University of Veterinary Medicine Budapest

Doctoral School of Veterinary Science

Comparative diagnostic imaging of the metacarpophalangeal joints in Thoroughbred racehorses: a longitudinal study

Ph.D. Dissertation

Dr. Koppány Boros

2026

Supervisor:

Dr. Annamária Nagy-Schuller tot Peursum, PhD habil. DipECVSMR DipACVSMR FRCVS

Department and Clinic of Equine Medicine

University of Veterinary Medicine Budapest

Consultant:

Dr. Sue Dyson, MA VetMB PhD

Independent Consultant

United Kingdom

Prepared in … copies, this is copy number …

Koppány Boros, DVM

Table of contents

1. Summary 9
2. Introduction 11
3. Literature review 13
3.1 Biomechanics and osseous adaptation in the aetiology of musculoskeletal injuries 13
3.2 Anatomy of the equine fore fetlock 13
3.3 Biomechanics of the fetlock 14
3.4 Adaptation of bone tissue 16
3.4.1 Modelling and remodelling 16
3.4.2 Effects of cyclic loading: bone adaptation, repair and fatigue damage 16
3.4.3 Adaptation during early training 18
3.5 Additional factors influencing musculoskeletal injuries 19
3.6 Articular and osseous abnormalities in the metacarpophalangeal joint of racehorses 21
3.6.1 Osteochondral lesions 21
3.6.2 Synovitis 22
3.6.3 Chronic proliferative (villonodular) synovitis 22
3.6.4 Sesamoiditis 23
3.6.5 Osteoarthritis 23
3.6.6 Palmar osteochondral disease 24
3.6.7 Fractures 25
3.6.7.1 Condylar fracture 26
3.6.7.2 Transverse fracture of the distal metaphysis of the third metacarpal bone 27
3.6.7.3 Fractures of the proximal phalanx 27
3.6.7.4 Fractures of the proximal sesamoid bones 28
3.7 Lameness diagnosis in Thoroughbred racehorses 28
3.8 Diagnostic imaging of the racehorse fetlock 29
3.8.1 Radiography 29
3.8.2 Ultrasonography 30
3.8.3 Magnetic Resonance Imaging 31

3.8.4 Computed Tomography 32
3.8.4.1 Spatial resolution and contrast resolution 36
3.8.5 Nuclear scintigraphy 37
3.8.6 Positron Emission Tomography 38
4. Knowledge gap addressed by the project 39
4.1 Computed tomographic evaluation of the sagittal ridge 39
4.2 Radiodensity and radiographic appearance of the proximal sesamoid bones 40
4.3 Comparative computed tomographic and magnetic resonance imaging evaluation of metacarpal condylar densification 40
5. Materials and methods 42
5.1 Cohort 42
5.2 Lameness examination 42
5.3 Image acquisition 42
5.4 Image analysis 44
5.4.1 Computed tomographic evaluation of the sagittal ridge 44
5.4.2 Radiodensity and radiographic appearance of the proximal sesamoid bones 47
5.4.3 Comparative computed tomographic and magnetic resonance imaging evaluation of metacarpal condylar densification 49
5.5 Data analysis 51
5.5.1 Computed tomographic evaluation of the sagittal ridge 51
5.5.2 Radiodensity and radiographic appearance of the proximal sesamoid bones 51
5.5.3 Comparative computed tomographic and magnetic resonance imaging evaluation of metacarpal condylar densification 53
6. Results 55
6.1 Horses 55
6.1.1 Lameness at follow-up examinations and responses to diagnostic anaesthesia 56
6.2 Computed tomographic evaluation of the sagittal ridge 56
6.2.1 Hounsfield Unit measurements 56
6.2.2 Hypoattenuating lesions 57
6.2.3 Subchondral bone plate thickening, trabecular bone hyperattenuation . 59

6.3 Radiodensity and radiographic appearance of the proximal sesamoid bones 59
6.3.1 Hounsfield Unit measurements 59
6.3.2 Abaxial margin changes 62
6.3.3 Proximal sesamoid bone grades 64
6.4 Comparative computed tomographic and magnetic resonance imaging evaluation of metacarpal condylar densification 65
6.4.1 Horses 65
6.4.2 Repeatability analysis 65
6.4.3 Location of maximal densification 66
6.4.4 Correlation between magnetic resonance imaging and computed tomographic measurements 67
6.4.5 Differences between magnetic resonance imaging and computed tomographic measurements 67
6.4.6 Association between magnetic resonance imaging and computed tomographic measurements and other variables 69
7. Discussion 72
7.1 Measurement methods 72
7.2 Changes in densification 73
7.3 Pattern of densification 74
7.4 Medial-lateral differences 75
7.5 Effect of sex 76
7.6 Effect of body size 76
7.7 Lameness 76
7.8 Findings in the sagittal ridge 77
7.9 Findings in the proximal sesamoid bones 79
7.10 Findings in the metacarpal condyles 80
8. Limitations 83
9. Conclusions 84
10. New scientific results 85
11. References 87
12. Scientific publications 110
12.1 Publications in peer-reviewed journals related to the thesis 110
12.2 Scientific posters, presentations 110

12.2.1 National 110
12.2.2 International 111
13. Supplementary material 113
14. Acknowledgements 123

List of abbreviations

ANOVA	Analysis of variance
CBCT	Cone-beam computed tomography/Cone-beam computed tomographic
CI	Confidence interval
CT	Computed tomography/Computed tomographic
CV	Coefficient of variance
DPa	Dorsopalmar
FBCT	Fan-beam computed tomography/Fan-beam computed tomographic
HU	Hounsfield unit
IQR	Interquartile range
IRU	Increased radiopharmaceutical uptake
IV	Intravenously
LM	Lateromedial
McIII	Third metacarpal bone
MR	Magnetic resonance
MRI	Magnetic resonance imaging
OR	Odds ratio
PET	Positron emission tomography
PSB	Proximal sesamoid bone
PSG	Parasagittal groove
POD	Palmar osteochondral disease
REML	Restricted maximum likelihood

ROI	Region of interest
SCB	Subchondral bone
SD	Standard deviation
SG	Sagittal groove
SL	Suspensory ligament
SR	Sagittal ridge
STIR	Short tau inversion recovery

1. Summary

The metacarpophalangeal joint of Thoroughbred racehorses is a major site of musculoskeletal injury, including fatigue-related osseous injury that may develop early in training when bone adaptation is insufficient to meet rapidly increasing mechanical demands. Repetitive cyclic loading during high-speed training and racing induces osseous adaptation, including changes in subchondral bone (SCB) density and morphology. When fatigue-related microdamage accumulates faster than it can be repaired, stress-related osseous injury and fracture may develop. In this thesis, densification is used as a descriptive term referring to an apparent increase in bone density on radiographs, computed tomographic (CT) and magnetic resonance (MR) images, without implying a specific pathological process. Advances in diagnostic imaging that can be performed in standing horses, particularly CT and low-field magnetic resonance imaging (MRI), have enabled detailed assessment of osseous structures, allowing early identification of osseous abnormalities associated with fatigue-related injury and pre-fracture changes.

This longitudinal study aimed to describe training-related asymptomatic changes in Thoroughbred racehorses in active training using repeated fan-beam CT (FBCT) and low-field MRI examinations. Radiographs acquired in parallel were compared with cross-sectional imaging results to help interpret radiographic findings. Over a two-and-a-half-year period, a cohort of forty Thoroughbred racehorses was followed from the onset of race training through multiple time points, providing one of the first prospective datasets combining morphologic and densitometric evaluation of the sagittal ridge (SR) and condyles of the third metacarpal bone (McIII) and the proximal sesamoid bones (PSBs).

The results demonstrated progressive, workload-related osseous changes at all three evaluated anatomical sites. Radiodensity of the SR and PSBs increased with training and racing exposure, whereas reduced training was associated with decreased overall PSB radiodensity. Some dorsal SR hypoattenuating lesions decreased in size or resolved during the first year of training, and radiographic improvement of PSB grades and abaxial margin abnormalities was observed despite continued training. Metacarpal condylar densification increased with racing exposure and was most frequently greatest in the middle third of the condyles. CT and MRI measurements of condylar densification were correlated but differed significantly, with CT consistently yielding greater measurements than MRI.

Overall, the findings demonstrate that substantial imaging-detectable osseous adaptation occurs in actively training Thoroughbred racehorses without clinically relevant lameness. Some imaging findings may represent dynamic, workload-related adaptation rather than

pathology, while the systematic difference between CT and MRI measurements highlights the need for modality-specific interpretation. These findings improve understanding of training-related osseous adaptation and provide longitudinal reference data that may support imaging-based screening, training management and future injury-prevention research in Thoroughbred racehorses.

2. Introduction

Musculoskeletal injury is the leading cause of lost training days, morbidity and catastrophic breakdown in Thoroughbred racehorses [1]. The fetlock, owing to its unique anatomy and the extreme mechanical loads encountered during gallop, is particularly vulnerable [2, 3]. Repetitive cyclic loading induces bone modelling, allowing bone mass and architecture to adapt to increased mechanical demand. In contrast, bone remodelling contributes to the removal and replacement of fatigued or microdamaged bone and may be inhibited during periods of sustained cyclic loading [4]. If microdamage accumulates faster than it can be repaired, fatigue-related osseous injury and fracture may develop. Understanding these processes and identifying early indicators of fatigue-related osseous injury are essential for improving equine welfare and reducing economic loss within the racing industry [5, 6].

Diagnostic imaging plays a key role in detecting and monitoring metacarpophalangeal joint pathology. Radiography remains a cornerstone for screening, yet its sensitivity to early detection of lesions is limited. Subjective CT and MRI appearance of the metacarpophalangeal joints of non-lame Thoroughbred yearlings at the beginning of racehorse training have already been described by our research group [7]. However, most published studies are cross-sectional or focus on horses already presenting with lameness. Consequently, at the outset of this project, there was limited longitudinal information on how training-related osseous changes evolve in apparently non-painful fetlocks during active race training.

The limited availability of longitudinal reference data limits the interpretation of imaging findings detected during screening or pre-race examinations, particularly when attempting to distinguish physiological adaptation from early pathological change. Establishing such baseline information is therefore fundamental for understanding the spectrum of osseous changes that may occur in actively training Thoroughbred racehorses.

The overall aim of this project was to document sequential osseous changes in the metacarpophalangeal joints of Thoroughbred racehorses using repeated FBCT, low-field MRI and radiographic examinations. Specific objectives are presented in Chapter 4. The working hypothesis was that osseous changes develop progressively in the metacarpophalangeal joint during race training and that, in some horses, adaptive alterations may evolve into pathological lesions associated with lameness.

This study represents one of the first longitudinal investigations describing adaptive and stress-related osseous changes in the metacarpophalangeal joints of actively training Thoroughbreds. It demonstrates that a range of osseous imaging findings may be observed in racehorses that remain non-lame throughout the study period. These findings provide

important context for the interpretation of diagnostic imaging examinations and may serve as reference data for future research on fatigue-related fetlock injuries.

3. Literature review

3.1 Biomechanics and osseous adaptation in the aetiology of musculoskeletal injuries

Horseracing, racehorse injuries and their welfare implications have been in the spotlight of public and professional forums [8]. Injuries occurring during racing or training may result in the premature ending of a horse's athletic career or even lead to catastrophic outcomes, and therefore have significant implications for animal welfare, jockey safety, and the economy of the racing industry [1]. These injuries most frequently involve the bones of the distal aspect of the limb [9]; fractures and other severe, career-limiting pathological changes occur predominantly in the fetlock region [2, 3]. To accurately assess fetlock region abnormalities in racehorses and to improve the identification of clinically relevant changes, it is essential to understand the spectrum of physiological and pathological changes that may occur in the fetlock during training and racing.

3.2 Anatomy of the equine fore fetlock

The horse’s metacarpophalangeal joints are formed by the complex articulation of four bones: McIII, the proximal phalanx, and the medial and lateral PSBs. The distal epiphysis of McIII consists of two convex condyles, a larger medial and a smaller lateral one, separated by the SR. The proximal articular surface of the proximal phalanx is an impression of the distal articular surface of McIII. The medial and lateral foveae articularis (glenoid cavities) are divided by the sagittal groove (SG), which accommodates the SR of McIII. The PSBs are pyramid-shaped bones embedded within the ligaments of the suspensory apparatus. In most horses the medial PSB has a smaller proximodistal length and greater mediolateral width than the lateral PSB [10].

The collateral ligaments, originating from the collateral fossae of McIII, are composed of two distinct parts on both the medial and lateral sides. The longer, vertical, superficial component inserts distal to the proximal articular surface of the proximal phalanx. The shorter, obliquely running deep component extends to the palmaromedial and palmarolateral aspects of the proximal phalanx and to the abaxial surface of the PSBs. Prevention of excessive extension of the joint is ensured by the passive static support system of the limb, which includes ligaments traversing the fetlock region, collectively referred to as the suspensory apparatus. The most prominent component is the suspensory ligament (SL). The majority of its fibres originate from the proximal aspect of the palmar cortex of McIII. The main component is complemented by accessory fibres arising from the axial portion of the base of the fourth metacarpal bone, as well as from the palmar aspect of the third and fourth carpal bones [11,

12]. The SL bifurcates distally forming the medial and lateral branches that attach abaxially to the palmaroproximal aspects of the PSBs [13]. The branches of the SL are connected to the distal end of the second and fourth metacarpal bones with fibrous bands [14].

Functionally, the SL is supplemented by the distal sesamoidean ligaments, which include three paired structures, the oblique, the short, and the cruciate sesamoidean ligaments, which insert on the proximal phalanx, as well as the straight sesamoidean ligament, which inserts on the proximal phalanx and contributes to the middle scutum [15, 16]. The collateral sesamoidean ligaments provide connections between the PSBs, McIII, and the proximal phalanx. The intersesamoidean ligament connects the two PSBs. Further support to the fetlock on the palmar aspect is provided by the metacarpointersesamoid ligament, connecting the intersesamoidean ligament to the palmar cortex of the McIII. Additionally, extensions of the SL from the PSBs form two extensor branches to the common digital extensor tendon, the tractus appositus, which play a role in the extension mechanism of the limb [16].

The metacarpophalangeal joint has three distinct recesses. The dorsal recess is located proximally between McIII and the common digital extensor tendon and extends about 2 cm proximally from the joint space [17]. The palmaroproximal recess lies proximally between McIII and the SL branches and extends about 4-5 cm proximally form the joint space. The palmarodistal recess is the smallest in extent and found between the distal sesamoidean ligaments and the proximal phalanx [16–18].

3.3 Biomechanics of the fetlock

Movement is generated through active contraction of muscles and passive tension of tendons and ligaments, which store and release energy [19]. Over the course of evolution, the structures of the equine limb have adapted to facilitate high-speed locomotion. In the distal limb, muscular elements are mainly replaced by robust tendons, which, together with their accessory ligaments, enhance the passive functionality of the limb [20]. The fetlock is one of the critical structures involved in limb stabilisation and shock absorption, enabling horses to perform high-speed work. While the primary movements of the fetlock are flexion and extension, small degrees of lateral movement and rotation also occur [21].

At low speed, the interaction between the SR of McIII and the SG of the proximal phalanx prevents excessive lateral movement and rotation. However, at high speeds, forces acting between the SR and the SG intensify [22], amplifying the biomechanical impact of non-sagittal movements on the components of the fetlock [23]. The degree of fetlock extension correlates with an increased frequency of these non-sagittal motions [23, 24]. During submaximal extension and tension of soft tissue structures, bones of the fetlock are compressed against

each other, and as the load increases, the extent of contact between the articular surfaces also increases [22, 23, 25]. With fetlock hyperextension, distal displacement of the PSBs occurs, resulting in the SL branches becoming articular surfaces that stabilise the metacarpal condyles between the PSBs and the proximal phalanx [20]. Extension of the fetlock occurs as a result of vertical forces, primarily through the passive function of the distal limb structures [26]. The passive elongation of tendons and ligaments reduces the need for active muscular effort [19]. During initial ground contact and early weight-bearing, the palmar tendons and ligaments of the fetlock absorb the impact through hyperextension of the joint, in conjunction with the simultaneous elongation of the digital flexor tendons and the SL [23]. Fetlock hyperextension is the excessive extension of the metacarpophalangeal joint beyond its neutral, weight-bearing position, occurring under load, most prominently during high-speed locomotion [27]. During weight transfer, the suspensory apparatus becomes tense and functions like a spring, playing a crucial role in dissipating ground reaction forces. In addition to the suspensory apparatus, the passive function of the superficial digital flexor muscle is essential for supporting the fetlock during hyperextension. The primary role of the superficial digital flexor muscle is not active limb flexion but rather the passive storage of energy during weight-bearing, which is later reutilized during push-off from ground [28, 29].

The primary gait of Thoroughbred racehorses is gallop, in which the sequence of footfalls is: trailing hindlimb, leading hindlimb, trailing forelimb, and finally the leading forelimb. During racing gallop, just before the suspension phase, the leading forelimb is the last to leave the ground and has the longest stance duration [30], making it subject to the highest loading forces and, consequently, the most injury-prone limb [31]. It is essential to differentiate the specific forces acting during gallop from those occurring in canter, where the trailing forelimb is subjected to the greatest ground reaction force [32]. Racing gallop exposes the musculoskeletal system to extreme forces. During trot, each forelimb bears approximately 120% of the horse's total body weight [33]. In canter this increases to 120–150% [32], and in gallop it reaches 170% [34]. Consequently, during the weight-bearing phase, fetlock hyperextension becomes extreme [28]. In this position, tension in the palmar tendons is at its maximum, which contributes to the increased forces between McIII and the PSBs. Additionally, the dorsoproximal portion of the proximal phalanx comes into contact with the dorsodistal aspect of McIII, indicating loading at or near the joint's physiological range of motion [35]. Fetlock hyperextension, together with elongation of the palmar tendons and suspensory ligament, contributes to energy absorption during the weight-bearing phase of the stride. However, excessive fetlock hyperextension (dorsal angle between McIII and proximal phalanx <110°) results in increased mechanical loading and may contribute to fetlock injury [35].

3.4 Adaptation of bone tissue

3.4.1 *Modelling and remodelling*

During skeletal growth, longitudinal development of long bones occurs through endochondral ossification. Bone modelling and bone remodelling are distinct, although potentially concurrent, processes. Bone modelling refers to the addition or removal of bone matrix resulting in a change in bone shape, size or volume. During modelling, osteoblast and osteoclast activity occurs independently in space and time [36]. Modelling therefore allows bone architecture and mass to adapt to changes in the mechanical loading environment. Bone remodelling, in contrast, refers to the removal and subsequent replacement of existing bone matrix at the same site, without a substantial net change in bone shape or volume [37]. Its principal role is the renewal and repair of bone tissue, including the replacement of fatigued or microdamaged bone. Remodelling occurs through a coordinated sequence of osteoclastic resorption followed by osteoblastic bone formation within basic multicellular units [38]. Following activation, osteoclasts resorb bone tissue and subsequently undergo apoptosis. During the reversal phase, mesenchymal stem cells, which are precursors of osteoblasts, are recruited to the remodelling site and differentiate into osteoblasts. During the formation phase, osteoblasts produce organic matrix, which subsequently undergoes mineralisation [36]. On average, it takes approximately four months for a single basic multicellular unit to complete an entire remodelling cycle [39]. Bone modelling and remodelling may occur concurrently in response to exercise; however, their biological roles should be distinguished. Modelling contributes to adaptation of bone mass and architecture to the loading environment, whereas remodelling contributes predominantly to tissue renewal and repair.

3.4.2 Effects of cyclic loading: bone adaptation, repair and fatigue damage

High-speed gallop training exposes the skeletal system to repeated cyclic loading [40]. Bone modelling occurs in response to training and contributes to adaptation of bone mass and architecture to increased mechanical demand. In contrast, bone remodelling is generally inhibited during periods of sustained cyclic loading and contributes primarily to the repair and replacement of fatigued or microdamaged bone [41]. Modelling allows bone to adapt to the mechanical loading environment, and training-induced increases in bone mass and structural properties can enhance resistance to fatigue [42]. However, once loading surpasses this threshold, the risk of injury increases.

Bone sclerosis refers to an increase in bone density, typically associated with reduced porosity [43, 44]. Histomorphometric studies have documented that the SCB of the metacarpal condyles in racehorses is often sclerotic and may contain abnormally stained bone matrix with

morphologically atypical osteocytes [40]. Although these findings have sometimes been interpreted as evidence of an adverse response to repetitive loading, increased bone formation or density should not in itself be considered pathological. Failure to adequately repair accumulated fatigue damage may be more relevant to the development of injury [41]. With prolonged cyclic loading, accumulation of microdamage may be accompanied by bone sclerosis, necrosis, microfractures and/or articular cartilage degradation [4, 22]. These findings may occur concurrently, but this does not establish that increased bone modelling or sclerosis itself is the cause of bone failure.

The formation of microdamage begins at the molecular level, involving collagen fibre degradation and disruption of the collagen-mineral interface [45]. With an increasing number of loading cycles during training, these molecular-level changes accumulate, resulting in diffuse matrix damage and the formation of microfractures [46]. The coalescence of microfractures can eventually lead to stress fractures [40], most commonly originating from the parasagittal groove (PSG) of McIII [40, 47]. These injuries are not the result of a single traumatic event but develop through progressive accumulation of fatigue damage associated with repetitive mechanical loading, particularly when damage accumulation exceeds the capacity for repair [48, 49]. Stress-related injuries compromise bone integrity, reducing its ability to withstand the loads experienced during racing and training [50]. Although stress-related injuries are increasingly recognised in non-racehorses [51, 52], stress fractures appear to be less frequently reported than in racehorses. However, several fatigue-related injuries are well recognised in sport horses, including short incomplete fractures of the proximal phalanx and proximopalmar cortical fatigue injuries of McIII [53–57].

The density and thickness of the SCB plate vary across different regions of the articular surface, depending on loading frequency, intensity, physical activity level, and limb conformation [58]. It is likely that in certain conformation variants, specific areas of bone are subjected to increased mechanical forces [53]. However, current knowledge is insufficient to establish direct correlations between conformation and stress-related bone injuries.

In racehorses in training, the average tissue density of the distal metacarpal epiphysis is 36.8% higher than in untrained horses [59]. The increase in metacarpal density begins in the palmarodistal epiphysis, at the contact point with the PSBs, and progresses in a dorsoproximal direction, leaving the dorsodistal region the least dense area [59]. This may at least partially explain why palmar osteochondral disease (POD), which is common in Thoroughbred racehorses, affects the palmarodistal region of the condyles [60]. However another study found that the dorsal half of the condyles has higher density compared to the palmar half [61]. These findings are not directly comparable because the studies differed in

anatomical sampling and region of interest (ROI) definition: the earlier study described regional density changes across the distal metacarpal epiphysis, whereas Putnoki et al. compared predefined dorsal and palmar condylar regions using longitudinal in vivo CT data [61]. Therefore, the apparently conflicting findings may reflect differences in how the condyle was subdivided and measured, rather than a true biological contradiction.

An imaging-based CT study reported higher density in the medial than the lateral condyle within the same limb [59]. This consistent mediolateral difference is more likely to reflect differences in loading magnitude between the condyles than the direction of training [22]. Biomechanical studies have demonstrated greater contact area and higher contact pressures in the medial aspect of the metacarpophalangeal joint compared with the lateral aspectIn contrast, a mechanical testing study of racehorse condyles found no significant differences between medial and lateral condyles or between left and right forelimbs of the same horse [44]. Although microstructural variables, including bone mineral density and bone volume fraction, were correlated with mechanical properties, density does not directly equate to mechanical strength or stiffness. Differences between studies may therefore reflect the fact that imaging-based density measurements and mechanical testing assess related but distinct aspects of bone adaptation.

Density of the proximal SCB of the proximal phalanx depends on anatomical location, physical activity, and the horse's developmental stage [62]. In racehorses that had suffered proximal phalanx fractures in the contralateral limb, SCB density variability between different parts of the proximal SCB of the proximal phalanx was greater than in those without fractures [62]. This variability likely reflects bone adaptation associated with training. Differences in bone density of the SG have been observed between active racehorses and those not in training, with the higher density reported in trained horses suggesting that this region is subjected to substantial mechanical loading during high-speed gallop [62].

3.4.3 Adaptation during early training

In Thoroughbred racehorses, particular attention must be paid to the period between one and two years of age. At this stage, McIII has its highest adaptive capacity, with pronounced bone adaptation occurring in response to the onset of training [63]. Since the bone tissue of young horses, still in the longitudinal growth phase, can adapt more rapidly before physeal closure than following closure, it is crucial to implement early but gradual training in Thoroughbreds, as they may begin racing at two years of age [53].

In Thoroughbreds, radiographic closure of the distal physis of McIII and the proximal physis of the proximal phalanx occurs between 8 and 14 months of age [64]. Complete

biological physeal closure occurs following radiographic closure [64], meaning that young racehorses are still in their growth phase at the beginning of their training regimen. Previous studies have demonstrated that SCB density increases within the first two months of training as part of the adaptive response of bone to mechanical loading [40, 65]. This physiological adaptation enhances the ability of growing racehorses to withstand repetitive mechanical loads associated with training [42].

The suspensory apparatus of young horses tends to be less stiff compared to adults, allowing greater fetlock hyperextension [31, 35]. A more compliant suspensory apparatus stores less elastic energy and is less effective in dampening ground reaction forces [31]. While training appears to have a strengthening effect on the SL [66–68], this raises concerns regarding whether the musculoskeletal system of young racehorses can adequately adapt to the cyclic high-intensity loads imposed during training. Supporting this concern, an increased risk of fatal distal limb fractures has been reported during the early racing career of Thoroughbreds, although this risk may vary according to training regimes and racing jurisdictions [9, 69]. The incidence of these catastrophic injuries increases again after five years of racing, potentially reflecting the cumulative effects of fatigue damage associated with repeated high-speed loading throughout a horse's career [9].

3.5 Additional factors influencing musculoskeletal injuries

Reducing racing speed can mitigate bone loading forces [53]. Several studies have found correlations between firmer racetrack surfaces (lower moisture content) and an increased incidence of injuries. This may be attributed to the fact that firmer surfaces allow racehorses to achieve higher speeds [70]. Conversely, on softer racetrack surfaces, the lower speeds and reduced mechanical load result in fewer catastrophic injuries compared to firmer surfaces [70, 71]. However, on soft, particularly deep track surfaces, the risk of soft tissue injuries may increase [72, 73].

Both longer race distances and larger field sizes increase the risk of injuries [69, 70]. The jockey's weight also contributes to the tension in the superficial digital flexor tendon and SL, thereby increasing the load on the fetlock [74]. In the racing industry, strict regulations govern jockey weight limits and monitoring. The less weight a horse carries, the greater its competitive advantage [75].

Training protocols that incorporate multiple short-speed sessions rather than prolonged gallop work are the most effective in reducing the risk of stress-related injuries while maintaining the necessary stimuli for bone tissue adaptation [76]. Inadequate exposure to speed work deprives the bone of sufficient stimuli to properly adapt to stresses encountered

during racing. However, excessive training volume, even at moderate speeds, can be harmful, as the cumulative distance covered (including both racing and training miles) increases injury risk [77, 78].

The timing of return to training following a period of reduced-intensity loading may also influence injury risk. Although rest from training may provide an opportunity for remodelling-mediated repair of accumulated bone damage, withdrawal from race training followed by pasture turnout has been associated with decreased McIII diaphyseal bone density approximately 147 days after training cessation [79]. Training-induced SCB adaptations may persist for up to six months after modifying an exercise programme [80, 81], however, this does not exclude earlier microstructural changes during periods of reduced loading. For example, racehorses resting from training for 1-16 weeks have been reported to have higher SCB porosity of the distal McIII than horses with condylar fractures, however, it cannot be excluded that, in some horses in that study, the duration of rest may have been insufficient to permit substantial remodelling-mediated repair, and this finding should therefore be interpreted with caution [82]. Therefore, both the duration and nature of reduced loading should be considered when planning the return to training. Increased bone porosity following a period of rest has been proposed to reduce the ability of bone to withstand subsequent loading [53]. However, mechanical properties under monotonic loading and resistance to fatigue under cyclic loading are distinct, and the mechanical consequences of post-rest increases in porosity remain incompletely characterised. Therefore, both the duration and nature of reduced loading should be considered when planning the return to training.

In addition to the environmental factors previously discussed, several studies have examined the influence of biological and early-life management factors on subsequent injury risk and racing performance. Stallions have been reported to sustain catastrophic limb injuries more frequently than mares [83]. Furthermore, first-born foals were less likely to suffer fractures, and increasing dam age was associated with a reduced fracture risk in the offspring [84]. These findings may partly relate to differences in early growth, as first-born foals and foals from older mares tend to have lower birth weights, which may influence subsequent athletic development and racing performance [85, 86]. More recently, early-life management factors have also been shown to be relevant: more extensive pasture turnout during the first six months of life, turnout in larger paddocks, and later weaning have been associated with improved later-life racing outcomes in Thoroughbreds, including the likelihood of racing, number of starts, and prizemoney earned [87]. These findings suggest that both prenatal and early postnatal factors may contribute to the development of a musculoskeletal system capable of tolerating the demands of race training.

3.6 Articular and osseous abnormalities in the metacarpophalangeal joint of racehorses

Every athlete, whether human or equine, is susceptible to orthopaedic injuries during training and racing. The high-speed work and skeletal immaturity of young racehorses predispose to musculoskeletal disorders that are rare or entirely absent in horses subjected to different types of workload and competing in other disciplines [49, 88]. The fetlock is a common site of these injuries, where repetitive loading during training and racing may contribute to fatigue-related osseous damage; cumulative racing workload has been associated with reduced fatigue life of equine SCB [89]. Injuries to the fetlock significantly contribute to loss of training and competition time, premature retirement of horses, and, in some cases, necessitate euthanasia [69, 71]. Severe injuries can often be prevented through early diagnosis and training modification. Given the substantial economic and welfare implications of established injuries, emphasis is placed on prevention. While regular screening examinations can contribute to early detection and risk reduction, they cannot completely eliminate the occurrence of injuries [90].

3.6.1 Osteochondral lesions

When the development of osteochondral lesions is due to insufficient blood supply to the growth cartilage, resulting in failure of endochondral ossification, the condition is referred to as osteochondrosis [91, 92]. Osteochondrosis dissecans occurs when an osteochondral fragment becomes detached from the affected area [91, 93]. The formation of osteochondral fragments is multifactorial, with pathogenesis potentially influenced by nutrition, conformation, body size, genetics, and traumatic impact [93, 94]. Most lesions undergo spontaneous healing during growth. However, lesions that persist beyond the horse's first year of life are likely to remain [95]. A previous radiographic study of yearling Thoroughbreds identified the metacarpophalangeal joint as the second most common location for osteochondral lesions (8% of the examined horses) after the femoropatellar joint [95]. In young Thoroughbred racehorses, osteochondral lesions are typically diagnosed in the absence of clinical signs during the evaluation of pre-sale radiographs [96, 97].

Osteochondral lesions affecting the SR of McIII fall within the domain of osteochondrosis [98]. Osteochondrosis of the SR generally presents as fragmentation of its dorsoproximal portion [99]. Similar lesions may also result from a separate centre of ossification or from traumatic impact. Minor SCB lesions, which manifest distally as flattening or concave contouring of the ridge surface, typically do not cause clinical signs and may resolve spontaneously [99, 100]. In more pronounced cases, radiographs reveal marked

irregularity in SR contour, as well as osteochondral fragments [99]. Osteochondrosis of the distal part of the SR rarely results in fragment formation; however, when fragments become detached, they can lead to joint effusion and lameness [100]. Such lesions are not always visible on standard weight-bearing lateromedial (LM) radiographs [101], but can be detected on LM (flexed) or dorsopalmar (flexed) views [100]. As long as fragments have not yet formed, spontaneous healing remains possible. Once fragments have detached, their removal is recommended, as they can lead to the development of osteoarthritis [99].

The aetiology of other osteochondral lesions in the metacarpophalangeal joint remains debated, as these cannot be unequivocally classified under osteochondrosis [91]. Osteochondral lesions of the metacarpal condyles are rare and may develop on both the dorsal and palmar aspects. Dorsal lesions tend to be more extensive [100]. The most common osteochondral lesion within the metacarpophalangeal joint is dorsoproximal osteochondral fragmentation of the proximal phalanx, which has been identified in 4% of yearling Thoroughbreds in a radiographic study [95]. This lesion rarely manifests clinically [98]. Small, rounded osteochondral fragments are typically located dorsomedially [99]. In young horses, fragments are more frequently positioned axially than in mature horses [100]. Initially, fragments detected on radiographs are small, but as they ossify during growth, they appear as larger radiopaque structures. Non-detached fragments can revascularize and reintegrate with the proximal phalanx [100]. Although lameness and clinical signs are rarely associated with this lesion, synovitis and articular cartilage fibrillation are commonly observed during arthroscopy [99]. Osteochondral fragments detached from the palmaroproximal aspect of the proximal phalanx (Birkeland fragments) occur more frequently on the medial than on the lateral side and are often asymptomatic [99, 102].

3.6.2 Synovitis

Metacarpophalangeal joint synovitis is common in young racehorses. It typically manifests with an increase in training intensity [13]. It is characterized by joint distension and mild lameness that improves with exercise. The joint's range of motion is usually reduced and radiographic examination does not reveal bony abnormalities [99].

3.6.3 Chronic proliferative (villonodular) synovitis

During hyperextension of the fetlock, the dorsoproximal aspect of the proximal phalanx exerts pressure on the dorsodistal region of McIII. Repeated trauma leads to inflammation and fibrosis of the synovial fold adjacent to the SR [13]. Fibrotic thickening of the fold causes further trauma, perpetuating a cycle of chronic inflammation [100]. The characteristic clinical presentation includes swelling of the dorsal aspect of the fetlock. Radiographic examination may reveal a crescent-shaped indentation just distal to the attachment site of the joint capsule

on the dorsal surface of McIII [13], which results from bone resorption caused by sustained pressure from the thickened fold [100]. Proximal to this indentation, new bone formation and increased radiopacity can be observed in advanced cases, indicating abnormal mineralisation [99]. Injection of contrast medium into the joint allows visualization of the thickened synovial fold, and ultrasonography can be used to measure its thickness, which is typically less than 2 mm in healthy joints [13].

3.6.4 Sesamoiditis

Traditionally sesamoiditis refers to inflammation of the PSBs and may be associated with desmitis of the branches of the SL at their insertion sites [100]. Clinically, sesamoiditis is characterized by pain upon palpation of the abaxial surface of the PSBs, often accompanied by lameness that becomes evident after prolonged, strenuous exercise [13]. Lameness resulting from pathology of the PSBs does not resolve with intra-articular anaesthesia of the metacarpophalangeal joint [13]. Radiographic findings indicative of sesamoiditis include periarticular osteophyte formation, enthesophyte formation, enlarged vascular channels and focal radiolucent lesions. There is often no direct correlation between the severity of clinical signs and radiographic changes [99]. Enlarged vascular channels attaining 2 mm in diameter, an increased number of vascular channels (more than two), or channels with irregular, non-parallel margins are not necessarily of clinical significance [13]. Importantly, the radiographic visibility of vascular channels may also be influenced by the degree of PSB densification. Lloyd et al. found that vascular channels were more likely to be identified radiographically in PSBs with a higher bone volume fraction and greater channel diameter, indicating that radiographic channel appearance reflects both channel morphology and the density of the surrounding bone [103]. Greater radiographic channel number and diameter were also associated with fewer career placings [103]. In light of the ambiguity surrounding the term sesamoiditis, recent research advocates replacing this terminology with the use of vascular channel grading and abaxial contour description [104]. Grading PSBs based on the number of enlarged (attaining 2 mm in diameter) vascular channels and describing changes of the abaxial margin (new bone formation, concave indentation) were deemed to enhance interpretation of radiographic findings [104]. In all cases of PSB pathology diagnosed via clinical examination and radiography, ultrasonographic evaluation of the SL is warranted. Suspensory ligament involvement influences treatment selection, rehabilitation protocols, and prognosis.

3.6.5 Osteoarthritis

Metacarpophalangeal joint osteoarthritis is common [13], affecting up to one-third of young, two- to three-year-old racehorses [105]. It may develop as a result of acute or repetitive trauma, osteochondrosis, biomechanical stress, or joint instability [106–109]. Due to the

biomechanics of the joint, lesions typically progress from the medial to the lateral aspect, presumably due to asymmetric load distribution resulting from the eccentric positioning of the horse's centre of gravity relative to the limb axis [109]. Osteoarthritis is often, but not always, accompanied by joint effusion and restricted range of motion [13]. The disease culminates in irreversible cartilage damage, structural changes in the SCB, soft tissue swelling and pain [107, 108, 110]. The severity of lameness varies from mild to severe, depending on the progression of the condition and the intensity of work [13]. Following perineural anaesthesia of the palmar and palmar metacarpal nerves at the junction of the proximal two-thirds and distal third of the metacarpal region (low four-point anaesthesia), lameness typically resolves [111]. Lameness may also be partially or completely alleviated by intra-articular anaesthesia [13]. Radiographic findings often include periarticular osteophyte formation along the proximal phalanx and McIII, both abaxially and on the dorsoproximal and dorsodistal aspects of the PSBs. Thickening of the SCB plate in the proximal aspect of the proximal phalanx is also observed, and in advanced cases, supracondylar lysis of McIII may occur [13]. In the final stage of osteoarthritis, significant cartilage loss results in joint space narrowing [13]. Cartilage loss due to osteoarthritis is typically more severe on the dorsal articular surface of the proximal phalanx and on the palmar aspect of the distal articular surface of McIII [112]. Early-stage lesions may not always be detectable on radiographs; therefore, advanced imaging techniques provide a more detailed assessment of joint abnormalities. Computed tomography can reveal heterogeneous attenuation of the SCB plate in the metacarpal condyles, with evidence of trabecular hyperattenuation and focal hypoattenuating (resorptive) lesions, which, due to previously mentioned biomechanical factors, more frequently affect the medial side [112]. The extent of SCB lesions is thought to correlate with the severity of overlying cartilage damage [112–114]. It remains unclear whether cartilage damage or SCB pathology occurs first; however, substantial evidence confirms their concurrent presence in osteoarthritis cases [113]. The most detailed imaging of articular cartilage is possible with high-field MRI, though this requires general anaesthesia [115]. Additional information about cartilage condition can be obtained through CT contrast arthrography or ultrasonographic assessment of the fetlock in a flexed position (distal McIII articular surfaces) [116, 117] and occasionally extensive cartilage damage can be detected in low-field MRI in standing horses [118–120]. Future efforts should focus on early lesion detection, which is becoming increasingly feasible with advanced imaging modalities.

3.6.6 Palmar osteochondral disease

Palmar osteochondral disease, also referred to as focal palmar necrosis, is a degenerative condition affecting the metacarpal condyles. It affects over 50% of Thoroughbred racehorses, with prevalence reaching 80-88% in certain populations [60, 121]. It is more

common in the forelimbs, where lesions are typically more severe in the medial condyle [121]. Initially, POD was classified as trauma-induced osteochondrosis and later as trauma-induced osteoarthritis [48]. The condition is associated with SCB fatigue due to repetitive trauma [122]. Although POD and condylar fatigue fractures both affect the distal metacarpal condyles, POD primarily involves the palmar articular and SCB region of the condyles, whereas condylar fatigue fractures most commonly originate from the PSG of McIII. Palmar osteochondral disease itself is not regarded as a predictor of future condylar fracture, and available evidence does not establish a direct association between POD and condylar fracture [121, 123, 124]. The disease is progressive, with different severity grades reflecting the advancement of POD. In early stages, mild surface irregularities of the palmar condyles are present, followed by SCB resorption, and in advanced stages, cartilage erosion and focal cartilage loss. It is hypothesized that beyond a certain threshold, these changes become irreversible, but some early lesions may resolve following training modification [121, 125]. Radiographic examination reveals both primary lesions characteristic of POD in advanced cases and secondary osteoarthritic changes. Primary lesions include focal areas of increased opacity (densification) with or without central radiolucent defects in the palmar aspect of the condyles, as well as irregular contour of the palmar SCB. Secondary changes include osteophyte formation on the PSBs and flattening of the palmar condyles [60]. In early stages, radiographic changes are mostly absent, making early diagnosis possible only through advanced imaging techniques [60]. In more advanced cases, condylar lesions become radiographically detectable, particularly with 35° dorsodistal-palmaroproximal (flexed) projections. There is an inconsistency between imaging findings and clinical signs, as marked POD lesions may occur in the absence of observable lameness or impaired performance [126]. Associations between condylar disease and reduced racing performance have been reported. Trope et al. found that horses with moderate or marked metacarpal/metatarsal condylar radiopharmaceutical uptake had fewer starts and reduced earnings compared with controls [127], while Beck et al. reported that CT-detected POD was associated with fewer placings per start in elite racing Thoroughbreds [128].

3.6.7 Fractures

With advancement of diagnostic imaging methods, numerous studies have confirmed that most fractures affecting the bones of the fetlock sustained by racehorses result from bone tissue fatigue due to repetitive loading [129–133]. The following fracture types share the characteristic that their site of origin and configuration within the bone are consistent, and they are frequently preceded by prodromal changes. Early changes include thickening of the SCB plate, bone resorption, periosteal and endosteal new bone formation, as well as bone oedema-type lesions on fluid-sensitive MRI sequences [134]. Recent-onset or recurrent exercise-

associated lameness, fetlock effusion, focal heat, swelling or pain over the metacarpal condyles or PSBs, asymmetrical loading, or exacerbation after fetlock flexion should raise suspicion of a stress-related osseous injury. In such cases, diagnostic imaging should precede diagnostic anaesthesia where possible, as continued exercise after pain that has been masked by anaesthesia could increase the risk of catastrophic fracture progression [13].

3.6.7.1 Condylar fracture

Condylar fractures represent a common and sometimes catastrophic injury in racehorses and are the leading cause of fatal musculoskeletal injuries in the United Kingdom [135]. These fractures originate parasagittally from the distal articular surface of the McIII [100, 136]. Their development is preceded by alterations in the SCB of the PSG or the condyles [137], from which a fissure progresses into a complete fracture [124]. The pathological process is associated with repetitive microtrauma sustained during high-speed work [100]. Since these fractures originate from the weight-bearing surface of the joint, bicortical (involving both the dorsal and palmar cortices) complete fractures typically result in severe lameness, swelling in the fetlock region, and pain on manipulation [13]. In contrast, unicortical fractures frequently occur in the absence of joint effusion or localizing signs [136]. Unicortical fissures originating from the PSG develop into complete fractures over weeks to months, extending towards the dorsal cortex [135]. Lateral condylar fractures are more frequent, tend to extend towards the lateral cortex, and rarely reach the diaphysis. Conversely, medial condyle fractures, which occur less frequently and are more common in hindlimbs, often propagate into the diaphysis [13]. Short unicortical fractures are primarily diagnosed using cross-sectional imaging modalities such as MRI or CT. Cross-sectional imaging techniques can aid in the prevention of catastrophic condylar fractures by detecting pre-fracture changes [137, 138]. The probability of returning to pre-injury performance levels exceeds 90% in cases of unicortical lateral condylar fractures [136]. Prognosis is less favourable for complete lateral condylar fractures, particularly displaced complete fractures, where only 33% of affected racehorses successfully return to racing [139]. Prognosis is also influenced by the extent of articular surface damage and the presence of intra-articular fragmentation. Comminution of the articular surface and free fragmentation within the joint are common in displaced condylar fractures, but may also be present in incomplete or complete nondisplaced fractures [140]. Importantly, comminution can be difficult to detect on standard radiographs, although dorsopalmar (DPa) (flexed) projections improve assessment of the dorsal and palmar articular surfaces [141]. Lateral condylar fractures with concurrent axial PSB fractures are associated with extensive articular surface damage and carry a hopeless prognosis for return to racing [13]. Outcomes are poorer for medial condylar fractures compared to lateral ones, regardless of unicortical or bicortical configuration. [139].

3.6.7.2 Transverse fracture of the distal metaphysis of the third metacarpal bone

Transverse fatigue fractures of the distal metaphysis of the McIII are relatively rare [130]. In many cases, they develop following return to training after a period of rest or at the initiation of training [131, 142]. These fractures are typically associated with acute, severe lameness and painful swelling in the palmarodistal region of the metacarpus [13], although they may also occur without these clinical signs [131]. Initial radiographs often do not reveal significant abnormalities. After seven to ten days, a horizontal radiolucent line may become visible, originating from the palmar or dorsal cortex of the distal metaphysis, surrounded by new bone formation. Additionally, the separation of the distal aspect of the second and fourth metacarpal bones from the palmar cortex of McIII may also be observed [13, 131]. In some cases, periosteal new bone formation occurs dorsally before the appearance of the radiolucent line, and paradoxically, a radiopaque line may even precede the radiolucent line [99]. In the absence of localizing, pathognomonic signs, lameness is alleviated by palmar and palmar metacarpal nerve blocks [13]. Although this condition does not directly involve the metacarpophalangeal joint, it is included in the differential diagnosis of conditions affecting the fetlock region.

3.6.7.3 Fractures of the proximal phalanx

Fractures of the proximal phalanx are among the most common long bone fractures in racehorses, accounting for up to 15% of fractures in certain populations [143, 144]. They occur more frequently during training than during racing and predominantly affect two-year-old horses [145]. The anatomical location and conformation of these fractures exhibit significant variability, influencing the severity of clinical signs and the prognosis for return to racing. The most frequently occurring type is a sagittal/parasagittal fracture originating from a fissure in the SG [13]. Incomplete fractures may be classified as short fractures if they are less than 30 mm in length, or long fractures if they meet or exceed this length [145]. A comminuted fracture is defined as one with three or more large fragments [146], while a complete separation of the proximal phalanx into multiple fragments without an intact bony column between the metacarpophalangeal joint and the proximal interphalangeal joint is referred to as a highly comminuted fracture [145]. Horses with long sagittal, displaced, comminuted, and highly comminuted fractures have distinct clinical signs, including swelling and pain in the affected region, even with mild manipulation [13]. Horses with short incomplete fractures may exhibit only mild or intermittent clinical signs. Frontal fractures of the proximal phalanx, which divide the bone into dorsal and palmar segments, are categorized into three groups: incomplete and complete dorsoproximal fractures and fractures originating from the midportion of the proximal articular surface [147].

3.6.7.4 Fractures of the proximal sesamoid bones

Fractures of the PSBs are generally associated with regional heat, swelling, pain on manipulation and lameness [13]. Their clinical significance is determined by their anatomical location and the extent of concurrent soft tissue injuries [99]. Their healing is hindered by inadequate blood supply and continuous biomechanical forces due to the extensive range of motion of the fetlock [13]. Small apical fractures of the PSBs typically cause mild to moderate lameness and often respond well to arthroscopic fragment removal. Prognosis may be less favourable for larger apical fractures involving most or all of the proximal third of the PSB, because these are more likely to compromise a greater portion of the SL branch attachment. Concurrent injury to the SL branches exacerbates clinical signs and further worsens the prognosis [13]. Abaxial fractures are avulsion fractures at the site of SL attachment. In horses with non-displaced fractures, stall rest may suffice for healing. Prognosis depends on fragment size and the extent of SL involvement. Since a larger proportion of the SL attachment is located at the site of abaxial fractures compared to apical fractures, SL branch injuries tend to be more severe in cases of abaxial fractures [100]. Basilar fractures involve the origin of the distal sesamoidean ligaments. Prognosis to return to racing depends on fragment size, displacement and the extent of associated distal sesamoidean ligament injury. [148]. Midbody transverse fractures extend through the central portion of the PSB and are particularly serious injuries because they can compromise the structural integrity of the bone and the function of the suspensory apparatus. Although they may present as acute catastrophic injuries, evidence suggests that midbody transverse fractures represent the end stage of a chronic fatigue-related process, in which repetitive high-speed loading and accumulation of microdamage progressively compromise bone integrity [133]. The prognosis to return to racing in case of midbody transverse fractures therefore depends not only on fragment configuration, but also on the degree of associated ligamentous injury and fetlock instability [149]. Axial fractures of the PSBs frequently occur in conjunction with lateral condylar fractures of the McIII. In the United States, these combined injuries are the most common catastrophic injuries occurring on racetracks [2]. Due to the concurrent injury of the intersesamoidean ligament and subsequent joint trauma, axial PSB fractures almost invariably result in the end of a horse's racing career [100].

3.7 Lameness diagnosis in Thoroughbred racehorses

Clinical examination and gait assessment form the cornerstone of lameness diagnosis. During clinical examination, the metacarpophalangeal joint should be assessed for distension of the dorsal and palmar pouches of the joint capsule. Digital pressure should be applied to the dorsoproximal aspect of the proximal phalanx and the dorsodistal aspect of McIII, as these

regions are common sites of fragmentation and impingement-associated pain, together with the abaxial margins of the PSBs, the SL branches and the proximal aspect of the distal sesamoidean ligaments. The joint is then flexed to evaluate range of motion and pain response, which should be compared between contralateral limbs. Standard protocols include visual gait evaluation, flexion tests, and diagnostic anaesthesia to localize pain to the fetlock region [3]. However, given that early fatigue-related osseous changes in racehorses may be subtle or subclinical, clinical findings may be equivocal. In Thoroughbreds in training, episodes of lameness of variable severity may be reported during or after exercise, typically improving rapidly with work, such clinical signs may be indicative of SCB pain [150]. In young Thoroughbreds, SCB injuries affecting the distal aspect of McIII are frequently associated with bilateral lameness, resulting in short steps and reduced performance [151]. Pain originating from the metacarpophalangeal joint and the surrounding region can most reliably be localized by perineural anaesthesia of the medial and lateral palmar nerves and the medial and lateral palmar metacarpal nerves just proximal to the fetlock (low four-point block), provided that more distal sources of pain have been excluded. It should nevertheless be acknowledged that both perineural anaesthesia of the medial and lateral palmar digital nerves at the level of the ungular cartilages (palmar digital block), or at the level of the base of the PSBs (abaxial sesamoid block) may improve pain originating from the fetlock region [111, 152, 153]. For more precise localization of pain, intra-articular anaesthesia may be required [154]. Lameness should first be assessed at 5 to 10 minutes; in most horses, intra-articular anaesthesia abolishes pain of articular origin within this time frame. In some cases of severe SCB pain, a longer period may be required to achieve meaningful clinical improvement. Conversely, horses with lesions confined predominantly to the SCB with intact articular cartilage, may show no improvement following intra-articular anaesthesia [155]. Walking the horse can facilitate intra-articular diffusion of the local anaesthetic solution, and in some instances, adding a low four-point perineural block is necessary to abolish pain of intra-articular origin [156].

3.8 Diagnostic imaging of the racehorse fetlock

3.8.1 Radiography

Standard radiographic evaluation of the metacarpophalangeal region typically includes four projections: weightbearing LM, dorsal10°proximal-palmarodistal oblique, dorsolateral-palmaromedial oblique and dorsomedial-palmarolateral oblique views [99]. On the LM projection, the condyles of McIII are superimposed [99]. In healthy joints, the articular surfaces appear smooth and curved, although a mild palmarodistal flattening of the metacarpal condyles are common. This projection also facilitates assessment of the articular margins of the proximal phalanx, the proximal aspect of the SR, the PSBs, and the contours of the condyles [157]. A

LM (flexed) view is particularly valuable to visualise the distal aspect of the SR and associated osteochondral changes, and also results in separation of the PSBs from the palmar aspect of McIII, thereby potentially enhancing evaluation of the dorsal aspects of the PSBs [98, 158]. Dorsoproximal-palmarodistal oblique views primarily evaluate condylar margins, the joint space and PSB contours [99, 157]. To further evaluate the joint space and the palmar aspect of the condyles, additional DPa views may be obtained with the fetlock flexed and the beam directed horizontally or tilted distoproximally. The latter is a standard projection in racehorse practice for assessing palmar condylar pathology [99]. Dorsolateral-palmaromedial/dorsomedial-palmarolateral oblique views provide complementary information, with 60° projections best highlighting the dorsal eminence of the proximal phalanx and axial PSB surfaces, while 45° projections show the PSB contours and dorsolateral and dorsomedial margins of the proximal phalanx [99]. A dorsoproximal–dorsodistal (flexed) (skyline) view enables detailed evaluation of the dorsal articular surface of McIII, including the SR [21]. While radiographs remain indispensable for routine screening, they should be interpreted cautiously in racehorses, as many clinically relevant lesions especially early signs of catastrophic injuries may be missed [131, 159–161]. Nevertheless, numerous racehorse fetlock lesions are still identified radiographically, especially on the DPa (flexed) view [99].

3.8.2 Ultrasonography

Ultrasonography is primarily employed to assess soft tissue structures and osseus surfaces of the fetlock. With appropriate technique, the integrity of articular cartilage can also be evaluated, although only a relatively small portion of the articular surface is accessible [116, 162]. Ultrasonography may detect some osseous changes, e.g., new bone formation, earlier than radiography, although agreement between the two modalities for fetlock-related findings has been reported to be only moderate, highlighting their complementary diagnostic value [163].

From the dorsal approach, the joint capsule, synovial plica, extensor tendons, dorsodistal condylar and SR cartilage, and the dorsoproximal margin of the proximal phalanx can be visualized [164]. Images obtained from either the medial or lateral side allow assessment of the collateral ligaments and the SL branches. From the palmar approach, the digital flexor tendon sheath, superficial and deep digital flexor tendons, the manica flexoria, the axial and abaxial surfaces of the PSBs, the intersesamoidean ligament and the distal sesamoidean ligaments can be evaluated [116]. Dynamic examination in flexion is useful for detecting adhesions between the flexor tendons and the tendon sheath, and for evaluating fragment mobility in cases of osteochondral lesions [116].

3.8.3 Magnetic Resonance Imaging

Magnetic resonance imaging allows simultaneous assessment of bone and soft tissues in multiple planes, without the use of ionising radiation [165]. Magnetic resonance imaging can identify alterations in osseus architecture, making it suitable for detecting osseous pathologies such as densification, oedema, fibrosis or necrosis [166]. Thus, MRI not only detects structural abnormalities but also provides information on associated physiological and pathological processes [165]. However, altered osseous signal intensity is not specific for a single underlying histopathological process, as similar signal patterns may reflect different combinations of changes. Therefore, osseous MRI findings should be interpreted according to their morphology and signal characteristics across multiple sequences and in conjunction with clinical findings and, where appropriate, complementary imaging [166]. By using multiple sequences, different anatomical structures and pathological changes can be highlighted. Equine MRI systems differ in both field strength and magnet configuration. Some low-field systems are suitable only for use with horses under general anaesthesia, whereas the Hallmarq (Hallmarq Veterinary Imaging Ltd., Guildford, UK) low-field open magnet is designed primarily for imaging standing sedated horses, although it can also be used with horses under general anaesthesia. High-field MRI offers superior image resolution and diagnostic accuracy but requires general anaesthesia. Low-field systems provide lower signal-to-noise ratio and spatial detail and are more prone to motion-artefacts [167]. Although low-field MRI performed in standing horses is limited by lower spatial resolution and susceptibility to motion artefact, it offers important practical and safety advantages by avoiding general anaesthesia and allowing imaging of the limb under load. This helps preserve more physiological anatomical relationships, and the modality remains valuable for detecting soft tissue injuries and osseous pathology in the equine distal limb [168, 169].

Magnetic resonance imaging is increasingly used in the racehorses to detect joint injuries early and reduce the risk of catastrophic failure [49]. In Thoroughbred racehorses, SCB injury of the metacarpophalangeal joint is a common MRI finding and includes a spectrum of lesions such as densification (hypointensity on all sequences), bone oedema-type lesions [T1-weighted hypointensity, short tau inversion recovery (STIR) hyperintensity and variable phase-cancellation artefact on out-of-phase T2*-weighted images], defects (interruption of normal contour in the SCB plate), resorption (area of trabecular SCB hyperintensity on all sequences) and stress-related fissures [49, 166, 170]. Palmar osteochondral disease appears on MR images as areas of low signal intensity with a central hyperintense region on T1- and T2*-weighted sequences, often accompanied by adjacent bone oedema-type lesions on fluid-sensitive sequences [49]. Stress fissures most commonly occur in the PSG, appearing as linear low-signal-intensity defects usually associated with surrounding bone oedema-type

signal [49, 125]. Thoroughbreds frequently have SCB abnormalities along the dorsal border of the proximal phalanx and marked involvement of the PSBs, characterised by increased densification and bone oedema-type signal [49]. Conversely, the dorsomedial aspect of the metacarpal condyles is relatively less affected by bone oedema-type lesions in racehorses [49].

Magnetic resonance imaging can reveal soft tissue injuries that are undetectable or only partially detectable with ultrasonography, facilitating the diagnosis of lesions affecting the distal sesamoidean ligaments and/or the collateral ligaments, as well as abnormalities within the deep and superficial digital flexor tendons within the digital flexor tendon sheath, which cannot be adequately diagnosed with conventional imaging techniques [171–173]. Magnetic resonance imaging has facilitated a more detailed understanding of fetlock pathology by enabling detection of bone oedema-type signal, SCB changes and soft tissue injuries not apparent on traditional imaging modalities. High-field MRI-based measurements of densification correlated with condylar fracture risk, suggesting a potential predictive value [137, 138].

3.8.4 Computed Tomography

Computed tomography is increasingly used in equine diagnostic imaging, particularly for the evaluation of osseous structures of the head, neck and distal limb. Two main CT acquisition geometries are currently relevant in veterinary and human medicine: FBCT, also referred to as conventional or multidetector CT, and cone-beam CT (CBCT). Although both techniques are based on X-ray attenuation and generate cross-sectional and three-dimensional images, they differ substantially in detector design, image quality characteristics and suitability for specific clinical applications.

Fan-beam CT uses a narrow, fan-shaped X-ray beam and a curved or multidetector array. During acquisition, the patient or ROI is scanned in sequential or helical fashion, and the data are reconstructed into cross-sectional images. In contrast, CBCT uses a cone-shaped X-ray beam and a flat-panel detector to acquire a volumetric dataset, often during a single rotation around the ROI. This acquisition geometry enables rapid volumetric imaging and can provide isotropic voxels and high spatial resolution, particularly when imaging relatively small, high-contrast structures such as teeth, cortical bone and articular margins. Consequently, CBCT has become widely used in human dental, maxillofacial and extremity imaging, and has gained increasing interest in veterinary dentistry and equine orthopaedic imaging [174–176].

Although CBCT can theoretically provide high spatial resolution, in currently available equine CBCT systems, the practical spatial resolution is considerably lower than that achieved

in small-field human or dental CBCT applications and may be insufficient for detecting subtle osseous detail compared with FBCT. In addition, the larger irradiated volume and flat-panel detector geometry make CBCT more susceptible to scattered radiation, beam hardening, noise and reconstruction artefacts. These factors reduce contrast-to-noise ratio and limit soft tissue contrast compared with FBCT. In addition, CBCT grey values are generally less reliable than Hounsfield Unit (HU) values obtained from FBCT, because CBCT attenuation values are more affected by scatter, field of view, patient size and acquisition parameters. Therefore, CBCT is less suitable for quantitative attenuation-based assessment, particularly when reliable measurement of bone density or comparison of attenuation values over time is required [175, 177].

Fan-beam CT, by contrast, generally provides superior contrast resolution, lower image noise, more consistent soft tissue differentiation and more reliable attenuation measurements. These characteristics are particularly important when evaluating osseus architecture, subtle density gradients, sclerosis, hypoattenuating defects, fracture morphology and soft tissue-related abnormalities. The ability to reconstruct images using different slice thicknesses and reconstruction algorithms also allows image quality to be adapted to the clinical or research question. In longitudinal equine studies, where repeated quantitative measurements of bone density or sclerosis extent are required, FBCT may therefore offer advantages over CBCT because of its greater consistency and reliability of attenuation-based data [61].

In horses, both CBCT and FBCT have been introduced to overcome the limitations of radiography, particularly anatomical superimposition and the inability to evaluate complex three-dimensional structures in detail. The emergence of standing CT systems has been especially important in equine practice, because image acquisition in standing sedated horses avoids general anaesthesia and thereby improves clinical practicality and patient safety.

The commercially available equine CBCT systems differ substantially in design and intended use. Hallmarq Vision CT (Hallmarq Veterinary Imaging Ltd, Guildford, UK) is a dedicated standing distal-limb CBCT system in which the scanner surrounds the limb and acquires images of the foot, pastern, fetlock and distal metacarpal/metatarsal region in the sedated standing horse [169, 178]. In contrast, robotics-controlled systems such as Equimagine (Equine Imaging LLC, Milwaukee, WI, USA) use robotically positioned x-ray sources and flat-panel detectors that move around the standing horse, allowing more flexible access to larger anatomical regions, including the head, neck and limbs [179]. Pegaso/Pegaso Forte (Epica Medical Innovations, San Clemente, CA, USA) represents another robotic equine CBCT platform designed for orthopaedic imaging in standing horses or under general anaesthesia, with published use for extremity imaging and case-based assessment of distal

limb lesions [180]. The mobile O-arm® system (Medtronic Inc., Minneapolis, MN, USA) is not equine-specific, but has been adapted for CBCT imaging of the equine head in standing sedated horses, where its mobility and short acquisition time are useful for selected indications [179]. Several studies have evaluated CBCT in equine patients. Stewart et al. (2021) reviewed the use of CBCT (Pegaso and Equimagine systems) and highlighted its potential for standing imaging of the head, neck and distal limb [176]. In a later cadaveric study of equine metacarpophalangeal joints [176]. Stewart et al. (2023) found that CBCT produced images of numerically comparable diagnostic quality for bone compared with FBCT, whereas FBCT was superior for soft tissue evaluation [181]. These findings support the use of CBCT for high-contrast osseous structures but also reinforce the limitation of CBCT for soft tissue assessment.

Direct comparisons between CBCT, FBCT and low-field MRI have also been performed in equine fetlock studies. Lin et al. (2024) compared CBCT, FBCT and low-field MRI for the detection of dorsoproximal osteochondral defects of the proximal phalanx using macroscopic pathology as a gold standard [169]. Diagnostic performance was best with FBCT, followed by CBCT and then low-field MRI, although CBCT measurements of defect size correlated strongly with macroscopic measurements[169]. In a related study of palmar/plantar osteochondral disease in Thoroughbred cadaver limbs, Lin et al. (2024) found that both CT techniques were more sensitive than low-field MRI for lesion detection. FBCT had the highest sensitivity, while CBCT showed similar imaging features and strong correlation with macroscopic lesion dimensions [178]. These studies are highly relevant for racehorse fetlock imaging because they indicate that CBCT and FBCT can both detect SCB and osteochondral lesions, but FBCT may provide superior diagnostic performance.

Additional equine studies have investigated the anatomical and diagnostic capabilities of CBCT and multidetector CT in other regions. Van Zadelhoff et al. (2021) compared CBCT and multidetector CT for detecting dental and sinus abnormalities in equine cadaver heads and found substantial agreement for most dental abnormalities. However, CBCT was less reliable for detecting pulp changes, probably because of scatter radiation, artefacts and non-calibrated grey values [182]. Bierau et al. (2024) compared CBCT and multidetector CT for visualization of anatomical structures in the equine fetlock region and found only minor differences between CBCT and multidetector CT for osseous structures, whereas multidetector CT was superior for soft tissue assessment [183].

Acquisition of FBCT images in standing horses is feasible and clinically useful. Brounts et al. (2022) reported the use of a novel helical FBCT system for distal limb imaging in 167 standing sedated horses. The system allowed rapid scanning of the distal limb, and CT

provided a specific imaging diagnosis more frequently than planar radiography [184]. More recently, combined low-field MRI and FBCT was described in horses with fetlock region pain, demonstrating that the two modalities provide complementary information [56]. In that study, FBCT was particularly useful for detecting incomplete fractures and resorptive SCB lesions that were not always evident on MRI images, whereas MRI provided additional information on bone oedema-type signal and soft tissue involvement.

Fan-beam CT systems that acquire images with the limb in weight-bearing or standing non-/semi-weight-bearing positions offer different advantages for equine distal limb imaging. Weight-bearing systems allow assessment of osseous structures under physiological load, which may better reflect functional joint alignment and anatomical relationships [185]. However, systems designed to accommodate both limbs generally require a larger field of view, which may affect image quality through reduced spatial resolution and increased scatter. In contrast, systems that allow standing non- or semi-weight-bearing acquisition, such as the system used in the present study, permit more controlled limb positioning and the use of a smaller field of view, which may improve image quality for the ROI, while still avoiding general anaesthesia. The main limitation of non-/semi-weight-bearing acquisition is that the absence of full physiological loading may restrict functional interpretation of joint mechanics. Although CT is primarily suited to osseous assessment and has lower soft tissue contrast than MRI, it can provide useful information on mineralised or gross soft tissue abnormalities [181]. In addition, CT contrast arthrography can improve assessment of intra-articular soft tissues, articular cartilage, synovial structures and communication between lesions and the joint space [116, 117].

Computed tomography permits both linear and attenuation-based assessment of osseous change. Linear measurements, as used in a standing CBCT study of young Thoroughbred fetlocks, can quantify lesion dimensions and changes in SCB morphology [186, 187]. In contrast, HU-based measurements within predefined ROIs can quantify regional bone attenuation and have been used in a FBCT study to assess longitudinal changes in metacarpal condylar radiodensity in non-lame Thoroughbred racehorses [61]. These approaches are complementary rather than interchangeable: linear measurements describe the extent or size of visible structural change, whereas HU-based measurements provide quantitative information on regional radiodensity.

Radiography and FBCT were compared for detection of condylar densification with CT achieving superior results [160]. Fan-beam CT also resulted in higher sensitivity and diagnostic accuracy for identifying hypoattenuating lesions in the condyles and PSG compared with radiography [161]. Computed tomography may be pivotal for identifying early fatigue-related

osseous abnormalities, fissures, and pre-fracture lesions that may precede catastrophic failure [3]. Longitudinal studies using both FBCT and CBCT have advanced the understanding of training-related osseous adaptation, with progressive densification documented in the metacarpal condyles and PSBs of Thoroughbreds, demonstrating that structural and density-related changes develop with continued training [61, 186, 187]. Fan-beam CT screening in standing horses has also recently been used to describe the prevalence and distribution of fetlock CT features in elite racing Thoroughbreds considered fit to race, further supporting the clinical relevance of CT-based assessment in high-risk racehorse populations [128].

In clinical practice, the choice between FBCT and CBCT is often determined by availability rather than by modality preference alone. Where both are available, selection should be guided by the anatomical region, clinical question and need for quantitative information, while recognising that FBCT generally involves substantially greater purchase and infrastructure costs than CBCT. Cone beam CT offers high spatial resolution, rapid volumetric acquisition and practical advantages for standing imaging of selected regions, particularly when the main target is cortical or high-contrast osseous detail. FBCT provides superior contrast resolution, lower image noise, more reliable attenuation values and better soft tissue discrimination, making it more appropriate for assessing trabecular and subchondral bone density, subtle sclerosis, fracture morphology and longitudinal quantitative changes. In equine distal limb imaging, both systems have important clinical and research applications, but their limitations must be recognised.

Overall, CT is superior to MRI for cortical and SCB assessment but inferior for bone oedema and soft tissue lesions [169]. Compared with scintigraphy and positron emission tomography (PET), CT provides structural rather than functional information, making the modalities complementary [188]. Limitations include radiation exposure, equipment costs, and restricted soft tissue evaluation [3]. Nevertheless, the advent and validation of CT systems that can be used in standing horses have transformed accessibility, establishing CT as a pivotal modality in the diagnosis and monitoring of fetlock lesions, with the potential to prevent catastrophic fetlock injuries in racehorses [189].

3.8.4.1 Spatial resolution and contrast resolution

Image quality is primarily determined by spatial resolution and contrast resolution. Spatial resolution refers to the ability of an imaging modality to distinguish two closely adjacent structures as separate entities. In digital imaging systems, spatial resolution is primarily determined by pixel size, which is influenced by the matrix size and field of view; smaller pixels generally result in improved spatial resolution [190]. Radiography generally provides superior

spatial resolution compared to CT, allowing excellent visualization of fine osseus detail and thus detection of incomplete non-displaced fractures.

While spatial resolution determines the ability to visualize fine anatomical detail, contrast resolution refers to the ability to distinguish between tissues with similar attenuation characteristics [191]. Computed tomography provides substantially greater contrast resolution than radiography, allowing the detection of markedly smaller differences in tissue attenuation and density [192]. This superior contrast resolution, combined with the elimination of anatomical superimposition and the ability to generate multiplanar and three-dimensional reconstructions, contributes to the increased sensitivity of CT for detecting lesions. Three-dimensional reconstructions can further aid lesion localization, assessment of complex osseous anatomy, visualization of fracture configuration and communication of findings for clinical decision-making or surgical planning.

3.8.5 Nuclear scintigraphy

Scintigraphy is highly sensitive for detecting bone modelling and remodelling; however, based solely on abnormal radiopharmaceutical uptake, the exact nature of the lesion cannot always be determined [193]. While highly sensitive, scintigraphy is limited by low specificity and poor spatial resolution, making precise lesion localization challenging. Furthermore, increased radiopharmaceutical uptake (IRU) does not necessarily indicate a clinically significant abnormality. Although multimodal interpretation is important for all imaging techniques, this is particularly relevant for scintigraphy, as it reflects increased bone metabolic and osteoblastic activity rather than specific structural pathology; therefore, scintigraphic findings should be interpreted in conjunction with clinical examination and complementary imaging modalities [194].

Scintigraphy has played an important role in the detection of stress-related osseous injury in racehorses, particularly before the widespread adoption of advanced cross-sectional imaging [195]. Patterns of IRU in the fetlock associated with repetitive loading and microdamage have been described [127], and scintigraphy can help determine the clinical relevance of abnormalities identified by other diagnostic methods. It may also detect subclinical osseous lesions before they progress to injuries that compromise athletic performance or racing careers [195]. Stress fractures and fissures may present as sudden but transient lameness; therefore, when radiography and ultrasonography fail to identify abnormalities in commonly affected regions, scintigraphic examination should be considered [196]. Although CT, MRI and PET are preferred over scintigraphy for pain causing lameness localized to the distal limb, particularly in the fetlock, scintigraphy remains valuable for whole-body assessment and for identifying stress fractures or areas of intense bone remodelling in regions that are less

accessible to other modalities, such as the pelvis, tibia and humerus [197]. It may also be useful in racehorses with bilateral or quadrilateral lameness, when multilimb stress-related injury is suspected [161, 198]. Overall, scintigraphy remains an important functional imaging modality in racehorses, particularly for whole-body screening, proximal limb and axial skeletal assessment, and cases in which pain cannot be confidently localized to a single distal limb region.

3.8.6 Positron Emission Tomography

Positron emission tomography has emerged as a promising advance over scintigraphy by providing higher spatial resolution and improved localization of lesions [198]. However, its current application remains largely confined to the carpus, tarsus, and more distal regions of the limb [195]. The first report in its application in racing Thoroughbreds demonstrated a superior lesion-to-background contrast and precise localization of increased bone turnover [199]. Subsequent studies validated standing PET as a safe and repeatable modality [188]. Comparison between PET and scintigraphy in a population of 33 racehorses confirmed PET's superior sensitivity and diagnostic value, particularly for detecting regions of IRU in the fetlock, most notably within the PSBs, where PET also yielded better inter-observer agreement and identified more sites of IRU potentially associated with early bone turnover [198]. Sites of IRU may correspond to predilection sites for catastrophic injury [200], however interpretation remains challenging, as physiological uptake patterns in clinically normal racehorses are not yet fully established. Further baseline studies are essential before PET can be reliably integrated into risk assessment protocols.

4. Knowledge gap addressed by the project

Despite the high prevalence of fetlock-related injuries in Thoroughbred racehorses, a critical knowledge gap exists in understanding how non-painful metacarpophalangeal joints remodel over time in response to race training. Although recent longitudinal standing CBCT studies have substantially advanced understanding of SCB morphology and pathology in the fetlocks of two-year-old Thoroughbred racehorses during their first year of training [186, 187], important knowledge gaps remain. Most other imaging studies are cross-sectional or focus on horses already presenting with lameness, and limited data are available from longer-term, repeated multimodality imaging of actively training, non-lame Thoroughbreds. In particular, sequential FBCT appearance of the SR, longitudinal changes in overall PSB radiodensity and radiographic PSB appearance, and the relationship between CT- and MRI-derived measurements of metacarpal condylar densification have not been systematically characterised in the same cohort. This PhD project aimed to address this gap by providing a prospective, longitudinal, multimodal imaging dataset, and improving interpretation of advanced imaging findings for injury prediction, training management, and welfare-oriented decision-making.

4.1 Computed tomographic evaluation of the sagittal ridge

Radiographic abnormalities of the SR of McIII are common in Thoroughbred yearlings, with reported prevalences varying widely between studies, and may be clinically and economically relevant since they have been associated with joint effusion, lameness and reduced sales prices [98, 158, 201–205]. Subjective CT, MRI and radiographic findings in the metacarpophalangeal joint of Thoroughbred yearlings have recently been described [7]. Abnormalities in the SR included hypoattenuating lesions, thickening of the SCB plate and increased attenuation of the trabecular bone. Longitudinal data are available on the change of SCB density at predilection sites in the metacarpophalangeal joints of young Thoroughbred racehorses, using CBCT [186]. However, this study did not evaluate abnormalities in the SR. To date, CT abnormalities of the SR have not been described in detail, and to our knowledge, there is no longitudinal information on the progression of SR lesions in young Thoroughbreds.

The aims of this study were to describe the CT appearance of the SR in young Thoroughbred racehorses, using subjective and objective evaluations, and to document the progression of these findings over three assessments in the first year of training and racing. We hypothesised that 1. the mean attenuation of the SR would increase during the study period, as an adaptative response to training; and 2. the appearance of some hypoattenuating lesions in the SCB of the dorsal aspect of the SR would change during the first year of training.

The SR analysis was restricted to the first three assessments (times 0-2), corresponding to the first year of training and racing, because this period was considered most relevant for documenting early training-related adaptation and changes in pre-existing or developing SR lesions.

4.2 Radiodensity and radiographic appearance of the proximal sesamoid bones

Radiographic abnormalities of the PSBs, particularly enlarged vascular channels and abaxial margin changes, may be clinically relevant and have been associated with reduced racing performance in Thoroughbred racehorses [97, 104, 158, 206]. Changes in frequency of occurrence of radiographic findings as a consequence of racehorse training have recently been described [104]. Nevertheless, data on longer term follow-up are limited. Longitudinal data are already available demonstrating changes in SCB radiodensity based on CBCT studies [186, 187] at various sites in the metacarpophalangeal/metatarsophalangeal joints of young Thoroughbreds, associated with racehorse training. Ex vivo studies have demonstrated regional alterations in PSB density of racehorses [133, 207, 208] and an increased overall density has been linked to commencement of race training and the development of PSB fractures [209, 210]. However, to date no longitudinal data exist on the cumulative effect of training and racing on overall radiodensity of the PSBs of young Thoroughbred racehorses in active training.

The aims of this study were 1. to evaluate the radiographic appearance of the PSBs in the forelimbs of Thoroughbred yearlings based on an objective grading system [104], 2. to follow changes in radiographic appearance over a period of 2.5 years with four re-examinations, 3. and to describe changes in overall radiodensity using objective CT measurements obtained from FBCT images. It was hypothesised that during the study period: 1. the overall radiodensity of the PSBs would increase; and 2. there would be alterations in the radiographic appearance of the PSBs with time spent in racehorse training and racing.

4.3 Comparative computed tomographic and magnetic resonance imaging evaluation of metacarpal condylar densification

Training-related densification of the metacarpal condyles is well recognised in Thoroughbred racehorses; however, longitudinal comparison of FBCT- and low-field MRI-derived measurements in the same actively training horses is lacking. Recent longitudinal investigations have demonstrated that densification and pathology accumulate over time in the palmar/plantar aspect of the condyles and the PSG of McIII [61, 186]. Magnetic resonance imaging can be used to detect linear hyperintensities and areas of increased signal intensity in fat supressed images associated with a lateral condylar fracture, with low-field MRI providing

diagnostic performance comparable to high-field systems on cadaver limbs [137, 138]. Despite advances in diagnostic imaging, establishing robust predictive thresholds for condylar fracture risk, using the extent of densification, remains challenging. The results of an MRI-based cadaver study suggested a cut-off value of 16 mm for the extent of densification in the SCB plate and underlying trabecular bone in the lateral PSG may be clinically relevant [137], however neither FBCT nor high-resolution peripheral quantitative CT has reliably identified fracture risk thresholds [210, 211]. Furthermore, this MRI-derived risk threshold for lateral condylar fracture should be interpreted with caution, because it was established in a pre-selected population with a high prevalence of lateral condylar fractures and therefore may not be directly applicable to real-world populations [137].

The main objectives of this study were (1) to measure the largest extent of densification in the axial, middle and abaxial thirds of the palmar aspect of the metacarpal condyles on FBCT and low-field MR images, (2) to follow the changes in extent of densification over a period of 2.5 years with four re-examinations and (3) to investigate correlation of CT and MRI measurements. It was hypothesised that (1) the extent of densification would increase with increasing racing activity and (2) there would be a correlation between CT and MRI measurements.

5. Materials and methods

5.1 Cohort

A convenience sample of 40 Thoroughbred racehorses was included in the study. Racehorse owners and trainers from Hungary were invited to participate. Participants were selected in order of application. Written informed consent was obtained from trainers or owners of the horses. The animal study protocol was approved by the Ethical and Animal Welfare Committee of the University of Veterinary Medicine Budapest and by the Government Office of Pest County (PE/EA/1051-7/2021; 23 September 2021). All horses were of yearling age and just entering racehorse training at the time of the first examination (time 0). Yearlings without lameness and a history of metacarpophalangeal joint disease were eligible. Data concerning signalment (sex, age in months, weight, height at the withers) and the number of total starts (starting from time 1) were collected. Re-examinations (times 1, 2, 3 and 4) were performed four times, approximately six months apart.

5.2 Lameness examination

All horses underwent clinical assessment with particular attention to the metacarpophalangeal region. The presence of the following findings was recorded for each forelimb: distension of the metacarpophalangeal joint capsule, diffuse or localised swelling and/or heat in the metacarpophalangeal region, pain on palpation or on manipulation, and restricted range of passive motion. Subjective and objective (Equinosis Q Lameness Locator®) lameness examinations were performed. For the subjective evaluation a numerical grading system, ranging from 0 to 8 [212], was used. At time 0, lameness evaluation was limited to walking and trotting in a straight line on a hard surface. At times 1-4, distal forelimb flexion tests and gait evaluation on the lunge/led in a circle on soft and hard surfaces, in trot, were also performed if permitted by the horse's behaviour. If a horse showed forelimb lameness at times 1-4, diagnostic anaesthesia was performed to localise the source of pain causing lameness.

5.3 Image acquisition

All diagnostic imaging of both metacarpophalangeal joints was performed in a standing position with the horses sedated using a combination of acepromazine (Vetoquinol, Lure, France) (0.04 mg/kg intramuscularly), romifidine (Boehringer Ingelheim, Ingelheim, Germany) [(0.01 mg/kg intravenously (IV)], detomidine (Orion Pharma, Budapest, Hungary) (0.01 mg/kg IV) and butorphanol (Bioveta, Ivanovice na Hané, Czech Republic) (0.02 mg/kg IV).

A comprehensive radiographic examination of both metacarpophalangeal joints was performed, including standard (LM, dorsal 10° proximal–palmarodistal oblique, dorsal 45° lateral–palmaromedial and dorsal 45° medial–palmarolateral oblique) and additional (LM [flexed], DPa [flexed], dorsal 70° proximal 45° lateral–palmarodistomedial oblique and dorsal 70° proximal 45° medial–palmarodistolateral oblique and dorsoproximal–dorsodistal [flexed] [skyline]) views (Fuji DR-ID1270, Fujifilm Corporation, Tokyo, Japan).

Fan-beam CT examinations of both metacarpophalangeal regions were performed with the horses in a standing position, with the limb extended forward and placed on the couch of a vertical gantry. The CT studies were acquired with a system specifically designed for examining horses while standing (Qalibra CT System, Vet-DICon GmbH, Zossen, Germany), featuring a 16-detector multislice helical scanner with a 90 cm bore diameter (Canon Aquilion LB; Canon Medical Systems Corporation, Otawara, Tochigi, Japan). Each limb was scanned from the distal third of the metacarpal region to at least the junction of the proximal and distal halves of the proximal phalanx. To ensure comparability and consistency, acquisition values affecting HU [213] were identical across all examinations: 135 kV and 350 ms, 300 mm range, 300 mm field of view, 0.5 mm slice thickness and 0.5 s rotation time. Given the system's internal calibration, standardised acquisition protocol, and consistent scanner settings, no external calibration phantom was used during scanning.

Low-field MRI was performed in a 0.27 T open magnet (Hallmarq Veterinary Imaging Ltd., Guildford, UK); T1-weighted and T2*-weighted gradient echo and short-tau inversion recovery sequences in sagittal, frontal and transverse planes, and T2-weighted fast spin echo sequences in transverse planes, were acquired (**Table 1**). All diagnostic imaging acquisitions were performed within 30 hours.

Pulse Sequence	TE (ms)	TR (ms)	Flip Angle (°)	Slice Thickness (mm)	Slice Gap (mm)	Matrix Size (FE × PE)	FOV (mm)
Pilot	7	66	45	7	0	150 × 120	220
Pilot of a pilot	7	66	45	7	0	150 × 120	220
STIR TEST	22	2100	50/60/85/110	4	0.8	256 × 144	200
T1W GRE MI	8	50	55	5	1	170 × 130	170
T2*W GRE MI	13	68	25	5	1	340 × 160	170
T2W FSE FAST	88	1544	90	5	1	168 × 168	170
STIR FSE FAST	22	2336	95	5	1	168 × 168	170

Table 1. Pulse sequence parameters used in a 0.27 T magnet to image the metacarpophalangeal joints. The same parameters were used for sagittal, frontal and transverse sequences. T1W GRE - T1-weighted gradient echo, T2*W GRE - T2*-weighted gradient echo, T2W FSE - T2-weighted fast spin echo, STIR FSE - short-tau inversion recovery fast spin echo, MI - motion insensitive, TE - echo time, ms - milliseconds, TR - repetition time, FE - frequency encoding, PE - phase encoding, FOV - field of view.

5.4 Image analysis

5.4.1 Computed tomographic evaluation of the sagittal ridge

Subjective and objective image analyses were performed by a single assessor (the author of the present thesis). A sagittal plane reconstruction was set transecting the most dorsal and palmar aspects of the SR. In this image, a circle was aligned to the outline of the SR, as precisely fitting as possible. The dorsoproximal and palmaroproximal extents of the SR were connected to the centre of the circle, and the SR was divided into eight radial segments of the same angle. The eight segments were categorized and also pooled in dorsal (1-4) and palmar (5-8) halves (**Figure 1**). The mean HU values of the whole SR, the dorsal and palmar halves and in each segment representing separate ROIs were recorded. Limbs were grouped as right or left in order to investigate any laterality in mean HU values.

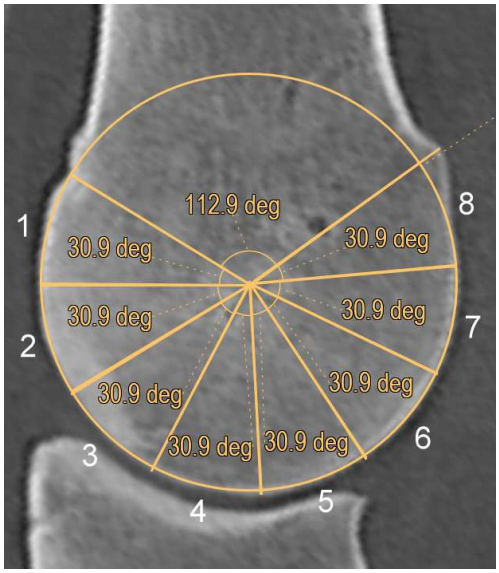

Figure 1. Sagittal CT reconstruction of the SR of McIII (dorsal is to the left) showing the eight radial segments of the SR, in which mean HU values were recorded. The segments were categorized into dorsal (1-4) and palmar (5-8) halves.

The presence, mediolateral location and proximodistal position of hypoattenuating lesions were recorded in each segment. The largest proximodistal and dorsopalmar extents of the hypoattenuating lesions were measured on sagittal plane reconstructions aligned to the lesion (**Figure 2**). The appearance of hypoattenuating lesions on the sagittal plane reconstructions was described as: 1. proximodistally elongated lesions (if the proximodistal extent of the lesion exceeded the dorsopalmar extent), 2. lesions extending towards trabecular bone (if the dorsopalmar extent of the lesion exceeded the proximodistal extent), 3. uneven depressions (a depression in the SCB surface with uneven margins), 4. indentations (a depression in the SCB surface with even margins), 5. subtle lesions (minor hypoattenuation that did not fit the description of any of the categories above) (**Figure 3**).

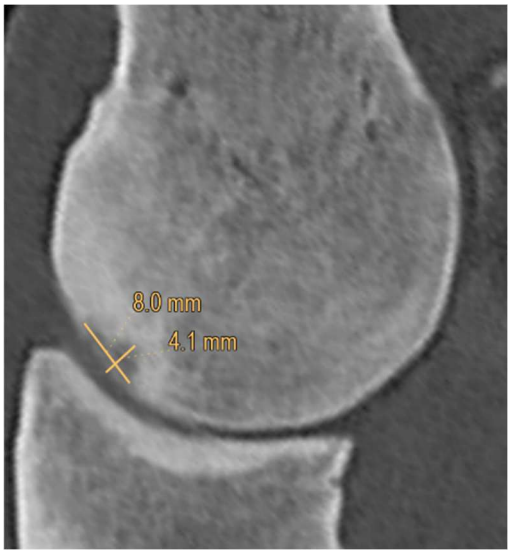

Figure 2. Sagittal CT reconstruction of the SR of McIII (dorsal is to the left) showing measurements of the proximodistal (8.0 mm) and DPa (4.1 mm) extents of a hypoattenuating lesion extending towards trabecular bone. Note the hyperattenuating area surrounding the lesion.

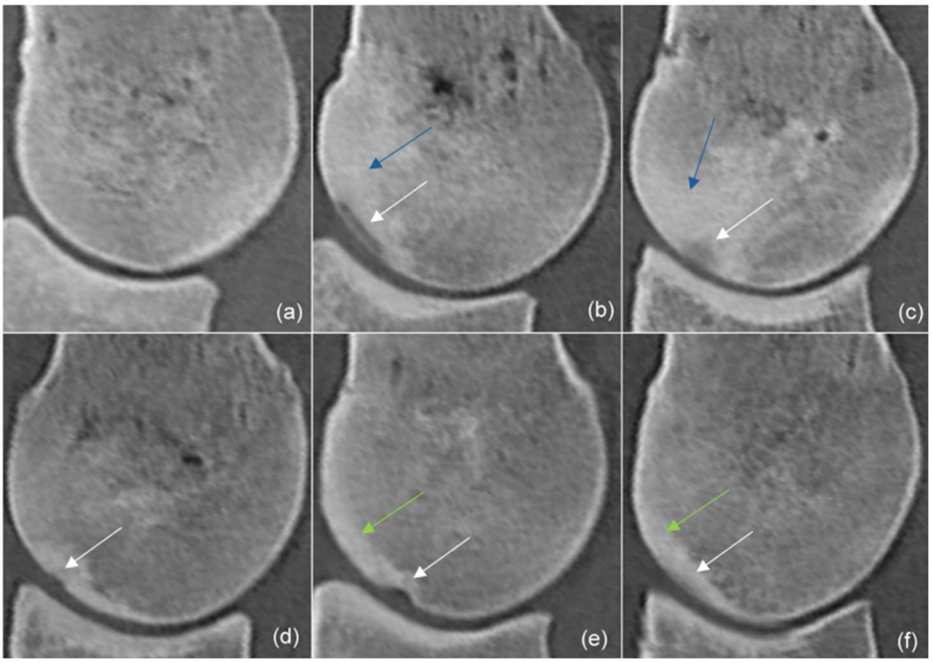

Figure 3. Sagittal CT reconstructions of the SR of McIII (dorsal is to the left): a normal dorsal contour (a) and different shapes of hypoattenuating lesions (white arrows) in the SCB of the SR: proximodistally elongated lesions: the proximodistal extent of the lesion exceeds the DPa extent (b), lesions extending towards trabecular bone: the DPa extent of the lesion exceeds the proximodistal extent (c), uneven depressions: a depression in the SCB surface with uneven margins (d), indentations: a depression in the SCB surface with even margins (e), subtle lesions: minor hypoattenuation that did not fit the description of any of the categories above (f). Note the hyperattenuating area (blue arrow) surrounding the hypoattenuating lesion (b), the cone-shaped hyperattenuation (blue arrow) in the trabecular bone extending from around the hypoattenuating lesion, occupying more than half of the DPa extent of the bone (c), and the thickening of the SCB plate (green arrow) (e, f).

Thickening of the SCB was recorded. The SCB plate was considered thickened if it did not run as an even line parallel to the dorsal outline of the SR (**Figures 3e,f**). The appearance of hyperattenuation in trabecular bone was recorded as being cone-shaped (**Figure 3c**) or patchy. A repeatability study was carried out obtaining all measurements three times on three limbs. Repeated measurements were performed on separate occasions, and the values from each measurement session were recorded separately and were not displayed during subsequent measurements. The coefficient of variance (CV) was calculated using Microsoft Excel (Microsoft Corporation One Microsoft Way, Redmond, WA 98052-6399 USA) with a result of <2% for all variables.

5.4.2 Radiodensity and radiographic appearance of the proximal sesamoid bones

Dorsal 45° lateral–palmaromedial and dorsal 45° medial–palmarolateral oblique radiographic images were assessed subjectively and objectively using a medical viewing software (JiveX DICOM Viewer® Version 5.2, Visus Health IT GmbH, Bochum, Germany). The width of the vascular channels was measured at three points equidistant from each other throughout the whole visible length of each vascular channel. Both PSBs were graded using a system previously developed by Peat et al [104] and modified by the addition of abaxial margin irregularity (**Table 2, Figures 4 and 5**).

Radiological grade	Definition
Grade 0 vascular channels	Any number of vascular channels that are <2 mm wide for at least two-thirds of their visible length
Grade 1 vascular channels	One vascular channel that is ≥2 mm wide for more than one third of its visible length. Any number of vascular channels <2 mm wide
Grade 2 vascular channels	Two vascular channels that are ≥2 mm wide for more than one third of their visible length[a]. Any number of vascular channels <2 mm wide
Grade 3 vascular channels	Three or more vascular channels that are ≥2 mm wide for more than one third of their visible length[b]. Any number of vascular channels <2 mm wide
Abaxial new bone	New bone formation on the abaxial margin of the PSB
Abaxial concavity	A distinct radiolucent concave defect on the abaxial margin of the PSB
Abaxial margin irregularity	Irregular surface of the distal half of the abaxial margin of the PSB

[a]Grade 2 can include one very enlarged vascular channel with a width equivalent to the combined width of two enlarged vascular channels, that is ≥4 mm total width.

[b]Grade 3 can include one or more very enlarged vascular channels with a total width equivalent to the combined width of three enlarged vascular channels, that is ≥6 mm total enlarged channel width.

Table 2. A grading system for each PSB based on the categories used by Peat et al. (2025) for the radiological appearance of vascular channels and other abaxial margin changes. A further category ‘abaxial margin irregularity’ was added.

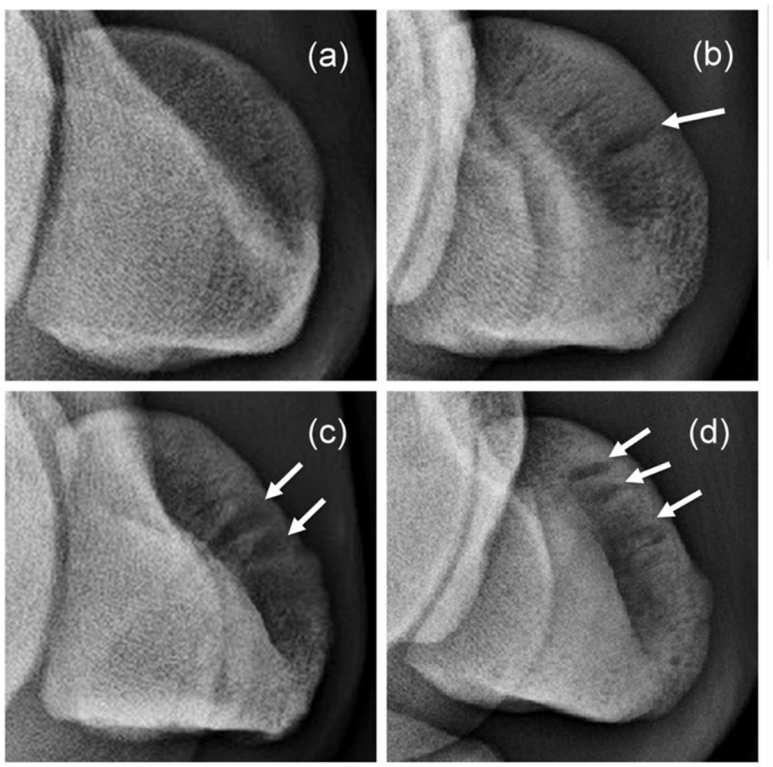

Figure 4. Segments of dorsal 45° lateral-palmaromedial or dorsal 45° medial-palmarolateral oblique radiographic images of the PSBs of the forelimbs of Thoroughbred racehorses. (a) Grade 0 vascular channel appearance: no enlarged vascular channels). (b) Grade 1 vascular channel appearance: one enlarged vascular channel (arrow). (c) Grade 2 vascular channel appearance: two enlarged vascular channels (arrows). (d) Grade 3 vascular channel appearance: three or more enlarged vascular channels (arrows).

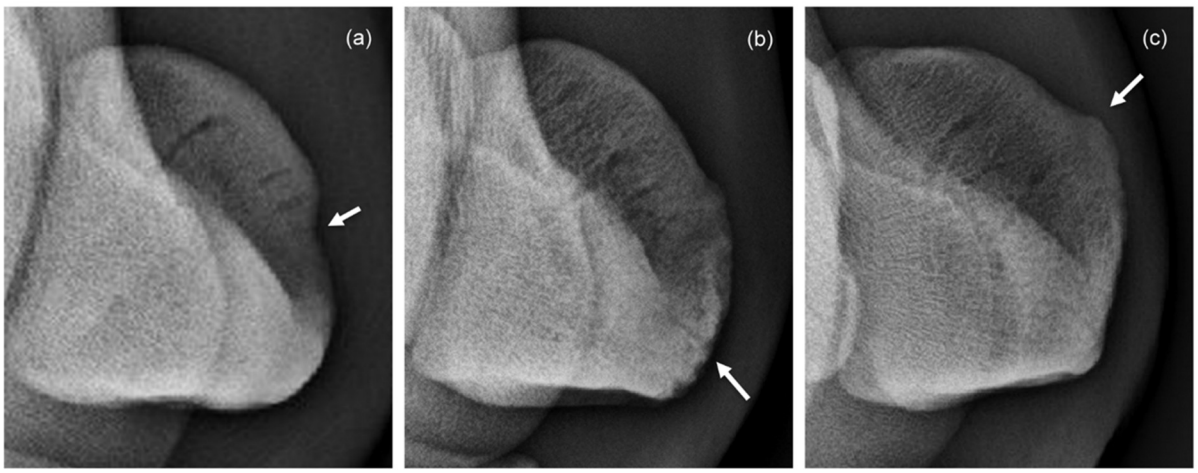

Figure 5. Segments of dorsal 45° lateral-palmaromedial or dorsal 45° medial-palmarolateral oblique radiographic images of the PSBs of the forelimbs of Thoroughbred racehorses

illustrating different types of abaxial margin changes. (a) abaxial margin smoothly marginated concavity (arrow), (b) irregularity of the distal half of the abaxial margin (arrow) and (c) smoothly marginated new bone formation (arrow).

Computed tomographic images were analysed in the image viewing software 3D Slicer (Brigham and Women's Hospital Inc., Boston, Massachusetts, USA) [214]. The PSBs were segmented on a multiplanar reconstruction by putting the threshold limit above 300 HU in order to be able to differentiate between bone and surrounding soft tissues [215]. Total mean HU values of both medial and lateral PSBs were measured. A repeatability study was conducted on the vascular channel width and HU measurements on six PSBs by measuring all values three times. The CV was calculated using Microsoft Excel (Microsoft Corporation) with a result of <0.8% for all variables.

5.4.3 Comparative computed tomographic and magnetic resonance imaging evaluation of metacarpal condylar densification

The greatest extent of hypointensity in the palmar aspect of the metacarpal condyles was measured perpendicular to the articular surface on three sagittal T1-weighted gradient recalled echo MR images (axial, middle and abaxial), the locations of which are illustrated on the transverse pilot images in **Figure 6**. Each condyle was divided into axial (including the PSG), middle and abaxial thirds (**Figure 7**) and the greatest extent of hyperattenuation within each third was measured perpendicular to the articular surface on sagittal CT reconstructions of 2 mm slice thickness. The repeatability of CT measurements was assessed on 12 condyles selected at random from the available dataset. Horses were identified using study-specific identification codes rather than by name. Repeated assessments were performed on separate occasions, and measurement values from each session were recorded separately and were not displayed during subsequent assessments. The repeatability assessment included both repeated selection of the sagittal measurement plane and repeated measurement of densification extent. For each repetition, the appropriate sagittal reconstruction was selected independently and the measurement was repeated using 0.5, 1, 2 and 3 mm reconstructions with slice distance equal to thickness. The CV was calculated using Microsoft Excel (Office 365; Microsoft Corporation, Redmond, Washington, USA). Measurements were obtained by a single assessor.

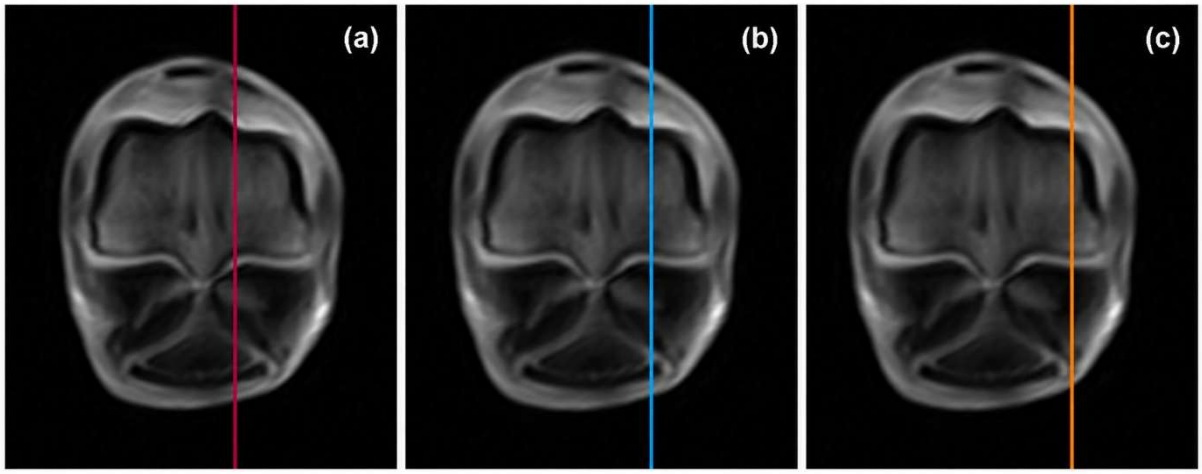

Figure 6. Transverse plane pilot MR images of the left metacarpophalangeal joint of a Thoroughbred racehorse. The coloured lines represent the locations of the sagittal plane images where measurements were acquired in the axial (a), middle (b) and abaxial (c) thirds of the lateral condyle.

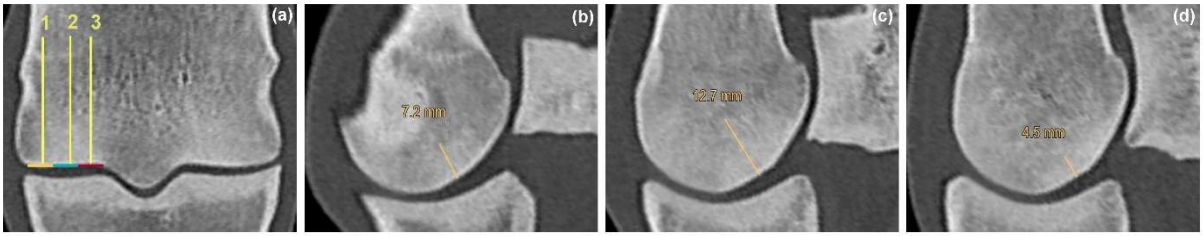

Figure 7. (a) Frontal plane CT reconstruction of the left metacarpophalangeal joint of a Thoroughbred racehorse. Medial is to the right. The yellow vertical lines represent planes for maximal densification measurements in the abaxial (1), middle (2) and axial (3) thirds of the lateral condyle of McIII. The horizontal lines represent the abaxial (orange), middle (blue) and axial (burgundy) thirds. (b-d) Sagittal plane CT reconstructions of the left metacarpophalangeal joint of a Thoroughbred racehorse illustrating maximal linear densification measurements. Dorsal is to the left. The planes of images b, c and d match lines 1, 2 and 3, respectively in (a). The densification measurements are b) 7.2 mm, c) 12.7 mm and d) 4.5 mm.

5.5 Data analysis

Data were collated and stored in a Microsoft Excel (Office 365; Microsoft Corporation) spreadsheet and imported into R Statistical Software (v4.3.1; R Foundation for Statistical Computing. https://www.R-project.org)[216] where all analyses were conducted. The statistical significance was set at $p<0.05$.

5.5.1 Computed tomographic evaluation of the sagittal ridge

Descriptive data analysis was performed on the location, shape and size [median, 95% confidence interval (CI)] of the hypoattenuating lesions of the SR; on the age of horses [(mean, ±standard deviation (SD)]; on the time since previous examination (mean, ±SD); on the sex and training/racing history of horses. A generalized linear mixed effects model [217] was used to investigate the mean HU values calculated separately for the dorsal half (segments 1–4) and palmar half (segments 5–8). To implement this, the lme() function from the nlme package [218, 219] in R was applied. For both dorsal HU values and palmar HU values the fixed factors were time of examinations (0, 1, 2), limb (right, left), sex of the horse (filly, colt), baseline age of the horse, body weight, height at withers and hypoattenuation (yes, no). Additionally, Thoroughbred racehorses were included as random subjects. The differences between the means at each round of examinations were also calculated using the generalized linear mixed effects model mentioned above. Subsequently, adjusted *p*-values were calculated for Tukey's pairwise multiple comparisons. The glht() function of the R multcomp package [220] was used to perform the analysis.

5.5.2 Radiodensity and radiographic appearance of the proximal sesamoid bones

The distribution of continuous variables (HU, age [months], body weight [kg] and height [cm]) was visualised via histograms and formally assessed for normality using the Shapiro–Wilk test. Body weight: height ratio was calculated to take into account the effect of both body weight and height as a single variable. Normally distributed data were summarised as means ±SD) and non-normally distributed and ordinal data (examination time, PSB grade and number of total starts) were described using medians with interquartile range (IQR) and range. Categorical variables (sex [colt, filly, gelding], left or right forelimb, medial or lateral PSB, examination number category, PSB grade category, age category [age in months divided into quartiles], presence of abaxial new bone formation, presence of abaxial margin concavity and presence of irregular abaxial surface on radiographs) were described as proportions (%).

A one-way analysis of variance (ANOVA) with a post-hoc Tukey's test for multiple comparisons was used to initially determine if and at which time points mean HU

measurements differed from each other, assuming in this instance that measurements were not related. A one-way repeated measures ANOVA with post-hoc pairwise paired t-tests could not be carried out because each horse had multiple HU values at each time point (left and right forelimb; lateral and medial PSB) and because a number of horses were lost to follow-up at each subsequent time point, leading to differing numbers of pairs across time points. A multivariable mixed-effects linear regression model was used to examine the association between HU as the outcome and the potential explanatory variables described above. The explanatory variables were included as fixed effects while horse (a unique identifier for each horse) was included as a random effect because data included repeated observations, resulting in a lack of independence between observations belonging to the same horse. Including horse as a random effect deals with this lack of independence by adjusting the model to account for any similarities between observations belonging to the same horse. The model using restricted maximum likelihood (REML) and t-tests based on Satterthwaite's method was fitted using the 'lme4' package [221]. No imputation of missing values was performed. Mixed-effects models were fitted using all available observations. Individual observations with missing values for any variable included in a given model were excluded from that model, while other available observations from the same horse were retained. Univariable mixed-effects linear regression models were used to test the initial association between HU and each explanatory variable individually. Variables where $p < 0.20$ were selected for inclusion in multivariable model building. Multivariable model building was performed using backward elimination by initially including all preselected variables from the univariable models with exclusion of non-significant effects. This was done using the automated step function of the 'lmerTest' package which uses least squares means and their differences for the fixed components of the model to select a final model that best fits the data [222]. To avoid multicollinearity, the relationship between variables likely to be closely correlated (e.g., age and examination number and age and number of total starts) was assessed using Spearman's rank correlation coefficient. Where two variables were highly correlated, the biologically most plausible variable was selected for inclusion in the model.

Multivariable mixed-effects logistic regression models were used to examine the association between the presence of abaxial margin changes (presence of new bone formation, abaxial margin concavity and irregular abaxial surface on radiographs as separate outcomes) and potential explanatory variables. As above, horse was included as a random effect. Initially, univariable mixed-effects logistic regression models were used to test the initial association between the outcomes and each individual explanatory variable. Variables where $p < 0.20$ were selected for inclusion in multivariable model building. Multivariable models were built using manual backward elimination with all preselected variables from univariable

modelling initially included in the model and excluded in a stepwise fashion based on whether they significantly improved model fit using the Wald p-value and lowest Akaike information criterion for guidance. Odds ratios (OR) and corresponding 95% confidence intervals (95% CI) were estimated.

5.5.3 Comparative computed tomographic and magnetic resonance imaging evaluation of metacarpal condylar densification

A body weight:height ratio was calculated to consider the effect of both body weight and height in a single variable. The distribution of continuous variables (all MRI and CT measurements at the location of maximal densification in the axial, middle and abaxial thirds of each condyle, age [months], body weight [kg], height [cm], body weight:height ratio and time since previous examination [days]) was visualised using histograms and formally tested for normality using the Shapiro-Wilk test. Normally distributed data were summarised using mean (±SD) and non-normally distributed and ordinal data (number of total starts) were described using medians with IQR. Categorical variables (sex [colt, filly, gelding], left or right forelimb, medial or lateral condyle, location of maximal densification for both MRI and CT [axial, middle or abaxial third]) were described as frequencies and percentages. For location of maximal densification, when identical measurements of maximal densification were present at more than one site, the observations were recategorised into a mixed category (e.g. middle/abaxial or axial/middle/abaxial).

The correlation between MRI and CT measurements in each condyle third were assessed using Spearman's rank correlation coefficient rho (ρ) and the strength of correlation was interpreted according to Chan, 2003 (poor: $\rho<0.3$; fair: $0.3\leq\rho<0.5$; moderate: $0.5\leq\rho<0.8$; strong: $\rho\geq0.8$) [223]. The Wilcoxon signed-rank test was used to compare MRI and CT measurements at the location of maximal densification for both pooled data and for data at each examination time point. For data at each time point, both the raw (unadjusted) p-value as well as the p-values adjusted using the Bonferroni correction (raw/unadjusted p-value multiplied by five) were estimated. The Kruskal-Wallis test (with a post-hoc Dunn's test where variables had more than two categories) was used to assess initial associations between MRI and CT measurements at the location of maximal densification and other variables of interest (including sex, right or left limb and lateral or medial condyle) at each time point. As above, both unadjusted and adjusted p-values were estimated.

Two multivariable mixed-effects linear regression models were used to examine the association between MRI and CT measurements at the location of maximal densification as two individual outcomes and the potential explanatory variables described above. The explanatory variables were included in the models as fixed effects, while the unique identifier

for each horse was included as a random effect. This is because data included repeated observations per horse, resulting in a lack of independence between observations belonging to the same horse. Including horse as a random effect adjusts the model to account for similarities between observations belonging to the same horse. The models were fitted using REML and t-tests based on Satterthwaite's method via the 'lme4' package [221]. Initially, univariable mixed-effects linear regression models were used to test the association between MRI and CT measurements and each explanatory variable individually. Variables with statistical significance of $p<0.20$ were selected for inclusion in multivariable model building. Backward elimination was used in the multivariable model building process by initially including all preselected variables from the univariable models and exclusion of non-significant effects. This was done using the automated *step* function of the 'lmerTest' package by using least squares means and their differences for the fixed components of the model to select the final best fitting models for the data [222]. The models were also checked manually to ensure that included variables and the direction of association made sense. To avoid multicollinearity, where two variables were strongly correlated (Spearman's $\rho \geq 0.80$), the biologically most plausible variable was selected for inclusion in the model (e.g., number of starts rather than age). Although the raw outcome data for MRI and CT measurements were not normally distributed, inspection of the residuals of the final models revealed an approximately normal distribution. Transformation of the outcome variables did not yield an improvement of raw data or residual normality, thus the mixed-effects linear regression models were considered robust and appropriate to be fitted.

6. Results

6.1 Horses

A total of 40 Thoroughbred yearlings (26 colts and 14 fillies) from 10 racehorse trainers were included at time 0. Signalment of horses at each examination is shown in **Table 3**. By time 4, 32 horses were lost to follow up. Fourteen were lost because of lack of long-term trainer/owner compliance (only one has not raced successfully following attrition), five did not undergo further training following time 0, 11 were retired, and two horses died due to causes unrelated to musculoskeletal injuries. Prior to the initial examination, 27/40 (67.5%) horses had been engaged in some form of training: 26 were exercised in trot (up to 30 min a day and up to seven times a week) and one also in canter (for four weeks). No horse had carried out any fast work. At time 1, 31 horses were examined. Nine horses had been trained in canter without any fast work and 22 horses had been engaged in fast speed training. Three fillies had raced once. At time 2, 23 horses were examined. Preceding this, 19/23 (82.6%) horses had raced (once n=4, twice n=6, three times n=6, and four times, n=3). Fillies had a significantly higher number of starts compared with colts (p=0.003). Two horses were trained in canter without any fast work and 21 horses were engaged in fast work training prior to time 2. By times 3 and 4 all participating horses were in active racehorse training including fast work and had already raced at least once.

		Time 0 (n=40)	Time 1 (n=31)	Time 2 (n=23)	Time 3 (n=13)	Time 4 (n=8)
Sex	**Colt**	26 (65.0%)	19 (61.3%)	12 (52.2%)	7 (53.8%)	3 (37.5%)
	Filly	14 (35.0%)	12 (38.7%)	8 (34.8%)	5 (38.5%)	2 (25.0%)
	Gelding	0 (0.0%)	0 (0.0%)	3 (13.0%)	1 (7.7%)	3 (37.5%)
Time since previous examination (days)	**Median**	-	194	198	213	175
	IQR and range	-	182.0, 202.5 168.0, 237.0	194.5, 203.5 171.0, 253.0	183.0, 217.0 154.0, 238.0	167.0, 203.5 160.0, 226.0
Age (months)	**Median**	20.0	26.0	33.0	38.0	45.0
	IQR and range	19.0, 20.3 17.0, 22.0	25.0, 27.0 23.0, 29.0	31.5, 33.0 29.0, 35.0	37.0, 39.0 36.0, 41.0	42.8, 45.3 41.0, 47.0
Body weight (kg)	**Median**	440.0	458.0	460.0	440.0	450.0
	IQR and range	403.8, 461.3 365.0, 490.0	420.0, 475.5 370.0, 518.0	421.0, 485.0 380.0, 540.0	430.0, 453.0 355.0, 490.0	447.5, 487.0 430.0, 500.0

Height (cm)	**Median**	155.0	156.0	158.0	158.0	159.5
	IQR and range	151.8, 157.0 148.0, 162.0	154.5, 160.0 151.0, 165.0	155.5, 161.0 152.0, 166.0	156.0, 160.0 154.0, 171.0	158.5, 160.5 154.0, 172.0
Body weight:height ratio	**Median**	2.8	2.9	2.9	2.8	2.9
	IQR and range	2.6, 2.9 2.4, 3.1	2.7, 3.0 2.4, 3.3	2.7, 3.1 2.5, 3.3	2.7, 2.9 2.3, 3.0	2.8, 3.0 2.6, 3.1

n— number of horses

Table 3. Signalment of 40 Thoroughbred racehorses which entered training, 31, 23, 13 and 8 of which were re-examined, respectively, at intervals of approximately six months.

6.1.1 Lameness at follow-up examinations and responses to diagnostic anaesthesia

At times 1, 3 and 4, three horses at each of these time points exhibited forelimb lameness. Lameness was abolished either by palmar digital blocks (*n*=5 limbs), or abaxial sesamoid blocks (*n*=1 limb); or by low four-point blocks (*n*=4 limbs). At time 2 no overt forelimb lameness was seen in any horse. Objective baseline lameness evaluation data, diagnostic anaesthesia findings and fetlock-related versus non-fetlock-related classification are provided in **Supplementary item 1** for horses that underwent diagnostic anaesthesia.

6.2 Computed tomographic evaluation of the sagittal ridge

6.2.1 Hounsfield Unit measurements

Observed mean (± SD) HU values of the dorsal half of the SR were 914.5 ± 92.2 HU at time 0, 998.1 ± 84.7 HU at time 1 and 999.8 ± 81.0 HU at time 2. Corresponding values for the palmar half were 741.9 ± 74.4 HU, 806.0 ± 80.9 HU and 813.1 ± 86.9 HU, respectively. Mean HU values at time 1 were significantly higher in both the dorsal (p<0.001) and palmar (p<0.001) halves of the SR than those measured at time 0 (**Table 4**). There was no significant difference between mean HU values of the dorsal (p=0.789) and palmar (p=0.853) halves measured at times 1 and 2. The mean HU value of the dorsal half of the SR was significantly higher than the mean for the palmar half (p=0.023). Mean HU values of the dorsal half were significantly higher in right forelimbs than in left forelimbs (p<0.001). Mean HU values of the dorsal half of fillies were significantly higher than mean HU values of the dorsal half of colts (p=0.037). There were no significant differences in mean HU values between the right and left forelimbs (p=0.082) and between colts and fillies in the palmar half (p=0.085).

	Mean HU dorsal			Mean HU palmar		
	Estimate	**95% CI**	**p-value**	**Estimate**	**95% CI**	**p-value**
Time 1 versus time 0	70.4	(48.9, 92.0)	<0.001*	59.7	(41.9, 77.4)	<0.001*
Time 2 versus time 0	63.7	(35.5, 91.9)	<0.001*	64.2	(40.8, 87.6)	<0.001*
Time 2 versus time 1	-6.7	(-30.9, 17.4)	0.789	4.5	(-15.3, 24.4)	0.853

Table 4. Model adjusted estimates and 95% confidence intervals for the difference in mean HU values between times of examination (initial = 0; first re-examination = time 1; second re-examination = time 2). P-values are adjusted for Tukey's multiple comparisons. There was a significant increase in the mean dorsal HU values for times 1 and 2 compared with time 0. The mean difference between times 1 and 2 was not significant. Similar results were also seen for the palmar HU values.

6.2.2 Hypoattenuating lesions

A hypoattenuating lesion in the SCB of the SR was identified in 33/80 (41.3%) limbs at time 0; in 14 horses bilaterally (**Table 5**). At time 1, a hypoattenuating lesion was identified in 22/62 (35.5%) limbs; in eight horses bilaterally. No new lesions, that could not be detected at time 0, were identified. At time 2, a hypoattenuating lesion was seen in 14/46 (30.4%) limbs; in five horses bilaterally. No new lesions that had not been detected at time 1 were identified. In horses with ≥2 examinations, in six limbs of four horses, the hypoattenuating lesion was no longer present at time 1; at time 2, the hypoattenuating lesion was not identifiable in a further five limbs of four horses (**Figure 8**). During the study period, no progression in the size of any of the lesions was detected.

		Time 0 (n=80)	**Time 1 (n=62)**	**Time 2 (n=46)**
Proximodistal extent (mm)	Median	5.3	4.3	4.0
	95% CI	4.3-11.7	3.6-12.3	2.9-14.5
DPa extent (mm)	Median	2.1	1.7	2.1
	95% CI	0.7-1.9	0.5-1.6	0.5-2.5

Shape			
Proximodistally elongated	12	6	5
Extending towards trabecular bone	16	10	5
Depression	1	1	1
Indentation	2	1	1
Subtle	2	4	2

Table 5. Proximodistal and DPa extents and the shape of hypoattenuating lesions in the SR of McIII in Thoroughbred racehorses measured at three subsequent CT examinations at intervals of approximately six months. n – number of limbs.

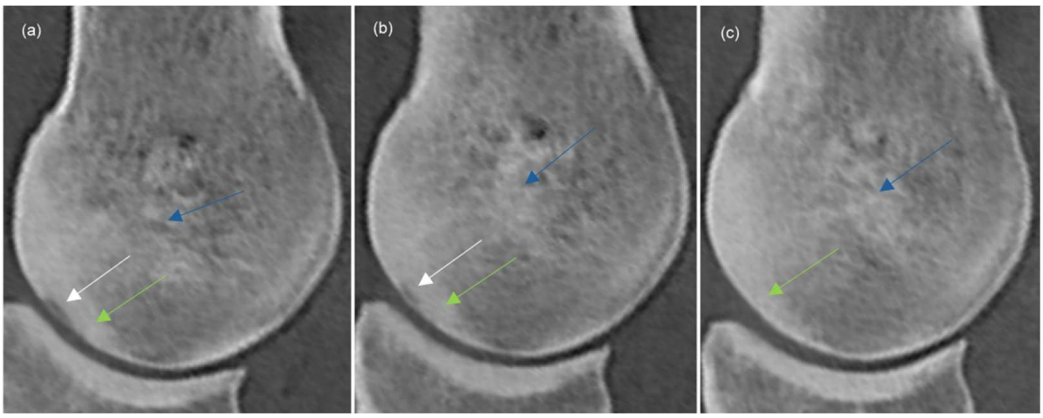

Figure 8. Sagittal CT reconstructions of the SR of McIII (dorsal is to the left) of the same metacarpophalangeal joint showing a hypoattenuating lesion (white arrows) in the SCB of the SR detected at the initial examination, time 0 (a) that decreased in size at the first re-examination (time 1) (b) and was no longer detectable at the second re-examination (time 2) (c). Note the thickening of the SCB plate (green arrows) (a, b, c) and patchy hyperattenuation in the trabecular bone (blue arrows) (a, b, c).

All hypoattenuating lesions were located in the dorsodistal aspect of the SR. Only the second, third and fourth segments of the SR were involved. At time 0, 18/33 (54.5%) lesions affected only the third segment, 1/33 (3.0%) lesion was only in the fourth segment, 9/33 (27.3%) lesions were present in both the second and third segments, 4/33 (12.1%) lesions were present in both the third and fourth segments, and 1/33 (3.0%) lesion involved all three segments. At time 1, 16/22 (72.7%) lesions affected only the third segment, 4/22 (18.2%) lesions were present in both the second and third segments, and 2/22 (9.1%) lesions were in both the third and fourth segments. At time 2, 8/14 (57.1%) lesions affected only the third

segment, 4/14 (28.6%) lesions were present in both the second and third segments, and 2/14 (14.3%) lesions involved both the third and fourth segments. At time 0, in 21/33 (63.6%) limbs the hypoattenuating lesion was located in the axial region of the SR, in 10/33 (30.3%) limbs in the lateral aspect and in 2/33 (6.1%) limbs in the medial aspect of the SR. Of the lesions that resolved over time (n = 11), seven were located in the axial region of the SR, three in the lateral aspect and one in the medial. The two most common shapes were proximodistally elongated hypoattenuating lesions and hypoattenuating lesions extending towards the trabecular bone.

6.2.3 Subchondral bone plate thickening, trabecular bone hyperattenuation

Thickening of the dorsal SCB plate of the SR was detected in 74/80 (92.5%) limbs at time 0, in 60/62 (96.8%) limbs at time 1 and in 45/46 (97.8%) limbs at time 2. Hyperattenuation in trabecular bone was detected with and without simultaneous presence of a hypoattenuating lesion in the SCB. Cone-shaped hyperattenuation was present in 5/80 (6.3%) limbs at time 0, in 7/62 (11.3%) limbs at time 1 and in 5/46 (10.1%) limbs at time 2. Hypoattenuating lesions surrounded by cone-shaped hyperattenuating zones had not resolved by the end of the study period. Patchy hyperattenuation in the trabecular bone was detected in 14/80 (17.5%) limbs at time 0, in 21/62 (33.8%) limbs at time 1 and in 24/46 (52.2%) limbs at time 2.

6.3 Radiodensity and radiographic appearance of the proximal sesamoid bones

6.3.1 Hounsfield Unit measurements

Assuming independence of HU values, a one-way ANOVA revealed an initial significant effect of examination time on mean HU value (F=43.98, p<0.001). Pairwise comparisons found mean HU differed between all time points (p<0.004) except for between times 1 and 4 (p=0.7), 1 and 2 (p>0.9) and 2 and 4 (p=0.7). Mean HU was lowest at baseline (time 0, 1064.0 ± 65.1) and highest at time 3 (1194.5 ± 78.6), after which mean HU decreased, but not below baseline (time 4, 1109.4 ± 77.2) (**Table 6 and Figure 9**). Times 0 and 3 were also the only time points that significantly differed from all others.

Pairwise comparison between examination time points	Difference in means	95% confidence interval of difference	Tukey's adjusted p-value
0 and 1	-62.28	-83,92, -40.63	<0.001
0 and 2	-62.72	-86.39, 39.04	<0.001
0 and 3	-130.50	-159.38, -101.62	<0.001

0 and 4	-45.41	-80.44, -10.37	0.004
1 and 2	-0.44	-25.33, 24.45	1.000
1 and 3	-68.22	-98.11, -38.33	<0.001
1 and 4	16.87	-19.00, 52.74	0.699
2 and 3	-67.78	-99.17, -36.39	<0.001
2 and 4	17.31	-19.82, 54.44	0.706
3 and 4	85.09	44.44, 125.74	<0.001

Table 6. Pairwise comparisons between total mean HU values measured in the PSBs in the metacarpophalangeal joints of Thoroughbred racehorses that were first examined as yearlings (time 0, n=40) and then four more times, at approximately six months' intervals (time 1 n=31, time 2 n=23, time 3 n=13, time 4 n=8).

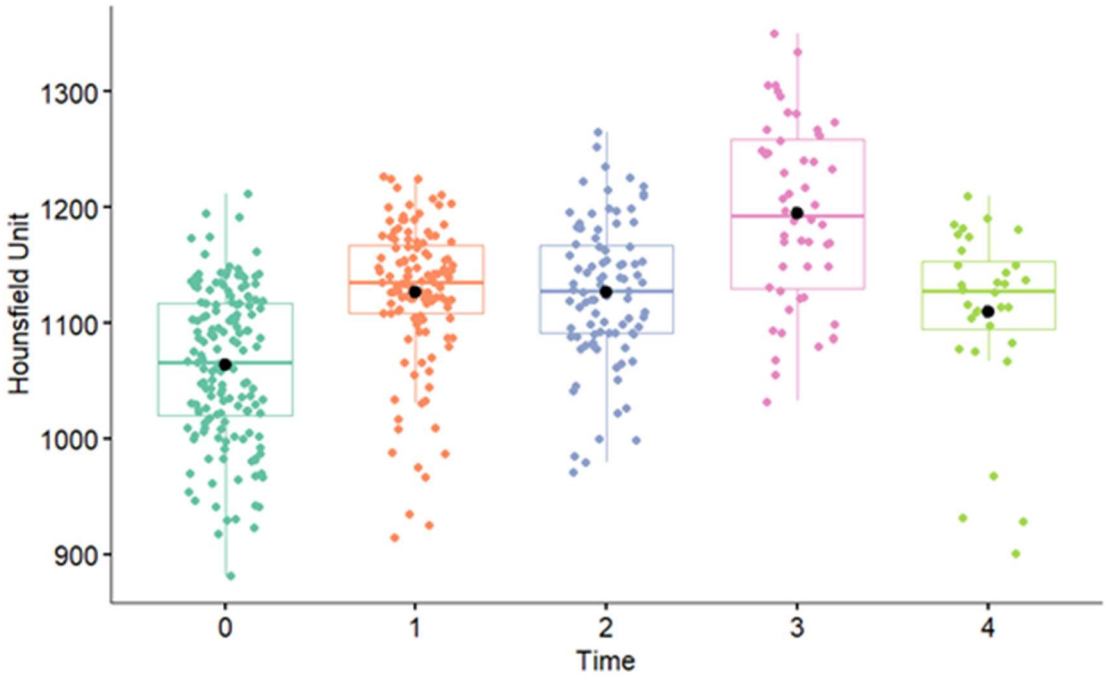

Figure 9. Distribution of total mean HU measurements in the PSBs in the metacarpophalangeal joints of Thoroughbred racehorses that were first examined as yearlings (time 0, n=40) and then four more times, at approximately six months' intervals (time 1 n=31, time 2 n=23, time 3 n=13, time 4 n=8). Boxes represent the median and IQR, whiskers the range, the black circles the mean and coloured circles the individual data points including outliers. The four lower outliers at time 4 belong to the same horse that had a period of eight weeks' rest and was gradually reintroduced to light training prior to time 4.

Univariable models of the association between HU and explanatory variables are presented in **Supplementary item 2**. It was decided that including the number of total starts would be most biologically plausible because it would show the effects of exercise on HU. Body weight: height ratio replaced individual body weight and height variables because both body weight and height were strongly associated with HU (p<0.001) and also moderately correlated with each other (Spearman's rho = 0.50, p<0.001).

The final multivariable model of variables associated with HU as the main outcome is presented in **Table 7**. Increasing HU measurements were associated with an increasing number of total starts (**Figure 10**), an increasing body weight: height ratio, and HU was higher in medial vs. lateral PSBs. For each additional start, the total mean HU increased by 6.1 (p<0.001); for each unit increase in body weight: height ratio, the total mean HU increased by 119.0 (p<0.001). The total mean HU was higher in the medial than in the lateral PSB (p=0.01).

Variable	Estimate	Standard error	t-value	p-value
Number of total starts	6.10	0.79	7.71	<0.001
Body weight:height ratio	119.03	22.16	5.37	<0.001
Medial or lateral PSB				
Lateral	Reference			
Medial	11.55	4.54	2.55	0.01

Table 7. The final multivariable mixed-effects linear regression model of variables associated with HU as the main outcome, with horse as a random effect, using data from Thoroughbred racehorses that were first examined as yearlings (time 0, n=40) and then four more times, at approximately six months' intervals (time 1 n=31, time 2 n=23, time 3 n=13, time 4 n=8). Estimate is the change in total mean HU for each additional start, for each unit increase in body weight:height ratio and comparing the medial and lateral PSB.

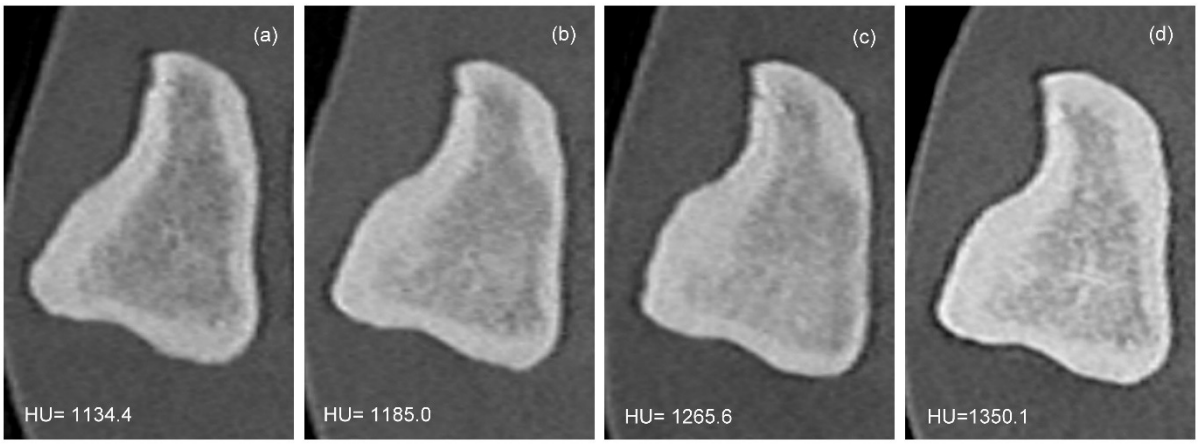

Figure 10. Frontal plane CT reconstructions of the same medial PSB (medial is to the left) of the right forelimb of a Thoroughbred racehorse acquired at four sequential examinations approximately six months apart, showing an increase in total mean HU values. (a) time 0, 1134.4 HU; (b) time 1, 1185.0 HU; (c) time 2, 1265.6 HU; (d) time 3, 1350.1 HU.

6.3.2 Abaxial margin changes

Univariable models of the association between abaxial margin changes and explanatory variables are presented in **Supplementary item 3**. For the analysis of abaxial margin changes, age was selected rather than examination number or number of total starts because these radiographic features were considered more likely to reflect developmental or maturational changes than cumulative racing exposure. In contrast to the previously selected number of total starts for the HU model, as PSB radiodensity was hypothesised to be more directly related to cumulative exercise exposure.

The final multivariable models of variables associated with abaxial margin changes as the main individual outcomes are presented in **Table 8**. Presence of new bone formation was associated with higher PSB grades, with the odds being >20 as likely in PSB grade 3 versus grade 0 (p=0.004). The odds of detecting new bone formation were higher for the lateral PSB compared with the medial PSB (p=0.04). The odds of detecting abaxial margin concavity decreased with increasing age (p=0.01) (**Figure 11**), but were higher for the medial PSB compared with the lateral PSB (p=0.03) and in the left forelimb compared with the right forelimb (p=0.03). The odds of detecting irregularity of the abaxial margin surface also decreased with increasing age (p=0.02) (**Figure 12**) but were higher in the medial PSB compared with the lateral PSB (p<0.001).

Outcome – Presence of new bone formation						
Variable	**Estimate**	**Standard error**	**Z-value**	**OR**	**95% CI**	**P-value**
PSB grade category						
0	Reference					
1	0.79	1.28	0.62	2.19	0.18, 26.71	0.538
2	0.23	1.37	0.16	1.25	0.08, 18.55	0.87
3	3.05	1.07	2.86	21.16	2.61, 171.82	0.004
Medial or lateral PSB						
Medial	Reference					
Lateral	1.16	0.56	2.06	3.18	1.06, 9.53	0.039
Outcome – Presence of abaxial margin concavity						
Variable	**Estimate**	**Standard Error**	**Z-value**	**OR**	**95% CI**	**P-value**
Age (months)	-0.25	0.1	-2.57	0.78	0.65, 0.94	0.01
Limb laterality						
Right fore	Reference					
Left fore	1.99	0.92	2.17	7.32	1.21, 44.15	0.03
Medial or lateral PSB						
Lateral	Reference					
Medial	1.99	0.92	2.17	7.32	1.21, 44.15	0.03
Outcome – Presence of irregular abaxial surface on radiographs						
Age (months)	-0.08	0.03	-2.36	0.93	0.87, 0.99	0.018
Medial or lateral PSB						
Lateral	Reference					
Medial	1.66	0.43	3.82	5.24	2.24, 12.28	<0.001

Table 8. The final multivariable mixed-effects logistic regression model of variables associated with three abaxial margin changes of the PSB as the main individual outcomes, with horse as a random effect, using data from Thoroughbred racehorses that were first examined as yearlings (time 0, n=40) and then four more times, at approximately six months' intervals (time 1 n=31, time 2 n=23, time 3 n=13, time 4 n=8).

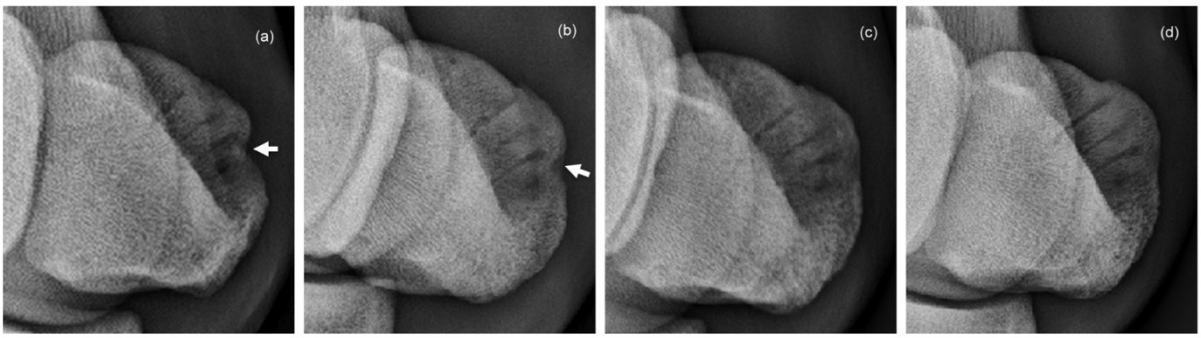

Figure 11. Segments of dorsal 45° medial–palmarolateral oblique radiographs highlighting the medial PSB of the left forelimb of a Thoroughbred racehorse, acquired at four sequential examinations approximately six months apart. There is a concavity of the abaxial margin (arrows) detected at time 0 (a), which became shallower at time 1 (b) and was undetectable at times 2 (c) and 3(d). Note the radiating radiolucent zones indicating vascular channels in the PSBs. The PSBs were graded 1, 1, 2 and 2 at times 0,1, 2 and 3, respectively.

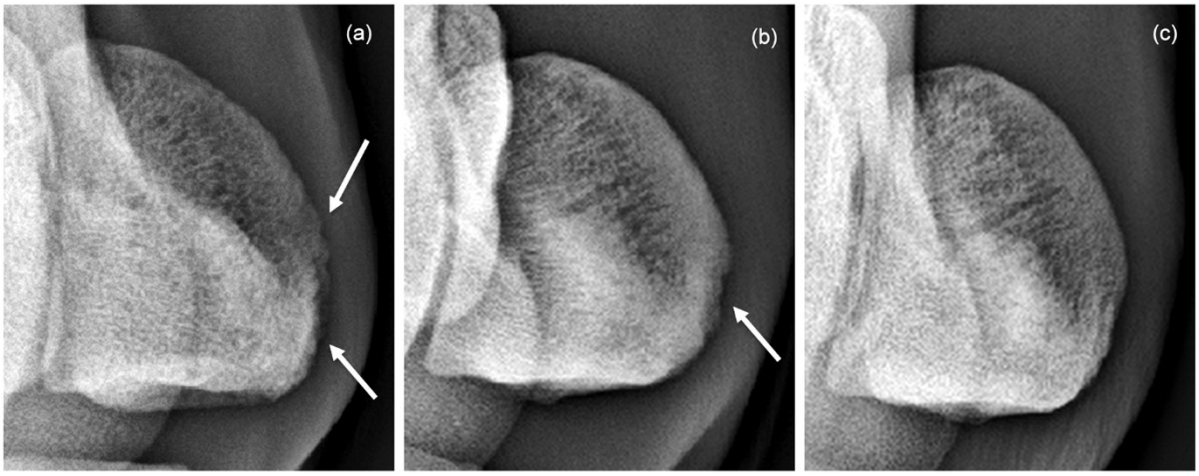

Figure 12. Segments of dorsal 45° medial–palmarolateral oblique radiographs highlighting the medial PSB of the right forelimb of a Thoroughbred racehorse, acquired at three sequential examinations approximately six months apart. The abaxial margin irregularity (arrows) detected at time 0 (a) was reduced in proximodistal length at time 1 (b) and by time 2 (c) the surface of the abaxial margin was smooth. The PSBs were graded 0 at all three times.

6.3.3 Proximal sesamoid bone grades

Frequency of PSB grades was described as proportions (%) throughout the five rounds of examinations (**Table 9**). The observed frequency of grade 0 and grade 3 PSBs increased, and grade 1 and grade 2 decreased from time 0 to time 4.

	Time 0 (n=160)		Time 1 (n=124)		Time 2 (n=92)		Time 3 (n=52)		Time 4 (n=32)	
	n	%	n	%	n	%	N	%	n	%
Grade 0	125	78.1	108	87.1	78	84.4	47	90.4	30	93.8
Grade 1	19	11.9	9	7.3	7	7.6	1	1.9	1	3.1
Grade 2	12	9.6	4	3.7	1	1.3	1	1.9	0	0.0
Grade 3	4	2.5	3	2.4	6	6.5	3	5.8	1	3.1

n – number of proximal sesamoid bones. % - percentage.

Table 9. Distribution of the radiological grades of the medial and lateral PSBs from the left and right forelimbs of 40 Thoroughbred racehorses examined at time 0 and four sequential examinations (31, 23, 13 and 8 horses, respectively) at intervals of approximately six months.

6.4 Comparative computed tomographic and magnetic resonance imaging evaluation of metacarpal condylar densification

6.4.1 Horses

At time 0, in one colt it was not possible to acquire MR images due to lack of cooperation and excessive motion. Therefore, a total of 39 Thoroughbred yearlings (25 colts and 14 fillies) were included. In some horses, slight change in limb position compared with the pilot scan, meant that fewer than three MRI slices per condyle could be obtained. A total of 17 condyles from 16 horses with missing MRI observations were removed from the statistical analysis. In total 438 (time 0: 146, time 1: 123, time 2: 90, time 3: 50, time 4: 29) complete condyles were analysed.

6.4.2 Repeatability analysis

Repeatability of CT measurements was best using 2 mm thick slices (CV: 7.6%). Measurements on different slice thicknesses resulted in poorer repeatability: CV of 10.8% for 0.5 mm, 12.2% for 1 mm and 10.4% for 3 mm thick slices. Consequently, subsequent image analysis was performed on 2 mm slice thickness.

6.4.3 Location of maximal densification

Regardless of imaging modality and examination round, the middle third of the condyle was the site of maximal densification in most condyles. Distribution of the greatest extent of densification within each third of the condyles is presented in **Table 10.**

	Time 0 (n=146)		**Time 1 (n=123)**		**Time 2 (n=90)**		**Time 3 (n=50)**		**Time 4 (n=29)**	
MRI maximal location										
	n	**%**	**n**	**%**	**n**	**%**	**n**	**%**	**n**	**%**
Abaxial	18	12.3	13	1.06	8	8.9	4	8.0	3	10.3
Axial	42	28.8	28	22.8	23	25.6	16	32.0	7	24.1
Axial/abaxial	0	0.0	0	0.0	0	0.0	0	0.0	1	3.4
Axial/middle	1	0.7	2	1.6	1	1.1	1	2.0	0	0.0
Axial/middle/abaxial	1	0.7	0	0.0	0	0.0	0	0.0	0	0.0
Middle	82	56.2	80	65.0	58	64.4	29	58.0	18	62.1
Middle/abaxial	2	1.4	0	0.0	0	0.0	0	0.0	0	0.0
CT maximal location										
	n	**%**	**n**	**%**	**n**	**%**	**n**	**%**	**n**	**%**
Abaxial	6	4.1	2	1.6	0	0.0	0	0.0	2	6.9
Axial	44	30.1	18	14.6	11	12.2	1	2.0	3	10.3
Axial/middle	2	1.4	0	0.0	0	0.0	0	0.0	1	3.4
Middle	94	64.4	103	83.7	79	87.8	49	98.0	23	79.3

n – number of condyles

Table 10: Distribution of the location of maximal densification in the metacarpal condyles of 39 Thoroughbred racehorses which entered training, 31, 23, 13 and 8 of which were re-examined, respectively, at intervals of approximately six months (times 1-4). The axial, middle, and abaxial thirds of the condyles were distinguished. Where two or three locations are indicated separated by a slash (/), identical values were measured at those locations.

Considering horses with at least one follow-up examination, at time 0 the site of maximum densification was axial or abaxial in 49 and 42 condyles on MR and CT images, respectively. However, of these, at the time of the final examination, maximum densification was in the middle third of the condyle in 22/49 (44.9%) on MR images and 33/42 (78.6%) on CT images.

6.4.4 Correlation between magnetic resonance imaging and computed tomographic measurements

There was a moderate positive correlation between maximal MRI and CT measurements for each condyle (Spearman's $\rho=0.69$, $p<0.001$) and in the middle one-third of each condyle (Spearman's $\rho=0.69$, $p<0.001$). There was fair positive correlation in the axial (Spearman's $\rho=0.31$, $p<0.001$) and abaxial (Spearman's $\rho=0.46$, $p<0.001$) thirds of each condyle.

6.4.5 Differences between magnetic resonance imaging and computed tomographic measurements

There was a significant difference between maximal MRI and CT measurements for each condyle and in all thirds, with CT values being consistently higher. This difference was observed in both the pooled dataset and in analyses performed at each time point. Differences between MRI and CT measurements are shown in **Table 11.** A significant difference between MRI and CT values was not detected in the abaxial third at times 0-3 and the axial third at times 3 and 4.

Pooled (n=438)	**Whole condyle**		**Axial third**		**Middle third**		**Abaxial third**	
	MRI	**CT**	**MRI**	**CT**	**MRI**	**CT**	**MRI**	**CT**
Median (mm)	4.7	8.1	3.7	5.0	4.5	8.1	3.1	3.5
IQR (mm)	3.6, 6.6	6.0, 10.1	2.8, 5.2	4.1, 6.4	3.3, 6.5	5.7, 10.1	2.2, 4.1	2.4, 4.8

P-value	<0.001		<0.001		<0.001		0.006	
Time 0 (n=146)								
Median (mm)	3.6	5.9	3.0	4.4	3.4	5.7	2.3	2.6
IQR (mm)	3.0, 4.5	4.7, 7.5	2.3, 3.7	3.7, 5.4	2.7, 4.4	4.0, 7.5	2.0, 3.1	1.6, 3.8
Unadjusted p-value	<0.001		<0.001		<0.001		0.119	
Adjusted p-value	<0.001		<0.001		<0.001		0.595	
Time 1 (n=123)								
Median (mm)	5.0	8.4	4.1	5.0	5.0	8.4	3.3	3.5
IQR (mm)	3.8, 7.2	6.9, 10.2	3.0, 5.4	4.1, 6.5	3.6, 6.7	6.6, 10.2	2.5, 4.3	2.6, 4.6
Unadjusted p-value	<0.001		<0.001		<0.001		0.482	
Adjusted p-value	<0.001		0.003		<0.001		1.000	
Time 2 (n=90)								
Median (mm)	5.8	9.1	4.2	5.6	5.7	9.1	3.5	4.2
IQR (mm)	4.4, 7.3	8.2, 10.6	3.2, 5.8	4.7, 6.9	4.2, 7.0	8.2, 10.6	2.8, 4.6	3.0, 5.2
Unadjusted p-value	<0.001		<0.001		<0.001		0.022	
Adjusted p-value	<0.001		0.001		<0.001		0.112	
Time 3 (n=50)								
Median (mm)	6.9	10.4	5.3	5.8	6.3	10.4	4.1	5.0
IQR (mm)	5.1, 9.5	8.4, 12.8	3.8, 7.1	4.8, 7.8	4.9, 9.5	8.4, 12.8	3.3, 5.8	3.5, 6.2
Unadjusted p-value	0.005		0.340		<0.001		0.169	
Adjusted p-value	0.026		1.000		0.001		0.845	
Time 4 (n=29)								
Median (mm)	5.3	10.0	4.0	4.8	5.0	10.0	3.2	4.3
IQR (mm)	3.6, 6.8	8.1, 11.7	3.2, 5.4	4.4, 6.0	3.1, 6.8	7.7, 11.7	1.9, 4.2	2.8, 5.5
Unadjusted p-value	<0.001		0.027		<0.001		0.009	
Adjusted p-value	<0.001		0.134		<0.001		0.043	

n – number of condyles, p-value – Wilcoxon signed-rank test p-value, adjusted p-value – Bonferroni correction for multiple pair-wise comparisons.

Table 11. Differences between MRI and CT measurements of maximal densification in the metacarpal condyles of 39 Thoroughbred racehorses which entered training, 31, 23, 13 and 8 of which were re-examined, respectively, at intervals of approximately six months.

6.4.6 Association between magnetic resonance imaging and computed tomographic measurements and other variables

There was no association between sex, limb (left/right) and whole condyle MRI/CT maximal measurements at any of the time points. Whole condyle maximal MRI measurements were significantly higher in the lateral condyle compared to the medial only at time 4 (p=0.045). However, this association was not retained when the p-value was adjusted for multiple pairwise comparisons (p=0.223).

Univariable models of the association between MRI measurements and explanatory variables are presented in **Supplementary item 4.** Age and number of total starts were strongly positively correlated (Spearman's ρ=0.83, p<0.001). It was decided that including the total number of starts rather than age in the multivariable model would be most biologically plausible because it would model the effects of exercise on densification. Body weight:height ratio replaced individual body weight and height variables in the multivariable model because both body weight and height were strongly associated with extent of densification (p<0.001) and moderately correlated with each other (Spearman's ρ=0.49, p<0.001). The final multivariable model of variables associated with extent of maximal MRI densification in the condyle as the main outcome is presented in **Table 12**. Increasing MRI measurements were associated with an increasing total number of starts (p<0.001) (**Figure 13**) and an increasing body weight:height ratio (p=0.001).

Variable	Estimate	Standard error	T-value	P-value
Total number of starts	0.39	0.04	9.91	<0.001
Body weight:height ratio	3.48	1.08	3.22	0.001

Table 12. The final multivariable mixed-effects linear regression model of variables associated with the extent of maximal densification on MR images in the metacarpal condyles as the main

outcome, with horse as a random effect, using data from Thoroughbred racehorses that were first examined as yearlings (time 0, n = 39) and then four more times, at approximately six months' intervals (time 1 n = 31, time 2 n = 23, time 3 n = 13, time 4 n = 8). Total number of observations was 438 from 39 horses.

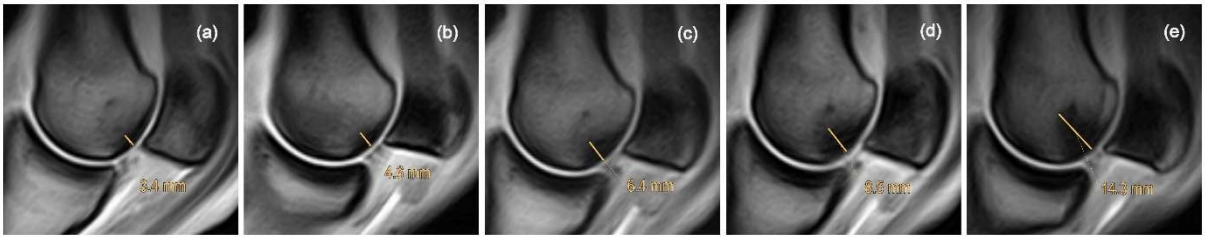

Figure 13. Sagittal plane T1-weighted gradient recalled echo MR images of the right metacarpophalangeal joint of the same Thoroughbred racehorse acquired at five sequential examinations approximately six months apart, showing an increase in extent of densification of the palmar aspect of the medial condyle of McIII. (a) time 0, 3.4 mm; (b) time 1, 4.6 mm; (c) time 2, 6.4 mm; (d) time 3, 8.5 mm; (e) time 4, 14.3 mm.

Univariable models of the association between CT measurements and explanatory variables are presented in **Supplementary item 5.** As in the MRI model, the number of total starts was included instead of age and body weight: height ratio replaced individual body weight and height variables in the multivariable model. The final multivariable model of variables associated with extent of maximal CT densification in the condyle as the main outcome is presented in **Table 13**. Increasing CT measurements were associated with an increasing number of total starts (p<0.001) (**Figure 14**) and an increasing body weight:height ratio (p=0.003). Measurements were higher in the middle third of the condyle compared with the abaxial third (p=0.05).

Variable	Estimate	Standard error	T-value	P-value
Total number of starts	0.41	0.04	10.99	<0.001
Body weight:height ratio	2.85	0.95	2.98	0.003
Maximal measurement location				
Abaxial	Reference			

Axial	-0.28	0.80	-0.35	0.731
Middle	1.50	0.75	1.99	0.047
Mixed	-3.56	1.51	-2.36	0.019

Table 13. The final multivariable mixed-effects linear regression model of variables associated with extent of maximal densification on CT images in the metacarpal condyles as the main outcome, with horse as a random effect, using data from Thoroughbred racehorses that were first examined as yearlings (time 0, n=39) and then four more times, at approximately six months' intervals (time 1 n=31, time 2 n=23, time 3 n=13, time 4 n=8). Total number of observations was 438 from 39 horses. Mixed location refers to observations in which equal values were recorded in different thirds (abaxial, axial, middle).

Figure 14. Sagittal plane CT reconstructions of the right metacarpophalangeal joint of the same Thoroughbred racehorse as shown in Figure 3 using 2 mm thick slices, acquired at five sequential examinations approximately six months apart. There is an increase in extent of densification of the palmar aspect of the medial condyle of McIII over time. (a) time 0, 1.0 mm; (b) time 1, 3.5 mm; (c) time 2, 6.7 mm; (d) time 3, 7.7 mm; (e) time 4, 10.0 mm.

7. Discussion

At the commencement of this project, longitudinal advanced diagnostic imaging data on metacarpophalangeal joint findings in Thoroughbred racehorses were not available. Although longitudinal studies have since become available, imaging data spanning extended periods remain scarce, as the published studies have monitored horses for no longer than one year [186, 187]. The studies included in this thesis are the first to provide a detailed fan-beam CT-based description and longitudinal evaluation of diagnostic imaging findings of the SR, PSBs and metacarpal condyles in young Thoroughbred racehorses within a cohort followed for up to two and a half years. In addition, this work is the first to compare MRI- and CT-derived measurements of metacarpal condylar densification in the same population.

7.1 Measurement methods

Changes in densification were assessed using two distinct measurement methods. In the SR and PSBs, densification was quantified using HU-based measurements, whereas in the metacarpal condyles it was evaluated based on the linear extent of the densified area. It has previously been shown that HU-based estimation of mineral density can be highly repeatable under identical imaging conditions, and that a linear relationship between HU and physical density can be applied to both cancellous and cortical bone [224]. Recent phantom-based work has shown that HU values may differ between conventional fan-beam CT scanners and CT systems designed for imaging standing sedated horses, particularly for denser materials, indicating that HU-based density measurements should be interpreted as system- and protocol-specific unless scanner-specific calibration is performed [225]. Although the same CT system and standardised acquisition parameters were used throughout the study, no external calibration phantom was included at each examination. Therefore, temporal stability of the relationship between HU and a calcium-equivalent reference could not be verified, and potential scanner-related drift in HU values cannot be excluded.

For the metacarpal condyles, selection of CT reconstruction slice thickness was an important methodological consideration. In the present study, repeatability analysis indicated that 2 mm reconstructions provided the most consistent linear measurements, whereas other slice thicknesses resulted in poorer repeatability. Although thinner slices improve spatial resolution and reduce partial-volume averaging, thicker reconstructions improve signal-to-noise ratio and, through a summation effect, may facilitate more consistent identification of low-contrast osseous changes such as mild densification [226–228]. Therefore, 2 mm reconstructions were considered to provide the most appropriate balance between spatial

resolution and reliable identification of the densification margin, although the CV for repeated measurements remained larger than ideal (7.6%).

The margin of densification may appear sharp or indistinct, and this influences the accuracy of linear measurements more than the absolute extent of densification itself. HU-based measurement of attenuation within predefined ROIs may reduce the subjectivity associated with identifying the margin between normal and densified bone, and previous HU-based measurements of the condyles in this population were more repeatable [61]. However, ROI-based HU analysis and linear measurement of densification extent quantify different aspects of bone adaptation. Hounsfield unit measurements assess attenuation within a defined region, reflecting both bone volume fraction and tissue mineral density, whereas linear measurements describe the extent of visually appreciable densification and may be more directly comparable with MRI-derived assessments.. Therefore, these methods should be regarded as complementary rather than interchangeable.

7.2 Changes in densification

Overall, the results support the hypothesis that densification of the SR, PSBs and metacarpal condyles increases in association with training and racing exposure. In the SR, mean HU values increased during the first year of training, with the most pronounced increase occurring between times 0 and 1. This suggests that adaptive changes may occur most rapidly during the early phase of training, when the workload increased from light training to fast work. This is consistent with previous studies showing that the density of distal regions of McIII increases within a few months after the onset of training as part of the adaptive response of bone to mechanical loading [186, 229–231]. Such adaptation is considered necessary for bone tissue to withstand the repetitive strains imposed by race training, and racehorses in training have been reported to have substantially greater density of the distal metacarpal epiphysis than horses not in training [42, 59].

A similar workload-related pattern was observed in the PSBs and metacarpal condyles. In the current population, horses with a greater number of starts had increased PSB radiodensity and greater condylar densification compared with horses with fewer starts, suggesting that cumulative loading from intensive training and racing is associated with progressive osseous adaptation. This is consistent with the concept that increased mechanical loading can induce increased bone density as part of the adaptive response to exercise [41, 207, 209]. Importantly, increased density alone should not be interpreted as evidence of accumulated microdamage or impending bone failure.

However, densification did not increase continuously between all time points. In the SR, no significant increase in mean HU values was detected at time 2 compared with time 1, and some horses showed a decrease in total mean SR attenuation between these time points. Most of these horses were in light training at time 2, commonly because of their winter rest period. Similarly, PSB radiodensity increased at times 1 and 3 compared with the preceding examinations, both of which occurred during racing seasons when the horses had been engaged in fast work, but no significant increase was detected at time 2 compared with time 1, and a significant decrease was observed at time 4 compared with time 3. Most horses at times 2 and 4 were in light training, usually because of winter rest. These findings support the concept that bone adaptation in young racehorses is dynamic and reflects recent workload rather than training status alone. One horse showed a marked decrease in radiodensity of all four forelimb PSBs at time 4 after 8 weeks of rest followed by a period of reduced training; however, removal of this horse from the statistical analysis did not alter the overall results. Decreased density of the distal aspect of McIII has previously been reported in racehorses undergoing rest or light training compared with those in full training, and focal decreases in density of the subchondral, compact and cancellous bone of the PSBs have also been described during periods of reduced training [207, 232–234]. However, focal decreases in SCB density previously linked to PSB fracture formation should be distinguished from the decrease in overall PSB radiodensity observed after periods of reduced work in the present study, because decreased overall radiodensity has not been shown to be associated with increased fracture risk.

7.3 Pattern of densification

The distribution of densification varied between anatomical regions. In the current study, the mean HU value of the dorsal half of the SR was significantly higher than the mean for the palmar half. This is in contrast to the results of a study, which evaluated single-slice FBCT reconstructions in the plane of the PSGs and the metacarpal condyles in two-year-old Thoroughbreds, in which there was an increase in density of the distal epiphysis of McIII, as a result of training, with the dorsodistal aspect being the least dense area [59]. However, the two studies assessed adjacent but different anatomical regions and used different measurement methods. The previous study evaluated regional density patterns across the metacarpal condyles, whereas the present study specifically compared the dorsal and palmar halves of the SR. Thus, the apparent difference is most likely related to ROI definition and measurement methodology.

In the PSBs, increased overall radiodensity with racing exposure is consistent with previous ex vivo studies of Thoroughbred racehorse PSBs that described regional and focal

density patterns within the subchondral, compact and cancellous bone, supporting the concept that PSBs undergo site-specific osseous adaptation in response to race training [207, 209]. To the author's knowledge, however, no previous study has longitudinally evaluated the effect of training and racing load on the overall radiodensity of the PSBs in racehorses in active training. The current findings therefore add longitudinal in vivo evidence that PSB radiodensity changes with workload. Densification of the SCB plate is expected to increase resistance to bone fatigue [41, 42] , although accumulation of microdamage in adjacent bone may also contribute to focal weakening and predisposition to PSB fracture [210, 235].

In the metacarpal condyles, the greatest extent of densification was most often observed in the middle third of the condyle. This agrees with a previous HU-based study of the same population, in which density was higher in the middle region of the condyles, from medial to lateral, than adjacent to the PSG [61]. The location of maximal densification was not constant but changed over time in the present study. This redistribution may reflect progressive adaptation of condylar bone structure to evolving loading patterns during early racehorse training. As with the SR and PSBs, condylar densification appears to represent a workload-related adaptive response; however, excessive or poorly distributed microdamage accumulation in adjacent bone may contribute to focal weakening and subsequent development of condylar fracture [235].

7.4 Medial-lateral differences

In this population of racehorses, the medial PSBs had higher radiodensity than the lateral PSBs. This is in agreement with the results of previous studies investigating density patterns of the PSBs of Thoroughbred racehorses ex vivo [209, 210]. The higher density observed in the medial PSBs was attributed to an increased bone volume fraction, primarily in the apical region [209]. There is a difference in shape and size of the forelimb PSBs, the medial being shorter and wider [10], hence the medial and lateral PSBs of the forelimbs experience different strains during high-speed gallop [236]. These findings support the results of a previous finite-element model which indicated that there is a difference between loading patterns of the medial and lateral PSBs, the medial PSB being under higher loads during gallop [237].

In the current study, evaluating the palmar aspect of the condyles, maximal MRI measurements were higher in the lateral condyle compared with the medial condyle at the final examination. The higher densification of the lateral condyle as determined by MRI is consistent with previous reports that lateral condylar fractures are more common than medial condylar fractures in Thoroughbred racehorses [238, 239]. However, in the current study using linear measurements, and in a previous study of the same population of horses using HU measurements [61], there were no mediolateral differences in the density of the palmar halves

of the condyles in the CT images. This discrepancy may reflect that MRI and CT delineate related but non-identical aspects of condylar densification. Linear MRI measurements were based on the maximal extent of hypointense signal change, whereas linear CT measurements were based on the visible extent of hyperattenuating bone. Therefore, subtle differences in trabecular architecture, or the distribution of densification may alter the apparent MRI extent without producing an equivalent mediolateral difference in the CT-defined extent or mean HU values. This finding should also be interpreted cautiously, as relatively few horses remained available at the final examination and the mediolateral difference was detected only at this time point.

7.5 Effect of sex

In this study there were significantly higher mean HU values of the dorsal half of the SR in fillies than in colts. The significantly higher number of starts of fillies compared to colts could provide one possible explanation at times 1 and 2. However, this difference was present at time 0 when the horses had not raced yet. Previous studies of training-related densification in the metacarpophalangeal joint have primarily focused on anatomical location, training status, limb laterality, mediolateral differences and body size, whereas the influence of sex has been less clearly established [40, 59, 62, 186, 187]. Therefore, the reason for the observed sex-related difference in SR attenuation is unknown and should be interpreted cautiously, particularly given the small sample size. In contrast, sex was not significantly associated with PSB radiodensity or metacarpal condylar densification measurements in the current study.

7.6 Effect of body size

All horses in the current study had a similar body condition score of 4–5/9; however, there was a positive relationship between increased radiodensity of the PSBs, condylar densification measurements and body weight:height ratio, in accordance with the study using HU measurements on the same condyles [61]. In horses with higher ratios, relatively greater forces may be transmitted through the joint surfaces, which may stimulate a more pronounced osseous adaptive response [240], including greater PSB radiodensity and metacarpal condylar densification. However, local stress also depends on factors such as bone cross-sectional area and joint surface area, which were not assessed in the present study. Therefore, the precise mechanism underlying the association between body size and densification cannot be determined from the present data.

7.7 Lameness

There is evidence that metacarpophalangeal joint pain related lameness can be resolved using ‘low four-point’, ‘abaxial sesamoid’ and even ‘palmar digital’ nerve blocks [56, 152, 241–

243]. Furthermore, selective blockade of the palmar metacarpal nerves results in more localised desensitisation of the metacarpal condyles [156]. During the study period, 10 forelimbs of nine horses had lameness abolished by one of these techniques. Since each technique affects multiple anatomical structures, it would be challenging to interpret their specific effects on the investigated regions. Moreover, all of these horses also had additional imaging abnormalities in the region to which pain causing the lameness was localised. To more thoroughly investigate the potential association between response to diagnostic anaesthesia and SR, PSB and condylar changes, a comprehensive imaging evaluation of all structures within the distal aspect of the limb would be required. Such analysis was beyond the scope of the current study. However the diagnostic anaesthesia technique resulting in improvement, and classification of the lameness as fetlock-related or unrelated to the fetlock are provided in **Supplementary item 1.** In only four horses was the lameness classified as fetlock-related. In one horse lameness was present due to unusual SCB resorption in the metacarpal condyles with mineralisation of the overlying cartilage. In two horses no overt MRI or CT abnormalities were detected in the fetlock and the owners denied further investigation. It cannot be excluded that in these cases foot-related pain was abolished only after low four-point block. In one horse, lameness improved following low four-point diagnostic anaesthesia on the first day of the examination, however, the degree of lameness was insufficient for intra-articular anaesthesia the following day. Therefore, it could not be determined whether this represented genuine clinical improvement or fluctuation in lameness severity. In this horse no overt MRI or CT abnormalities were detected, only densification in the metacarpal condyles without concurrent STIR hyperintensity (greatest extent of densification medial condyle CT: 9.2 mm, MRI: 7.4 mm; lateral condyle CT: 14.4 mm, MRI: 9.9 mm).

Subjective and objective lameness assessments were performed throughout the study, and objective baseline lameness data for horses undergoing diagnostic anaesthesia are provided in **Supplementary item 1**. However, objective lameness variables were not included as primary outcome measures in the present analyses, and the small number of horses in which lameness was localized by diagnostic anaesthesia precluded meaningful statistical investigation of associations between objective lameness parameters and SR, PSB or condylar imaging findings.

7.8 Findings in the sagittal ridge

This is the first study to document longitudinal data on hypoattenuating lesions detected with CT examination in the SR of McIII. It was hypothesised that the appearance of some hypoattenuating lesions in the SCB of the dorsal aspect of the SR would change during the first year of training. These findings may be consistent with osteochondrosis [158, 201];

however, histological evaluation would be needed to confirm this. On radiographs osteochondrosis of the SR can be detected as flattening or depression of the dorsal contour or lucency within the SCB [101]. Such radiographic changes were reported with a wide range of frequency of occurrence (4.8–37.1%) in Thoroughbred yearlings, often (39–53%) bilaterally [158, 202, 205]. The large range among different studies can be related to different populations of racehorses and to different radiographic views obtained to assess SR changes. In most studies, only standard radiographic views and LM (flexed) images were examined. However, in a recent study based on subjective evaluation of MRI and CT images and radiographs of the same population at yearling age [7], DPa (flexed) and dorsoproximal-dorsodistal (flexed) ('skyline') views of the metacarpophalangeal joints were included in the radiographic protocol, revealing hypoattenuating lesions which were not identified in standard views. The use of digital radiography [7] compared with conventional radiography used in earlier studies [158] may have facilitated increased detection of radiolucent lesions.

Computed tomography allows three-dimensional visualisation; thus, superimposition of anatomical structures can be avoided [184, 186, 244]. At the initial examination, hypoattenuating lesions were detected with greater frequency than the highest reported numbers of SR radiolucent lesions in yearling pre-sale radiographs. It is likely that not all lesions detected in CT images are identifiable radiographically. In our related study that compared CT and radiographic findings at time 0, 76% of SR hypoattenuating lesions were identified radiographically [7]. Osteochondrosis lesions have the potential to heal depending on various factors in the first year of life [245]. Radiological studies investigating the development of equine osteochondrosis established that in the hock, osteochondrosis of the distal cranial aspect of the intermediate ridge of the tibia and osteochondrosis of the distal aspect of the lateral trochlea of the talus can resolve in the first five month of life [246]. In the stifle, osteochondrosis of the mid region of the lateral femoral trochlea can resolve in the first eight months of life [246]. In a radiographic study, osteochondrosis lesions of McIII appeared, disappeared or evolved between the age of 12 and 36 months in Warmblood sports horses [247]. This concurs with the results of the present study which demonstrated that osteochondrosis lesions of the SR of McIII have the potential to resolve even in two-year-old Thoroughbreds. Some of these lesions were surrounded by a cone-shaped hyperattenuating zone, consistent with a local increase in trabecular bone density [7]. The evolution of hypoattenuating lesions in the SCB of the SR with and without surrounding trabecular hyperattenuation requires further investigation. These lesions can occur in various shapes on the dorsodistal aspect of the SR. Longer term follow-up is required to assess the long-term clinical significance of SR lesions during and after racehorse training.

7.9 Findings in the proximal sesamoid bones

In this study, in accordance with the hypotheses there were alterations in the radiographic appearance of the PSBs. In the current study, changes of the abaxial margin of the PSBs were only examined on radiographs. Cross-sectional imaging, such as CT, potentially offers greater detail compared with radiography. However, it was observed that radiography was more reliable in detecting subtle abaxial margin changes because the shape of the PSBs hindered proper alignment of multiplanar CT reconstructions on the abaxial margin. New bone formation was primarily observed in higher-grade PSBs. This is consistent with the findings of Peat et al. (2025) [104], who established a correlation between abaxial new bone formation and grade 3 PSBs. New bone formation, along with the presence of enlarged vascular channels, suggests a response to prior or ongoing mechanical stress. This finding is thought to be consistent with sesamoiditis [248]. In this population of racehorses, new bone formation on the abaxial margin was more often detected in lateral PSBs compared with medial PSBs. Forelimb PSBs are subjected to different strains during gallop; more external rotation of the medial PSB and more abduction of the lateral PSB are present during axial limb loading [236]. This specific strain experienced by the lateral PSB might make it more prone to consequent productive osseous changes at the abaxial margin. Furthermore, entheseous new bone formation may develop at the palmar annular ligament enthesis. Whether the aetiology of smoothly marginated new bone formation differs from active osseous changes warrants further investigation.

In this population, there was a decrease in the occurrence of abaxial margin concavity and irregularity over time. This decrease in the occurrence of abaxial concavities with increasing age of horses is consistent with previous findings [104]. This suggests that abaxial margin concavity, initially observed in younger horses, could be a normal variation or a developmental abnormality and should not be considered a sign of pathology. The lack of new concavities observed following the initial examination in the current study further supports this concept. An irregular contour of the distal half of the abaxial margin of the PSBs was frequently observed in young Thoroughbreds and also decreased over time. Moreover, no new irregular abaxial margins were detected following the initial examination. This finding could indicate incomplete ossification and might represent a normal stage in the maturation of the PSBs, which become more angular in shape and form bony ridges at sites of entheses [249].

In the current study by time 3, over 90% of PSBs were graded as grade 0, compared with 78% at time 0, indicating radiographic improvement, despite stresses encountered during training and racing. Similar improvement in radiographic grades of the PSBs was documented previously [104]. The results of the current study could be biased by some horses with higher

grade PSBs being lost to follow-up. During the study period, 10 PSBs of 10 horses were graded 3/3 at least at one examination. Three of these horses were lost to follow-up after time 0, only one of which raced subsequently according to race records. In three other horses, there was an improvement in PSB grades despite the horses being in active training, although at the time when improvement was detected, all three horses were in reduced/light training. Only one horse with a grade 3 PSB completed the study; this horse had raced successfully without improvement in PSB grade and without related lameness. Two horses were retired during the study period due to lameness caused by desmitis of the SL branches attached to grade 3 PSBs. One horse with a grade 3 PSB suffered an apical fracture of the contralateral grade 2 medial PSB and injury of the medial SL branch three months prior to time 2. The measurements conducted on the parent bone remained in the statistical analysis because this did not alter the results. In the latter three cases, lameness could be related to PSB changes and SL branch injury. To determine the clinical significance of grade 3 PSBs, a long-term follow-up on a larger sample size of actively racing Thoroughbreds would be required.

An increase in the number and size of vascular channels and the presence of lytic lesions on the abaxial margin of the PSBs was previously associated with higher bone volume fraction calculated from micro-CT images [103, 209]. In this study, no similar association was found between radiographic changes and radiodensity objectively measured on FBCT images. This discrepancy highlights potential differences in imaging modalities, measurement techniques, or study populations, and underscores the need for further research to clarify the relationship between radiographic appearance and radiodensity in the PSBs of racehorses.

7.10 Findings in the metacarpal condyles

In accordance with the hypotheses there was a positive correlation between MRI- and CT-derived measurements. Fracture risk assessment of the racehorse fetlock has previously been approached separately using MRI and CT. Previous high-field MRI studies have reported associations between the extent and distribution of low-signal subchondral bone change in the metacarpal condyles and subsequent condylar fracture risk [137, 138]. These findings suggest that MRI-based evaluation of condylar densification may contribute to fracture risk assessment. Computed tomography has also become increasingly important for fracture risk assessment because it can directly depict osseous morphology, sclerosis and lysis with high spatial resolution. Hypointensity on T1-weighted MR images is not specific for densification and may represent a combination of densification and intraosseous fluid [49, 120, 171]. However, T1-weighted GRE sequences were used in the present study due to their superior anatomical detail and clearer delineation of densification margins, which are essential for consistent linear measurements. T2-weighted sequences may represent densification more

specifically than T1-weighted images as densely mineralised trabecular bone remains low in signal intensity on T2-weighted images [49, 166]. However, in low-field systems, lower spatial resolution and signal-to-noise ratio limit the suitability of T2-weighted images for precise measurement of lesion extent [167]. Furthermore, in none of the condyles in which hyperintense signal was observed on STIR sequences, did the hyperintensity extend to the margin of the densified region, indicating that the potential presence of bone oedema was unlikely to have influenced the measurements performed on T1-weighted images. This distinction is important because the current study assessed the extent of low-signal densification rather than fracture-associated bone oedema signal or CT features of microdamage.

To the author's knowledge there are no data directly comparing extent of condylar densification on low-field MR and FBCT images in Thoroughbred racehorses in active training. In the current study there was a moderate positive correlation between MRI- and CT-derived measurements of condylar densification, however, CT measurements were consistently larger than those obtained from MRI. Consequently, low-field MRI may underestimate the extent of condylar densification compared with FBCT. Fan-beam CT had greater sensitivity than low-field MRI for detection of osseus changes in the fetlocks of Thoroughbred racehorses in a previous study [178]. Recent CT-based work has further highlighted the importance of not only the extent, but also the morphology and distribution of sclerosis and lysis when considering fracture risk. Beck et al. performed a post-mortem CT study of fetlocks from racing Thoroughbreds and identified CT features associated with fracture [206]. Hypoattenuation within the SCB underlying the medial and/or lateral PSG and palmar SCB hyperattenuation projecting proximoaxially were associated with condylar fracture, whereas PSB hypoattenuating lesions and increased medial PSB radiodensity were associated with PSB fracture [210]. Importantly, the shape of the region of sclerosis, particularly in the lateral condyle, was specifically assessed in that study, and inter-rater reliability for this feature was reported to be moderate. The present study did not include subjective assessment of the shape of densification or CT features such as PSG lysis; however, measurements were performed at three predefined condylar locations, allowing partial assessment of the regional distribution of densification. Therefore, the present findings should not be interpreted as direct fracture-risk assessment, but they provide relevant background information by showing how MRI- and FBCT-derived measurements of condylar densification compare. The significant differences observed in the current study between condylar densification measurements obtained using low-field MRI and FBCT may be attributed to differences in slice thickness between the two imaging modalities and the effects of volume averaging. Previous research comparing quantitative CT, FBCT and high-field MRI demonstrated that metacarpal sclerosis scores

derived from both CT and MRI correlated significantly with quantitative CT-derived bone mineral density, although CT likely provides a more direct representation of mineral density, whereas MRI reflects these changes indirectly through alterations in signal intensity [113]. It remains unclear which modality reflects more accurately the true underlying tissue characteristics, as direct validation against postmortem or histological measurements is lacking. The complementary strengths and limitations of MRI and CT suggest that combined imaging may be beneficial in selected cases [56]. Computed tomography may better characterize mineralised osseous change, lysis, fissure configuration and sclerosis morphology, whereas MRI may provide additional information on bone oedema-type signal and associated soft tissue or osteochondral abnormalities. Accordingly, although the present results do not establish fracture-risk thresholds, they indirectly contribute to fracture-risk interpretation by demonstrating that MRI and FBCT measurements are correlated but not interchangeable.

8. Limitations

The present study had certain limitations. The high attrition rate of racehorses from research projects is a frequently encountered problem [186, 187, 234]. Out of the 32 horses lost to follow up 14 were lost due to lack of long-term trainer/owner compliance (only one has not raced successfully following attrition), five did not undergo further training following time 0, 11 were retired (in two cases related to the study, due to lameness caused by desmitis of the suspensory ligament branches attached to grade 3 PSBs), and two horses died due to causes unrelated to musculoskeletal injuries. The eight horses completing all five rounds of examinations remained in training and racing throughout the study period. Results based solely on these horses may introduce survivorship bias [250] thereby potentially confound interpretation of findings, as horses that returned could be those that remained racing and training, therefore representing a 'healthy horse effect' [251]. Lameness assessments at time 0 were not comprehensive in every case because some yearlings were unhandled at the time. Intrasynovial anaesthesia was not performed in horses that developed lameness during the study period; therefore, the potential contribution of synovial structures to the lameness could not be further assessed. No post-mortem histological examinations were performed; therefore, the aetiopathogenesis of detected changes could not be determined. Results may not be representative of all racehorse populations since they were collected from a relatively small geographical area. Some results could be influenced by differences in training regimes and the low sample size, particularly when investigating the effect of sex. All participating horses were trained on dirt training tracks, however slight differences in surface composition could exist. The influence of conformation, gait patterns, trimming and shoeing was not investigated. No calibration phantom was included to improve precision of quantitative measurements, nevertheless assessment of relative changes in HU remains valid due to consistent imaging parameters [225]. However, without repeated phantom-based calibration, temporal stability of HU values relative to a calcium-equivalent reference could not be confirmed, and a degree of scanner-related drift cannot be excluded.

9. Conclusions

In conclusion, repeated CT, MRI and radiographic examinations demonstrated progressive osseous adaptation of the metacarpophalangeal joint in young Thoroughbred racehorses during active training and racing. Densification of the SR, PSBs and metacarpal condyles increased with training and racing exposure, whereas reduced PSB radiodensity during periods of lighter work supported the dynamic relationship between workload and bone adaptation.

The results also indicated that some imaging findings in young Thoroughbreds are not necessarily clinically significant. Dorsal SR hypoattenuating lesions decreased in size or disappeared in some horses during the first year of training and were not associated with lameness, while PSB abaxial margin concavities, irregularities and radiographic grades may improved despite continued training.

Fan-beam CT and low-field MRI measurements of metacarpal condylar densification were correlated but differed significantly, with CT measurements consistently exceeding MRI measurements. Therefore, modality-specific interpretation is required, particularly in longitudinal monitoring and when imaging findings are considered in relation to injury risk.

10. New scientific results

- A prospective longitudinal multimodality imaging dataset of the metacarpophalangeal joints of Thoroughbred racehorses without clinically relevant lameness was established, with horses being followed from the onset of race training through repeated CT, MRI, and radiographic examinations over approximately two and a half years.
- Substantial training-related osseous adaptation was demonstrated at the evaluated sites (the metacarpal condyles, PSBs, and SR) in the metacarpophalangeal joints of Thoroughbred racehorses during race training, in the absence of overt lameness, demonstrating progressive changes in bone density and morphology associated with repetitive high-speed loading.

- Sagittal ridge of McIII:
    - An increase in density was observed in the SR during the first six months of race training.
    - Greater density was observed in the dorsal half compared with the palmar half.
    - Variation in shape was identified among the hypoattenuating lesions in the dorsal aspect.
    - A decrease in hypoattenuating lesion size was observed, and resolution of some lesions was recorded during the first year of training.

- Proximal sesamoid bones:
    - An increase in radiodensity was identified in association with the number of race starts.
    - A decrease in overall radiodensity was associated with light or reduced training.
    - Radiographic improvement of PSB grades, abaxial margin concavities, and irregularities was observed, despite active training.

- Metacarpal condyles:
    - Computed tomographic reconstructions with 2 mm slices were found to be the most consistent for densification measurements.
    - The greatest extent of densification was most frequently measured in the middle third of the condyles.

- Metacarpal condyle densification measurements obtained on FBCT and low-field MR images were found to be correlated but differed significantly, with CT measurements being larger than MRI measurements.
- An increase in density was identified in association with the number of race starts and the body weight ratio.

11. References

1. Spargo KE, Rubio-Martinez LM, Wheeler DP, Fletcher L, Carstens A (2019) Catastrophic musculoskeletal injuries in Thoroughbred racehorses on racetracks in Gauteng, South Africa. J S Afr Vet Assoc 90:1–5. https://doi.org/10.4102/jsava.v90i0.1640

2. Cresswell EN, McDonough SP, Palmer SE, Hernandez CJ, Reesink HL (2019) Can quantitative computed tomography detect bone morphological changes associated with catastrophic proximal sesamoid bone fracture in Thoroughbred racehorses? Equine Vet J 51:123–130. https://doi.org/10.1111/evj.12965

3. Denoix J-M, Coudry V (2020) Clinical insights: Imaging of the equine fetlock in Thoroughbred racehorses: Identification of imaging changes to predict catastrophic injury. Equine Vet J 52:342–343. https://doi.org/10.1111/evj.13226

4. Davidson E (2011) Pathophysiology and Clinical Diagnosis of Cortical and Subchondral Bone Injury. In: Dyson S, Ross M (eds) Diagnosis and Management of Lameness in the Horse, 2nd ed. Elsevier Saunders, St. Louis, pp 935–946

5. Colgate VA, Riggs CM, The FRAT Group II (2025) IFHA Global Summit of Equine Safety and Technology: Fracture prediction and prevention. Equine Vet J 57:290–295. https://doi.org/10.1111/evj.14458

6. Keen J, Whitton C (2025) IFHA Global Summit on Equine Safety & Technology: What veterinary scientists want from racing. Equine Vet J 57:287–289. https://doi.org/10.1111/evj.14432

7. Nagy A, Boros K, Dyson S (2023) Magnetic Resonance Imaging, Computed Tomographic and Radiographic Findings in the Metacarpophalangeal Joints of 40 Non-Lame Thoroughbred Yearlings. Animals 13:3466. https://doi.org/10.3390/ani13223466

8. Heleski C, Stowe CJ, Fiedler J, Peterson ML, Brady C, Wickens C, MacLeod JN (2020) Thoroughbred Racehorse Welfare through the Lens of 'Social License to Operate—With an Emphasis on a U.S. Perspective. Sustainability 12:1706. https://doi.org/10.3390/su12051706

9. Parkin TDH, Clegg PD, French NP, Proudman CJ, Riggs CM, Singer ER, Webbon PM, Morgan KL (2004) Horse-level risk factors for fatal distal limb fracture in racing Thoroughbreds in the UK. Equine Vet J 36:513–519. https://doi.org/10.2746/0425164044877387

10. Beccati F, Gialletti R, Giontella A, Davanzo S, Di Meo A, Pepe M (2014) Morphologic radiographic study of the proximal sesamoid bones of the forelimb in thoroughbred racehorses in training. Anat Histol Embryol 43:403–407. https://doi.org/10.1111/ahe.12075

11. Denoix J -M., Coudry V, Jacquet S (2008) Ultrasonographic procedure for a complete examination of the proximal third interosseous muscle (proximal suspensory ligament) in the equine forelimbs. Equine Vet Educ 20:148–153. https://doi.org/10.2746/095777308X282381

12. Nagy A, Dyson S (2009) Magnetic resonance anatomy of the proximal metacarpal region of the horse described from images acquired from low- and high-field magnets. Vet Radiol Ultrasound Off J Am Coll Vet Radiol Int Vet Radiol Assoc 50:595–605. https://doi.org/10.1111/j.1740-8261.2009.01589.x

13. Richardson D, Dyson S (2011) The Metacarpophalangeal Joint. In: Dyson S, Ross M (eds) Diagnosis and Management of Lameness in the Horse, 2nd ed. Elsevier Saunders, St. Louis, pp 394–410

14. Dyson SJ, Arthur RM, Palmer SE, Richardson D (1995) Suspensory Ligament Desmitis. Vet Clin North Am Equine Pract 11:177–215. https://doi.org/10.1016/S0749-0739(17)30319-X

15. Moiroud C, Audigié F, Denoix J-M (2021) The middle scutum: Functional anatomy and normal images. Equine Vet Educ 33:288–292. https://doi.org/10.1111/eve.13337

16. Liebich H, König H, Maierl J (2004) Forelimb or thoracic limb (membra thoracica). In: König H, Liebich H (eds) Veterinary Anatomy of Domestic Mammals, 1st ed. Schattauer, Stuttgart, pp 129–196

17. Velásquez JM, Tamayo-Arango L, Santos-Silva T, Miglino MA (2025) Casting techniques of equine hand and foot synovial cavities for the development of teaching models. Front Vet Sci 12:1524549. https://doi.org/10.3389/fvets.2025.1524549

18. Vanderperren K, Ghaye B, Snaps FR, Saunders JH (2008) Evaluation of computed tomographic anatomy of the equine metacarpophalangeal joint. Am J Vet Res 69:631–638. https://doi.org/10.2460/ajvr.69.5.631

19. Harrison SM, Whitton RC, King M, Haussler KK, Kawcak CE, Stover SM, Pandy MG (2012) Forelimb muscle activity during equine locomotion. J Exp Biol 215:2980–2991. https://doi.org/10.1242/jeb.065441

20. Denoix JM (1994) Functional anatomy of tendons and ligaments in the distal limbs (manus and pes). Vet Clin North Am Equine Pract 10:273–322. https://doi.org/10.1016/s0749-0739(17)30358-9

21. Fehér G (2000) A csontok összeköttetései, juncturae ossium. In: Fehér G (ed) A háziállatok funkcionális anatómiája 1. A mozgás szervei, 1st ed. Mezőgazda Kiadó, Budapest, pp 101–126

22. Easton KL, Kawcak CE (2007) Evaluation of increased subchondral bone density in areas of contact in the metacarpophalangeal joint during joint loading in horses. Am J Vet Res 68:816–821. https://doi.org/10.2460/ajvr.68.8.816

23. Singer E, Garcia T, Stover S (2013) How do metacarpophalangeal joint extension, collateromotion and axial rotation influence dorsal surface strains of the equine proximal phalanx at different loads in vitro? J Biomech 46:738–744. https://doi.org/10.1016/j.jbiomech.2012.11.028

24. Clayton HM, Sha D, Stick J, Elvin N (2007) 3D kinematics of the equine metacarpophalangeal joint at walk and trot. Vet Comp Orthop Traumatol 20:86–91. https://doi.org/10.1160/vcot-07-01-0011

25. Den Hartog SM, Back W, Brommer H, van Weeren PR (2009) In vitro evaluation of metacarpophalangeal joint loading during simulated walk. Equine Vet J 41:214–217. https://doi.org/10.2746/042516409x395570

26. Northrop AJ, Dagg L-A, Martin JH, Brigden CV, Owen AG, Blundell EL, Peterson ML, Hobbs SJ (2013) The effect of two preparation procedures on an equine arena surface in relation to motion of the hoof and metacarpophalangeal joint. Vet J Lond Engl 1997 198 Suppl 1:e137-142. https://doi.org/10.1016/j.tvjl.2013.09.048

27. Santschi EM (2008) Articular Fetlock Injuries in Exercising Horses. Vet Clin North Am Equine Pract 24:117–132. https://doi.org/10.1016/j.cveq.2007.11.011

28. Swanstrom MD, Zarucco L, Hubbard M, Stover SM, Hawkins DA (2005) Musculoskeletal modeling and dynamic simulation of the thoroughbred equine forelimb during stance phase of the gallop. J Biomech Eng 127:318–328. https://doi.org/10.1115/1.1865196

29. Smith RKW, Birch HL, Sinclair C, Goodship AE (2025) Tendon and Ligament Physiology. In: Equine Sports Medicine and Surgery, 3rd ed. Elsevier, St. Louis, pp 252–279

30. Leach DH, Sprigings EJ, Laverty WH (1987) Multivariate statistical analysis of stride-timing measurements of nonfatigued racing Thoroughbreds. Am J Vet Res 48:880–888

31. Butcher MT, Ashley-Ross MA (2002) Fetlock joint kinematics differ with age in Thoroughbred [was thoroughbred] racehorses. J Biomech 35:563–571. https://doi.org/10.1016/s0021-9290(01)00223-8

32. Merkens HW, Schamhardt HC, van Osch GJ, Hartman W (1993) Ground reaction force patterns of Dutch Warmbloods at the canter. Am J Vet Res 54:670–674

33. Hjertén G, Drevemo S (1994) Semi-quantitative analysis of hoof-strike in the horse. J Biomech 27:997–1004. https://doi.org/10.1016/0021-9290(94)90216-x

34. Kingsbury HB, Quddus MA, Rooney JR, Geary JE (1978) A laboratory system for production of flexion rates and forces in the forelimb of the horse. Am J Vet Res 39:365–369

35. Symons JE, Hawkins DA, Fyhrie DP, Upadhyaya SK, Stover SM (2017) Modelling the effect of race surface and racehorse limb parameters on in silico fetlock motion and propensity for injury. Equine Vet J 49:681–687. https://doi.org/10.1111/evj.12672

36. Langdahl B, Ferrari S, Dempster DW (2016) Bone modeling and remodeling: potential as therapeutic targets for the treatment of osteoporosis. Ther Adv Musculoskelet Dis 8:225–235. https://doi.org/10.1177/1759720X16670154

37. Bentolila V, Boyce TM, Fyhrie DP, Drumb R, Skerry TM, Schaffler MB (1998) Intracortical remodeling in adult rat long bones after fatigue loading. Bone 23:275–281. https://doi.org/10.1016/s8756-3282(98)00104-5

38. Raggatt LJ, Partridge NC (2010) Cellular and Molecular Mechanisms of Bone Remodeling. J Biol Chem 285:25103–25108. https://doi.org/10.1074/jbc.R109.041087

39. Frost HM (1989) Transient-steady state phenomena in microdamage physiology: a proposed algorithm for lamellar bone. Calcif Tissue Int 44:367–381. https://doi.org/10.1007/BF02555964

40. Muir P, Peterson AL, Sample SJ, Scollay MC, Markel MD, Kalscheur VL (2008) Exercise-induced metacarpophalangeal joint adaptation in the Thoroughbred racehorse. J Anat 213:706–717. https://doi.org/10.1111/j.1469-7580.2008.00996.x

41. Firth EC (2006) The response of bone, articular cartilage and tendon to exercise in the horse. J Anat 208:513–526. https://doi.org/10.1111/j.1469-7580.2006.00547.x

42. Martig S, Hitchens PL, Lee PVS, Whitton RC (2020) The relationship between microstructure, stiffness and compressive fatigue life of equine subchondral bone. J Mech Behav Biomed Mater 101:103439. https://doi.org/10.1016/j.jmbbm.2019.103439

43. Stewart HL, Kawcak CE (2018) The Importance of Subchondral Bone in the Pathophysiology of Osteoarthritis. Front Vet Sci 5:178. https://doi.org/10.3389/fvets.2018.00178

44. Rubio-Martínez LM, Cruz AM, Gordon K, Hurtig MB (2008) Mechanical properties of subchondral bone in the distal aspect of third metacarpal bones from Thoroughbred racehorses. Am J Vet Res 69:1423–1433. https://doi.org/10.2460/ajvr.69.11.1423

45. Burr DB, Forwood MR, Fyhrie DP, Martin RB, Schaffler MB, Turner CH (1997) Bone microdamage and skeletal fragility in osteoporotic and stress fractures. J Bone Miner Res Off J Am Soc Bone Miner Res 12:6–15. https://doi.org/10.1359/jbmr.1997.12.1.6

46. Kh Z, Js K, Rb M, Mab W, Nl F (2005) New insights into the propagation of fatigue damage in cortical bone using confocal microscopy and chelating fluorochromes. Eur J Morphol 42:81–90. https://doi.org/10.1080/09243860500096206

47. Muir P, McCarthy J, Radtke CL, Markel MD, Santschi EM, Scollay MC, Kalscheur VL (2006) Role of endochondral ossification of articular cartilage and functional adaptation

of the subchondral plate in the development of fatigue microcracking of joints. Bone 38:342–349. https://doi.org/10.1016/j.bone.2005.08.020

48. Janes JG, Kennedy LA, Garrett KS, Engiles JB (2017) Common lesions of the distal end of the third metacarpal/metatarsal bone in racehorse catastrophic breakdown injuries. J Vet Diagn Investig Off Publ Am Assoc Vet Lab Diagn Inc 29:431–436. https://doi.org/10.1177/1040638717717948

49. Olive J, Serraud N, Vila T, Germain J-P (2017) Metacarpophalangeal joint injury patterns on magnetic resonance imaging: A comparison in racing Standardbreds and Thoroughbreds. Vet Radiol Ultrasound Off J Am Coll Vet Radiol Int Vet Radiol Assoc 58:588–597. https://doi.org/10.1111/vru.12512

50. Easton K (2012) Effect of bone geometry on stress distribution patterns in the equine metacarpophalangeal joint. Dissertation, Colorado State University

51. Faulkner JE, Joostens Z, Broeckx BJG, Hauspie S, Mariën T, Vanderperren K (2023) Follow-Up Magnetic Resonance Imaging of Sagittal Groove Disease of the Equine Proximal Phalanx Using a Classification System in 29 Non-Racing Sports Horses. Animals 14:34. https://doi.org/10.3390/ani14010034

52. Faulkner JE, Joostens Z, Broeckx BJG, Hauspie S, Mariën T, Vanderperren K (2025) Low-field magnetic resonance imaging of sagittal groove disease of the proximal phalanx in non-racing sport horses. Equine Vet J 57:140–152. https://doi.org/10.1111/evj.14088

53. Martig S, Chen W, Lee PVS, Whitton RC (2014) Bone fatigue and its implications for injuries in racehorses. Equine Vet J 46:408–415. https://doi.org/10.1111/evj.12241

54. Ross MW, Ford TS, Orsini PG (1988) Incomplete Longitudinal Fracture of the Proximal Palmar Cortex of the Third Metacarpal Bone in Horses. Vet Surg 17:82–86. https://doi.org/10.1111/j.1532-950X.1988.tb00282.x

55. Morgan R, Dyson S (2012) Incomplete longitudinal fractures and fatigue injury of the proximopalmar medial aspect of the third metacarpal bone in 55 horses. Equine Vet J 44:64–70. https://doi.org/10.1111/j.2042-3306.2011.00371.x

56. Nagy A, Dyson SJ (2025) Combined standing low-field magnetic resonance imaging and fan-beam computed tomographic diagnosis of fetlock region pain in 27 sports horses. Equine Vet J 57:1313–1327. https://doi.org/10.1111/evj.14504

57. Kuemmerle JM, Auer JA, Rademacher N, Lischer CJ, Bettschart-Wolfensberger R, Fürst AE (2008) Short Incomplete Sagittal Fractures of the Proximal Phalanx in Ten Horses Not Used for Racing. Vet Surg 37:193–200. https://doi.org/10.1111/j.1532-950X.2007.00359.x

58. Beccati F, Pepe M, Di Meo A, Davanzo S, Moriconi F (2011) Radiographic evaluation of changes in the proximal phalanx of Thoroughbreds in race training. Am J Vet Res 72:1482–1488. https://doi.org/10.2460/ajvr.72.11.1482

59. Firth EC, Rogers CW, Jopson N (2000) Effects of racetrack exercise on third metacarpal and carpal bone of New Zealand thoroughbred horses. J Musculoskelet Neuronal Interact 1:145–147

60. Davis AM, Fan X, Shen L, Robinson P, Riggs CM (2017) Improved radiological diagnosis of palmar osteochondral disease in the Thoroughbred racehorse. Equine Vet J 49:454–460. https://doi.org/10.1111/evj.12636

61. Putnoki V, Pollard D, Dyson S, Boros K, Nagy A (2026) Objective, Longitudinal Computed Tomographic Evaluation of the Metacarpal Condyles in Non-Lame Thoroughbred Racehorses. Animals 16:973. https://doi.org/10.3390/ani16060973

62. Noble P, Singer ER, Jeffery NS (2016) Does subchondral bone of the equine proximal phalanx adapt to race training? J Anat 229:104–113. https://doi.org/10.1111/joa.12478

63. Nunamaker DM, Butterweck DM, Provost MT (1990) Fatigue fractures in thoroughbred racehorses: relationships with age, peak bone strain, and training. J Orthop Res Off Publ Orthop Res Soc 8:604–611. https://doi.org/10.1002/jor.1100080417

64. Rogers CW, Gee EK, Dittmer KE (2021) Growth and Bone Development in the Horse: When Is a Horse Skeletally Mature? Animals 11:3402. https://doi.org/10.3390/ani11123402

65. Rubio-Martínez LM, Cruz AM, Gordon K, Hurtig MB (2008) Structural characterization of subchondral bone in the distal aspect of third metacarpal bones from Thoroughbred racehorses via micro--computed tomography. Am J Vet Res 69:1413–1422. https://doi.org/10.2460/ajvr.69.11.1413

66. Bukowiecki CF, Bramlage LR, Gabel AA (1987) In Vitro Strength of the Suspensory Apparatus in Training and Resting Horses. Vet Surg 16:126–130. https://doi.org/10.1111/j.1532-950X.1987.tb00923.x

67. Birch HL, Wilson AM, Goodship AE (2008) Physical activity: does long-term, high-intensity exercise in horses result in tendon degeneration? J Appl Physiol 105:1927–1933. https://doi.org/10.1152/japplphysiol.00717.2007

68. Guest DJ, Birch HL, Thorpe CT (2025) A review of the equine suspensory ligament: Injury prone yet understudied. Equine Vet J 57:1167–1182. https://doi.org/10.1111/evj.14447

69. Parkin TDH, Clegg PD, French NP, Proudman CJ, Riggs CM, Singer ER, Webbon PM, Morgan KL (2005) Risk factors for fatal lateral condylar fracture of the third metacarpus/metatarsus in UK racing. Equine Vet J 37:192–199. https://doi.org/10.2746/0425164054530641

70. Parkin TDH, Clegg PD, French NP, Proudman CJ, Riggs CM, Singer ER, Webbon PM, Morgan KL (2004) Race- and course-level risk factors for fatal distal limb fracture in racing Thoroughbreds. Equine Vet J 36:521–526. https://doi.org/10.2746/0425164044877332

71. Boden LA, Anderson GA, Charles JA, Morgan KL, Morton JM, Parkin TDH, Clarke AF, Slocombe RF (2007) Risk factors for Thoroughbred racehorse fatality in flat starts in Victoria, Australia (1989-2004). Equine Vet J 39:430–437. https://doi.org/10.2746/042516407x183162

72. Butcher MT, Hermanson JW, Ducharme NG, Mitchell LM, Soderholm LV, Bertram JEA (2007) Superficial digital flexor tendon lesions in racehorses as a sequela to muscle fatigue: A preliminary study. Equine Vet J 39:540–545. https://doi.org/10.2746/042516407X212475

73. Peterson M, Sanderson W, Kussainov N, Hobbs SJ, Miles P, Scollay MC, Clayton HM (2021) Effects of Racing Surface and Turn Radius on Fatal Limb Fractures in Thoroughbred Racehorses. Sustainability 13:539. https://doi.org/10.3390/su13020539

74. Riemersma DJ, van den Bogert AJ, Jansen MO, Schamhardt HC (1996) Tendon strain in the forelimbs as a function of gait and ground characteristics and in vitro limb loading in ponies. Equine Vet J 28:133–138. https://doi.org/10.1111/j.2042-3306.1996.tb01605.x

75. Wilson G, Drust B, Morton JP, Close GL (2014) Weight-making strategies in professional jockeys: implications for physical and mental health and well-being. Sports Med Auckl NZ 44:785–796. https://doi.org/10.1007/s40279-014-0169-7

76. Nunamaker DM (2002) Relationships of exercise regimen and racetrack surface to modeling/remodeling of the third metacarpal bone in two year-old Thoroughbred racehorses. Vet Comp Orthop Traumatol 15:195–199. https://doi.org/10.1055/s-0038-1632738

77. Cogger N, Perkins N, Hodgson DR, Reid SWJ, Evans DL (2006) Risk factors for musculoskeletal injuries in 2-year-old Thoroughbred racehorses. Prev Vet Med 74:36–43. https://doi.org/10.1016/j.prevetmed.2006.01.005

78. Reed SR, Jackson BF, Wood JLN, Price JS, Verheyen KLP (2013) Exercise affects joint injury risk in young Thoroughbreds in training. Vet J 196:339–344. https://doi.org/10.1016/j.tvjl.2012.11.014

79. Firth EC, Rogers CW (2005) Musculoskeletal responses of 2-year-old Thoroughbred horses to early training. Conclusions. N Z Vet J 53:377–383. https://doi.org/10.1080/00480169.2005.36581

80. Firth EC, Rogers CW, van Weeren PR, Barneveld A, McIlwraith CW, Kawcak CE, Goodship AE, Smith RKW (2012) The effect of previous conditioning exercise on

diaphyseal and metaphyseal bone to imposition and withdrawal of training in young Thoroughbred horses. Vet J 192:34–40. https://doi.org/10.1016/j.tvjl.2011.05.016

81. Brama P a. J, Firth EC, van Weeren PR, Tuukkanen J, Holopainen J, Helminen HJ, Hyttinen MM (2009) Influence of intensity and changes of physical activity on bone mineral density of immature equine subchondral bone. Equine Vet J 41:564–571. https://doi.org/10.2746/042516409x429437

82. Whitton RC, Trope GD, Ghasem-Zadeh A, Anderson GA, Parkin TDH, Mackie EJ, Seeman E (2010) Third metacarpal condylar fatigue fractures in equine athletes occur within previously modelled subchondral bone. Bone 47:826–831. https://doi.org/10.1016/j.bone.2010.07.019

83. Estberg L, Stover SM, Gardner IA, Johnson BJ, Case JT, Ardans A, Read DH, Anderson ML, Barr BC, Daft BM, Kinde H, Moore J, Stoltz J, Woods LW (1996) Fatal musculoskeletal injuries incurred during racing and training in thoroughbreds. J Am Vet Med Assoc 208:92–96

84. Verheyen KLP, Price JS, Wood JLN (2007) Fracture rate in Thoroughbred racehorses is affected by dam age and parity. Vet J 174:295–301. https://doi.org/10.1016/j.tvjl.2006.07.023

85. Barron JK (1995) The effect of maternal age and parity on the racing performance of thoroughbred horses. Equine Vet J 27:73–75. https://doi.org/10.1111/j.2042-3306.1995.tb03036.x

86. Finocchio E, Rosenzweig M (1995) Significance of birthrank, maternal age and parity on race performance in Thororughbreds. In: Proceedings of the Annual Convention of the American Association of Equine Practitioners. American Association of Equine Practitioners, Lexington, Kentucky, pp 64–67

87. R M, Am de M, Jc A-S, Kl V (2026) Born to run? Associations between gestational and early-life exposures and later-life performance outcomes in Thoroughbreds. Equine Vet J 58:. https://doi.org/10.1111/evj.70084

88. Rouette J, Cockram MS, Sanchez J, MacMillan KM (2021) Musculoskeletal injuries in Standardbred racehorses on Prince Edward Island. Can Vet J 62:987–993

89. Morrice-West AV, Hitchens PL, Walmsley EA, Tasker K, Lim SL, Smith AD, Whitton RC (2022) Relationship between Thoroughbred workloads in racing and the fatigue life of equine subchondral bone. Sci Rep 12:11528. https://doi.org/10.1038/s41598-022-14274-y

90. Wright I, Minshall G, Young N, Riggs C (2024) Fractures in Thoroughbred racing and the potential for pre-race identification of horses at risk. Equine Vet J 56:424–436. https://doi.org/10.1111/evj.14046

91. Hendrickson EHS, Lykkjen S, Dolvik NI, Olstad K (2018) Prevalence of osteochondral lesions in the fetlock and hock joints of Standardbred horses that survived bacterial infection before 6 months of age. BMC Vet Res 14:390. https://doi.org/10.1186/s12917-018-1726-3

92. Olstad K, Østevik L, Carlson CS, Ekman S (2015) Osteochondrosis Can Lead to Formation of Pseudocysts and True Cysts in the Subchondral Bone of Horses. Vet Pathol 52:862–872. https://doi.org/10.1177/0300985814559399

93. Etiology and Pathogenesis of Osteochondrosis - B. Ytrehus, C. S. Carlson, S. Ekman, 2007. https://journals.sagepub.com/doi/10.1354/vp.44-4-429. Accessed 19 Aug 2025

94. Mol BV, Janssens S, Meyermans R, Chapard L, Oosterlinck M, Pille F, Buys N (2026) Leveraging Joint-Specific Phenotypes for Genome-Wide Association Studies and SNP Heritability Estimation of Equine Osteochondrosis and Fetlock Osteochondral Fragments

95. Russell J, Matika O, Russell T, Reardon RJM (2017) Heritability and prevalence of selected osteochondrosis lesions in yearling Thoroughbred horses. Equine Vet J 49:282–287. https://doi.org/10.1111/evj.12613

96. McIlwraith CW (2004) Developmental orthopedic disease: problems of limbs in young horses. J Equine Vet Sci 24:475–479. https://doi.org/10.1016/j.jevs.2004.10.004

97. Kane AJ, McIlwraith CW, Park RD, Rantanen NW, Morehead JP, Bramlage LR (2003) Radiographic changes in Thoroughbred yearlings. Part 2: Associations with racing performance. Equine Vet J 35:366–374. https://doi.org/10.2746/042516403776014307

98. Yovich JV, McIlwraith CW, Stashak TS (1985) Osteochondritis dissecans of the sagittal ridge of the third metacarpal and metatarsal bones in horses. J Am Vet Med Assoc 186:1186–1191

99. Butler J, Colles C, Dyson S, Kold S, Poulos P (2017) Metacarpophalangeal and metatarsophalangeal (fetlock) joints. In: Butler J, Colles C, Dyson S, Kold S, Poulos P (eds) Clinical Radiology of the Horse, 4th ed. John Wiley & Sons Ltd, West Sussex, pp 175–213

100. Bramlage L (2009) Part I: Operative Orthopedics of the Fetlock Joint of the Horse: Traumatic and Developmental Diseases of the Equine Fetlock Joint. In: Proceedings of the Annual Convention of the American Association of Equine Practitioners. American Association of Equine Practitioners, Las Vegas, Nevada

101. Wright IM, Minshall GJ (2014) Identification and treatment of osteochondritis dissecans of the distal sagittal ridge of the third metacarpal bone. Equine Vet J 46:585–588. https://doi.org/10.1111/evj.12187

102. Carmalt JL, Borg H, Näslund H, Waldner C (2014) Racing performance of Swedish Standardbred trotting horses with proximal palmar/plantar first phalangeal (Birkeland)

fragments compared to fragment free controls. Vet J 202:43–47. https://doi.org/10.1016/j.tvjl.2014.07.017

103. Lloyd KA, Ayodele BA, Hitchens PL, Beck C, Mackie EJ, Whitton RC (2020) Associations between the radiographic appearance of vascular channels in proximal sesamoid bones, their microstructural characteristics and past racing performance in Thoroughbreds. Equine Vet J 52:670–677. https://doi.org/10.1111/evj.13239

104. Peat FJ, Kawcak CE, McIlwraith CW, Keenan DP, Berk JT, Mork DS (2025) Radiological findings in the proximal sesamoid bones of yearling and 2-year-old Thoroughbred sales horses: Prevalence, progression and associations with racing performance. Equine Vet J 57:87–100. https://doi.org/10.1111/evj.14051

105. H. Neundorf R, B. Lowerison M, M. Cruz A, J. Thomason J, J. McEwen B, B. Hurtig M (2010) Determination of the prevalence and severity of metacarpophalangeal joint osteoarthritis in Thoroughbred racehorses via quantitative macroscopic evaluation. Am J Vet Res 71:1284–1293. https://doi.org/10.2460/ajvr.71.11.1284

106. Pool R (1995) Joint disease in the athletic horse: a review of pathologic findings and pathogenesis. In: Proceedings of the Annual Convention of the American Association of Equine Practitioners. American Association of Equine Practitioners, Lexington, Kentucky, pp 20–34

107. Pool, RR (1996) Pathologic manifestations of joint disease in the athletic horse. In: McIlwraith CW, Trotter G (eds) Joint disease in the horse, 1st ed. Saunders, Philadelphia, pp 87–104

108. Johnston SA (1997) Osteoarthritis. Vet Clin North Am Small Anim Pract 27:699–723. https://doi.org/10.1016/S0195-5616(97)50076-3

109. Brommer H, Brama PAJ, Barneveld A, Van Weeren PR (2004) Differences in the topographical distribution of articular cartilage degeneration between equine metacarpo- and metatarsophalangeal joints. Equine Vet J 36:506–510. https://doi.org/10.2746/0425164044877369

110. Strand E, Martin GS, Crawford MP, Kamerling SG, Burba DJ (1998) Intra-articular pressure, elastance and range of motion in healthy and injured racehorse metacarpophalangeal joints. Equine Vet J 30:520–527. https://doi.org/10.1111/j.2042-3306.1998.tb04528.x

111. Bassage II L, Ross, MW (2011) Diagnostic analgesia. In: Ross M, Dyson S (eds) Diagnosis and Management of Lameness in the Horse, 2nd ed. Elsevier Saunders, St. Louis, pp 100–135

112. Young BD, Samii VF, Mattoon JS, Weisbrode SE, Bertone AL (2007) Subchondral bone density and cartilage degeneration patterns in osteoarthritic metacarpal condyles of horses. Am J Vet Res 68:841–849. https://doi.org/10.2460/ajvr.68.8.841

113. Olive J, D'Anjou M-A, Alexander K, Laverty S, Theoret C (2010) Comparison of magnetic resonance imaging, computed tomography, and radiography for assessment of noncartilaginous changes in equine metacarpophalangeal osteoarthritis. Vet Radiol Ultrasound 51:267–279. https://doi.org/10.1111/j.1740-8261.2009.01653.x

114. Lacourt M, Gao C, Li A, Girard C, Beauchamp G, Henderson JE, Laverty S (2012) Relationship between cartilage and subchondral bone lesions in repetitive impact trauma-induced equine osteoarthritis. Osteoarthritis Cartilage 20:572–583. https://doi.org/10.1016/j.joca.2012.02.004

115. Evrard L, Audigié F, Bertoni L, Jacquet S, Denoix J-M, Busoni V (2019) Low field magnetic resonance imaging of the equine distal interphalangeal joint: Comparison between weight-bearing and non-weight-bearing conditions. PLOS ONE 14:e0211101. https://doi.org/10.1371/journal.pone.0211101

116. Cauvin E, Smith, R (2014) Ultrasonography of the Fetlock. In: Kidd J, Lu K, Frazer M (eds) Atlas of Equine Ultrasonography, 1st ed. John Wiley & Sons Ltd, West Sussex

117. Hoey S, Fogarty U, McAllister H, Puggioni A, Cloak B, Richard H, Skelly C, Laverty S (2025) Ultrasonographic assessment of equine metacarpal cartilage thickness is more accurate than computed tomographic arthrography. Vet Radiol Ultrasound 66:e13444. https://doi.org/10.1111/vru.13444

118. Olive J (2010) Distal interphalangeal articular cartilage assessment using low-field magnetic resonance imaging. Vet Radiol Ultrasound 51:259–266. https://doi.org/10.1111/j.1740-8261.2009.01663.x

119. van Zadelhoff C, Schwarz T, Smith S, Engerand A, Taylor S (2019) Identification of Naturally Occurring Cartilage Damage in the Equine Distal Interphalangeal Joint Using Low-Field Magnetic Resonance Imaging and Magnetic Resonance Arthrography. Front Vet Sci 6:508. https://doi.org/10.3389/fvets.2019.00508

120. Smith MA, Dyson SJ, Murray RC (2012) Reliability of high- and low-field magnetic resonance imaging systems for detection of cartilage and bone lesions in the equine cadaver fetlock. Equine Vet J 44:684–691. https://doi.org/10.1111/j.2042-3306.2012.00561.x

121. Pinchbeck GL, Clegg PD, Boyde A, Riggs CM (2013) Pathological and clinical features associated with palmar/plantar osteochondral disease of the metacarpo/metatarsophalangeal joint in T horoughbred racehorses. Equine Vet J 45:587–592. https://doi.org/10.1111/evj.12036

122. Whitton RC, Ayodele BA, Hitchens PL, Mackie EJ (2018) Subchondral bone microdamage accumulation in distal metacarpus of Thoroughbred racehorses. Equine Vet J 50:766–773. https://doi.org/10.1111/evj.12948

123. Riggs CM, Whitehouse GH, Boyde A (1999) Pathology of the distal condyles of the third metacarpal and third metatarsal bones of the horse. Equine Vet J 31:140–148. https://doi.org/10.1111/j.2042-3306.1999.tb03807.x

124. Radtke CL, Danova NA, Scollay MC, Santschi EM, Markel MD, Gómez TDC, Muir P (2003) Macroscopic changes in the distal ends of the third metacarpal and metatarsal bones of Thoroughbred racehorses with condylar fractures. Am J Vet Res 64:1110–1116. https://doi.org/10.2460/ajvr.2003.64.1110

125. Powell SE (2012) Low-field standing magnetic resonance imaging findings of the metacarpo/metatarsophalangeal joint of racing Thoroughbreds with lameness localised to the region: a retrospective study of 131 horses. Equine Vet J 44:169–177. https://doi.org/10.1111/j.2042-3306.2011.00389.x

126. Ramzan PHL (2021) Mind the gaps: The science of POD and the racehorse fetlock. Equine Vet J 53:217–220. https://doi.org/10.1111/evj.13369

127. Trope GD, Anderson GA, Whitton RC (2011) Patterns of scintigraphic uptake in the fetlock joint of Thoroughbred racehorses and the effect of increased radiopharmaceutical uptake in the distal metacarpal/tarsal condyle on performance. Equine Vet J 43:509–515. https://doi.org/10.1111/j.2042-3306.2010.00316.x

128. Beck C, Hitchens PL, Muir P, Whitton RC (2025) Computed tomography features of the fetlock joint in elite racing Thoroughbred horses. Equine Vet J evj.70106. https://doi.org/10.1111/evj.70106

129. Ramzan PHL, Powell SE (2010) Clinical and imaging features of suspected prodromal fracture of the proximal phalanx in three Thoroughbred racehorses. Equine Vet J 42:164–169. https://doi.org/10.2746/042516409X478695

130. Ramzan PHL (2009) Transverse stress fracture of the distal diaphysis of the third metacarpus in six Thoroughbred racehorses. Equine Vet J 41:602–605. https://doi.org/10.2746/042516409X444764

131. Shan R, Johnston AS, Rosanowski SM, O'Shea J, Riggs CM (2022) Stress fracture of the palmar, distal cortex of the third metacarpal bone: A diagnostic challenge with a good prognosis. Equine Vet J 54:74–81. https://doi.org/10.1111/evj.13426

132. Dubois M-S, Morello S, Rayment K, Markel MD, Vanderby R, Kalscheur VL, Hao Z, McCabe RP, Marquis P, Muir P (2014) Computed Tomographic Imaging of Subchondral Fatigue Cracks in the Distal End of the Third Metacarpal Bone in the Thoroughbred Racehorse Can Predict Crack Micromotion in an Ex-Vivo Model. PLoS ONE 9:e101230. https://doi.org/10.1371/journal.pone.0101230

133. Shaffer SK, To C, Garcia TC, Fyhrie DP, Uzal FA, Stover SM (2021) Subchondral focal osteopenia associated with proximal sesamoid bone fracture in Thoroughbred racehorses. Equine Vet J 53:294–305. https://doi.org/10.1111/evj.13291

134. Smith MRW, Wright IM (2014) Are there radiologically identifiable prodromal changes in T horoughbred racehorses with parasagittal fractures of the proximal phalanx? Equine Vet J 46:88–91. https://doi.org/10.1111/evj.12093

135. Ramzan PHL, Palmer L, Powell SE (2015) Unicortical condylar fracture of the T horoughbred fetlock: 45 cases (2006–2013). Equine Vet J 47:680–683. https://doi.org/10.1111/evj.12349

136. Brown HR, Peloso JG, Clay-Werner W, Mecholsky JJ, Cohen ND, Vogler JB (2019) A Thoroughbred racehorse with a unicortical palmar lateral condylar fracture returned to training 14 days after surgery: a hypothesis on the role of a single bone screw on crack propagation. J Equine Sci 30:7–12. https://doi.org/10.1294/jes.30.7

137. Tranquille CA, Murray RC, Parkin TDH (2017) Can we use subchondral bone thickness on high-field magnetic resonance images to identify Thoroughbred racehorses at risk of catastrophic lateral condylar fracture? Equine Vet J 49:167–171. https://doi.org/10.1111/evj.12574

138. Tranquille CA, Parkin TDH, Murray RC (2012) Magnetic resonance imaging-detected adaptation and pathology in the distal condyles of the third metacarpus, associated with lateral condylar fracture in Thoroughbred racehorses. Equine Vet J 44:699–706. https://doi.org/10.1111/j.2042-3306.2011.00535.x

139. Bassage LH, Richardson DW (1998) Longitudinal fractures of the condyles of the third metacarpal and metatarsal bones in racehorses: 224 cases (1986-1995). J Am Vet Med Assoc 212:1757–1764

140. Cianci JM, Wulster KB, Richardson DW, Stefanovski D, Ortved KF (2022) Computed tomographic assessment of fracture characteristics and subchondral bone injury in Thoroughbred racehorses with lateral condylar fractures and their relationship to outcome. Vet Surg 51:426–437. https://doi.org/10.1111/vsu.13770

141. O'Brien TR, Hornof WJ, Meagher DM (1981) Radiographic detection and characterization of palmar lesions in the equine fetlock joint. J Am Vet Med Assoc 178:231–237

142. Gray SN, Spriet M, Garcia TC, Uzal FA, Stover SM (2017) Preexisting lesions associated with complete diaphyseal fractures of the third metacarpal bone in 12 Thoroughbred racehorses. J Vet Diagn Invest 29:437–441. https://doi.org/10.1177/1040638717704866

143. Ramzan PHL, Palmer L (2011) Musculoskeletal injuries in Thoroughbred racehorses: A study of three large training yards in Newmarket, UK (2005–2007). Vet J 187:325–329. https://doi.org/10.1016/j.tvjl.2009.12.019

144. Bathe A (1994) 245 Fractures in Thoroughbred racehorses: results of a 2-year prospective study in Newmarket. In: Proceedings of the Annual Convention of the

American Association of Equine Practitioners. American Association of Equine Practitioners, Vancouver, Kanada, p 175

145. Smith MRW, Wright IM (2014) Radiographic configuration and healing of 121 fractures of the proximal phalanx in 120 T horoughbred racehorses (2007–2011). Equine Vet J 46:81–87. https://doi.org/10.1111/evj.12094

146. Kraus BM, Richardson DW, Nunamaker DM, Ross MW (2004) Management of comminuted fractures of the proximal phalanx in horses: 64 cases (1983–2001). J Am Vet Med Assoc 224:254–263. https://doi.org/10.2460/javma.2004.224.254

147. Ruggles A (2011) The Proximal and Middle Phalanges and Proximal Interphalangeal Joint. In: Dyson S, Ross M (eds) Diagnosis and Management of Lameness in the Horse, 2nd ed. Elsevier Saunders, St. Louis, pp 387–393

148. Nixon AJ (2019) Phalanges and the Metacarpophalangeal and Metatarsophalangeal Joints. In: Equine Surgery, 5th ed. Elsevier, St. Louis, pp 1587–1618

149. Busschers E, Richardson DW, Hogan PM, Leitch M (2008) Surgical repair of mid-body proximal sesamoid bone fractures in 25 horses. Vet Surg 37:771–780. https://doi.org/10.1111/j.1532-950X.2008.00445.x

150. Findley J, Hewitt-Dedman C (2024) Diagnosis and management of stress fractures and fatigue injuries in horses. UK-Vet Equine 8:58–64. https://doi.org/10.12968/ukve.2024.8.2.58

151. Pilsworth, R.C. (2011) The European Thoroughbred. In: Mike W. R, Sue J. D (eds) Diagnosis and Management of Lameness in the Horse, 2nd ed. Elsevier Saunders, St. Louis, pp 994–1013

152. Nagy A, Bodo G, Dyson SJ, Szabo F, Barr ARS (2009) Diffusion of contrast medium after perineural injection of the palmar nerves: an in vivo and in vitro study. Equine Vet J 41:379–383. https://doi.org/10.2746/042516409x372502

153. Malton R, Nagy A (2015) Clinical Research Abstracts of the British Equine Veterinary Association Congress 2015. Equine Vet J 47 Suppl 48:15. https://doi.org/10.1111/evj.12486_33

154. McIlwraith CW, Frisbie D, Kawcak CE, Weeren P van (2016) General Anatomy and Physiology of Joints. In: McIlwraith CW, Kawcak CE (eds) Joint disease in the horse, 2nd ed. Elsevier Saunders, St. Louis, pp 1–24

155. Schumacher J, Schramme MC, Schumacher J, DeGraves FJ (2013) Diagnostic analgesia of the equine digit. Equine Vet Educ 25:408–421. https://doi.org/10.1111/eve.12001

156. Pilsworth R, Dyson S (2015) Where does it hurt? Problems with interpretation of regional and intra-synovial diagnostic analgesia. Equine Vet Educ 27:595–603. https://doi.org/10.1111/eve.12392

157. McKnight AL (2004) Digital Radiography in Equine Practice. Clin Tech Equine Pract 3:352–360. https://doi.org/10.1053/j.ctep.2005.02.013

158. Kane AJ, Park RD, McIlwraith CW, Rantanen NW, Morehead JP, Bramlage LR (2003) Radiographic changes in Thoroughbred yearlings. Part 1: Prevalence at the time of the yearling sales. Equine Vet J 35:354–365. https://doi.org/10.2746/042516403776014280

159. Meagher DM, Bromberek JL, Meagher DT, Gardner IA, Puchalski SM, Stover SM (2013) Prevalence of abnormal radiographic findings in 2-year-old Thoroughbreds at in-training sales and associations with racing performance. J Am Vet Med Assoc 242:969–976. https://doi.org/10.2460/javma.242.7.969

160. Morgan JW, Santschi EM, Zekas LJ, Scollay-Ward MC, Markel MD, Radtke CL, Sample SJ, Keuler NS, Muir P (2006) Comparison of radiography and computed tomography to evaluate metacarpo/metatarsophalangeal joint pathology of paired limbs of thoroughbred racehorses with severe condylar fracture. Vet Surg 35:611–617. https://doi.org/10.1111/j.1532-950X.2006.00198.x

161. Irandoust S, O'Neil LM, Stevenson CM, Franseen FM, Ramzan PHL, Powell SE, Brounts SH, Loeber SJ, Ergun DL, Whitton RC, Henak CR, Muir P (2025) Comparison of radiography and computed tomography for identification of third metacarpal structural change and associated assessment of condylar stress fracture risk in Thoroughbred racehorses. Equine Vet J 57:723–736. https://doi.org/10.1111/evj.14131

162. Denoix J-M, Audigié, Fabrice (2001) Ultrasonographic Examination of Joints in Horses. In: Proceedings of the Annual Convention of the American Association of Equine Practitioners. American Association of Equine Practitioners, San Diego

163. Hoey S, McAllister H, Laverty S, O'Sullivan J, Toomey W, Connolly S, Skelly C (2025) Screening ultrasonographic findings of Thoroughbred weanling horses show agreement with concurrent radiographic examination and with subsequent yearling sales radiographs. Equine Vet Educ 37:148–160. https://doi.org/10.1111/eve.13994

164. Denoix JM, Jacot S, Bousseau B, Perrot P (1996) Ultrasonographic anatomy of the dorsal and abaxial aspects of the equine fetlock. Equine Vet J 28:54–62. https://doi.org/10.1111/j.2042-3306.1996.tb01590.x

165. Gonzalez LM, Schramme MC, Robertson ID, Thrall DE, Redding RW (2010) MRI features of metacarpo(tarso)phalangeal region lameness in 40 horses. Vet Radiol Ultrasound 51:404–414. https://doi.org/10.1111/j.1740-8261.2010.01676.x

166. Murray R, Werpy N (2010) Image interpretation and artefacts. In: Murray RC (ed) Equine MRI, 1st ed. Wiley, Chichester, UK, pp 101–145

167. Byrne CA, Marshall JF, Voute LC (2021) Clinical magnetic resonance image quality of the equine foot is significantly influenced by acquisition system. Equine Vet J 53:469–480. https://doi.org/10.1111/evj.13330

168. Peloso JG, Vogler Iii JB, Cohen ND, Marquis P, Hilt L (2015) Association of catastrophic biaxial fracture of the proximal sesamoid bones with bony changes of the metacarpophalangeal joint identified by standing magnetic resonance imaging in cadaveric forelimbs of Thoroughbred racehorses. J Am Vet Med Assoc 246:661–673. https://doi.org/10.2460/javma.246.6.661

169. Lin S-T, Bolas NM, Sargan DR, Restif O, Peter VG, Pokora R, Patrick H, Foote AK, Murray RC (2024) Comparison of cone-beam and fan-beam computed tomography and low-field magnetic resonance imaging for detection of proximal phalanx dorsoproximal osteochondral defects. Equine Vet J 56:484–493. https://doi.org/10.1111/evj.13973

170. Sampson SN, Schneider RK, Tucker RL, Gavin PR, Zubrod CJ, Ho CP (2007) Magnetic resonance imaging features of oblique and straight distal sesamoidean desmitis in 27 horses. Vet Radiol Ultrasound 48:303–311. https://doi.org/10.1111/j.1740-8261.2007.00247.x

171. Dyson S, Murray, R. C. (2007) Magnetic Resonance Imaging of the Equine Fetlock. Clin Tech Equine Pract 6:62–77

172. King JN, Zubrod CJ, Schneider RK, Sampson SN, Roberts G (2013) MRI findings in 232 horses with lameness localized to the metacarpo(tarso)phalangeal region and without a radiographic diagnosis. Vet Radiol Ultrasound 54:36–47. https://doi.org/10.1111/j.1740-8261.2012.01983.x

173. Magnetic resonance imaging of the distal limb of the standing horse - Mair - 2005 - Equine Veterinary Education - Wiley Online Library. https://beva.onlinelibrary.wiley.com/doi/10.1111/j.2042-3292.2005.tb00340.x. Accessed 20 Aug 2025

174. Miracle AC, Mukherji SK (2009) Conebeam CT of the head and neck, part 1: physical principles. Am J Neuroradiol 30:1088–1095. https://doi.org/10.3174/ajnr.A1653

175. Lechuga L, Weidlich GA (2016) Cone Beam CT vs. Fan Beam CT: A Comparison of Image Quality and Dose Delivered Between Two Differing CT Imaging Modalities. Cureus 8:e778. https://doi.org/10.7759/cureus.778

176. Stewart HL, Siewerdsen JH, Nelson BB, Kawcak CE (2021) Use of cone-beam computed tomography for advanced imaging of the equine patient. Equine Vet J 53:872–885. https://doi.org/10.1111/evj.13473

177. Zhao W, Vernekohl D, Zhu J, Wang L, Xing L (2016) A model-based scatter artifacts correction for cone beam CT. Med Phys 43:1736–1753. https://doi.org/10.1118/1.4943796

178. Lin S-T, Bolas NM, Peter VG, Pokora R, Patrick H, Foote AK, Sargan DR, Murray RC (2024) Comparison of cone-beam and fan-beam computed tomography and low-field magnetic resonance imaging for detection of palmar/plantar osteochondral disease in Thoroughbred horses. Equine Vet J 56:999–1007. https://doi.org/10.1111/evj.14023

179. Bregger MDK, Koch C, Zimmermann R, Sangiorgio D, Schweizer-Gorgas D (2019) Cone-beam computed tomography of the head in standing equids. BMC Vet Res 15:289. https://doi.org/10.1186/s12917-019-2045-z

180. Koch C, Pauwels F, Schweizer-Gorgas D (2021) Technical set-up and case illustrations of orthopaedic cone beam computed tomography in the standing horse. Equine Vet Educ 33:255–262. https://doi.org/10.1111/eve.13290

181. Stewart HL, Siewerdsen JH, Selberg KT, Bills KW, Kawcak CE (2023) Cone-beam computed tomography produces images of numerically comparable diagnostic quality for bone and inferior quality for soft tissues compared with fan-beam computed tomography in cadaveric equine metacarpophalangeal joints. Vet Radiol Ultrasound 64:1033–1036. https://doi.org/10.1111/vru.13309

182. van Zadelhoff C, Liuti T, Dixon PM, Reardon RJM (2021) Multidetector CT and cone-beam CT have substantial agreement in detecting dental and sinus abnormalities in equine cadaver heads. Vet Radiol Ultrasound 62:413–420. https://doi.org/10.1111/vru.12978

183. Bierau J, Cruz AM, Koch C, Manso-Diaz G, Büttner K, Staszyk C, Röcken M (2023) Visualization of anatomical structures in the fetlock region of the horse using cone beam computed tomography in comparison with conventional multidetector computed tomography. Front Vet Sci 10:1278148. https://doi.org/10.3389/fvets.2023.1278148

184. Brounts SH, Lund JR, Whitton RC, Ergun DL, Muir P (2022) Use of a novel helical fan beam imaging system for computed tomography of the distal limb in sedated standing horses: 167 cases (2019-2020). J Am Vet Med Assoc 260:1351–1360. https://doi.org/10.2460/javma.21.10.0439

185. Computed tomographic evaluation of the distal limb in the standing sedated horse: Technique, imaging diagnoses, feasibility, and artifacts - Mathee - 2023 - Veterinary Radiology & Ultrasound - Wiley Online Library. https://onlinelibrary.wiley.com/doi/10.1111/vru.13182. Accessed 19 Aug 2025

186. Ciamillo SA, Wulster KB, Gassert TM, Richardson DW, Brown KA, Stefanovski D, Ortved KF (2025) Prospective, longitudinal assessment of subchondral bone morphology and pathology using standing, cone-beam computed tomography in fetlock joints of 2-year-old Thoroughbred racehorses in their first year of training. Equine Vet J 57:126–139. https://doi.org/10.1111/evj.14048

187. Ciamillo SA, Bills KW, Gassert TM, Richardson DW, Brown KA, Stefanovski D, Ortved KF (2025) Effect of high-speed exercise on subchondral bone in the

metacarpo−/metatarsophalangeal joints of 2-year-old Thoroughbred racehorses in their first year of training. Equine Vet J evj.14524. https://doi.org/10.1111/evj.14524

188. Spriet M (2022) Positron emission tomography: a horse in the musculoskeletal imaging race. Am J Vet Res 83:ajvr.22.03.0051. https://doi.org/10.2460/ajvr.22.03.0051

189. Curtiss AL, Ortved KF, Dallap-Schaer B, Gouzeev S, Stefanovski D, Richardson DW, Wulster KB (2021) Validation of standing cone beam computed tomography for diagnosing subchondral fetlock pathology in the Thoroughbred racehorse. Equine Vet J 53:510–523. https://doi.org/10.1111/evj.13414

190. Jones J, Porter AH, Niknejad MT (2009) Spatial resolution. In: Radiopaedia.org. Radiopaedia.org

191. Niknejad MT, Bell D, Luijkx T (2013) Contrast resolution. In: Radiopaedia.org. Radiopaedia.org

192. Goldman LW (2007) Principles of CT: Radiation Dose and Image Quality. J Nucl Med Technol 35:213–225. https://doi.org/10.2967/jnmt.106.037846

193. Winter MD, Berry CR, Reese DJ (2010) Nuclear scintigraphy in horses. Compend Contin Educ Vet 32:E5

194. Weaver MP (1995) Twenty years of equine scintigraphy--a coming of age? Equine Vet J 27:163–165. https://doi.org/10.1111/j.2042-3306.1995.tb03057.x

195. Dyson S (2014) Musculoskeletal scintigraphy of the equine athlete. Semin Nucl Med 44:4–14. https://doi.org/10.1053/j.semnuclmed.2013.08.003

196. O'Neill H, Fraser B (2009) Equine scintigraphy: Part 1 Basic principles, the generation of images and radiation safety. Companion Anim 14:11–14. https://doi.org/10.1111/j.2044-3862.2009.tb00324.x

197. MacKinnon MC, Bonder D, Boston RC, Ross MW (2015) Analysis of stress fractures associated with lameness in Thoroughbred flat racehorses training on different track surfaces undergoing nuclear scintigraphic examination. Equine Vet J 47:296–301. https://doi.org/10.1111/evj.12285

198. Spriet M, Arndt S, Pige C, Pye J, O'Brion J, Carpenter R, Blea J, Dowd JP (2023) Comparison of skeletal scintigraphy and standing 18 F-NaF positron emission tomography for imaging of the fetlock in 33 Thoroughbred racehorses. Vet Radiol Ultrasound 64:123–130. https://doi.org/10.1111/vru.13169

199. Spriet M, Espinosa-Mur P, Cissell DD, Phillips KL, Arino-Estrada G, Beylin D, Stepanov P, Katzman SA, Galuppo LD, Garcia-Nolen T, Murphy B, Stover SM (2019) 18 F-sodium fluoride positron emission tomography of the racing Thoroughbred fetlock: Validation and comparison with other imaging modalities in nine horses. Equine Vet J 51:375–383. https://doi.org/10.1111/evj.13019

200. Pye J, Spriet M, O'Brion J, Carpenter R, Blea JA, Dowd JP (2022) Longitudinal monitoring of fetlock lesions in Thoroughbred racehorses using standing 18F-sodium fluoride positron emission tomography. Am J Vet Res 83:ajvr.22.03.0062. https://doi.org/10.2460/ajvr.22.03.0062

201. Howard B, Embertson R, Rantanen NW, Bramlage L (1992) Survey radiographic findings in Thoroughbred sales yearlings. In: Proceedings of the Annual Convention of the American Association of Equine Practitioners. American Association of Equine Practitioners, Anaheim, California, USA, pp 397–402

202. Scott N, Hance S, Todhunter P, Adams P, Adkins A (2005) Incidence of radiographic changes in Thoroughbred yearlings. 755 cases. In: Pagan J (ed) Advances in Equine Nutrition III. Nottingham University Press, Notthingham, UK, p 347

203. Preston SA, Zimmel DN, Chmielewski TL, Trumble TN, Brown MP, Boneau JC, Hernandez JA (2010) Prevalence of various presale radiographic findings and association of findings with sales price in Thoroughbred yearlings sold in Kentucky. J Am Vet Med Assoc 236:440–445. https://doi.org/10.2460/javma.236.4.440

204. Furniss C, Carstens A, Berg SSV den (2011) Radiographic changes in Thoroughbred yearlings in South Africa. J S Afr Vet Assoc 82:194–204. https://doi.org/10.4102/jsava.v82i4.74

205. Cohen ND, Carter GK, Watkins JP, O'Conor MS (2006) Association of racing performance with specific abnormal radiographic findings in Thoroughbred yearlings sold in Texas. J Equine Vet Sci 26:462–474. https://doi.org/10.1016/j.jevs.2006.08.004

206. Spike-Pierce DL, Bramlage LR (2003) Correlation of racing performance with radiographic changes in the proximal sesamoid bones of 487 Thoroughbred yearlings. Equine Vet J 35:350–353. https://doi.org/10.2746/042516403776014262

207. Young DR, Nunamaker DM, Markel MD (1991) Quantitative evaluation of the remodeling response of the proximal sesamoid bones to training-related stimuli in Thoroughbreds. Am J Vet Res 52:1350–1356

208. Noordwijk KJ, Chen L, Ruspi BD, Schurer S, Papa B, Fasanello DC, McDonough SP, Palmer SE, Porter IR, Basran PS, Donnelly E, Reesink HL (2023) Metacarpophalangeal Joint Pathology and Bone Mineral Density Increase with Exercise but Not with Incidence of Proximal Sesamoid Bone Fracture in Thoroughbred Racehorses. Animals 13:827. https://doi.org/10.3390/ani13050827

209. Ayodele BA, Hitchens PL, Wong ASM, Mackie EJ, Whitton RC (2021) Microstructural properties of the proximal sesamoid bones of Thoroughbred racehorses in training. Equine Vet J 53:1169–1177. https://doi.org/10.1111/evj.13394

210. Beck C, Hitchens PL, Whitton RC (2025) Post-mortem computed tomography features associated with fracture of the fetlock joint in racing Thoroughbreds. Equine Vet J evj.14465. https://doi.org/10.1111/evj.14465

211. Trope GD, Ghasem-Zadeh A, Anderson GA, Mackie EJ, Whitton RC (2015) Can high-resolution peripheral quantitative computed tomography imaging of subchondral and cortical bone predict condylar fracture in Thoroughbred racehorses? Equine Vet J 47:428–432. https://doi.org/10.1111/evj.12312

212. Dyson S (2011) Can lameness be graded reliably? Equine Vet J 43:379–382. https://doi.org/10.1111/j.2042-3306.2011.00391.x

213. Papanikolaou N, Battista JJ, Boyer AL, Kappas C, Klein E, Mackie TR, Sharpe M, Dyk JV (2004) Tissue Inhomogeneity Corrections for Megavoltage Photon Beams. AAPM

214. Fedorov A, Beichel R, Kalpathy-Cramer J, Finet J, Fillion-Robin J-C, Pujol S, Bauer C, Jennings D, Fennessy F, Sonka M, Buatti J, Aylward S, Miller JV, Pieper S, Kikinis R (2012) 3D Slicer as an image computing platform for the Quantitative Imaging Network. Magn Reson Imaging 30:1323–1341. https://doi.org/10.1016/j.mri.2012.05.001

215. Greenway K, Campos A, Knipe H (2015) Hounsfield unit. In: Radiopaedia.org. Radiopaedia.org

216. R Core Team (2023) R: A Language and Environment for Statistical Computing

217. Brown H, Prescott R Applied Mixed Models in Medicine, 3rd ed. John Wiley & Sons Ltd, Hoboken, NJ, USA

218. Pinheiro J, Bates D (2000) Mixed-Effects Models in S and S-PLUS. Springer, New York, NY, USA

219. Pinheiro J, Bates D, R Core Team (2023) nlme: Linear and Nonlinear Mixed Effects Models

220. Hothorn T, Bretz F, Westfall P (2008) Simultaneous Inference in General Parametric Models. Biom J 50:346–363. https://doi.org/10.1002/bimj.200810425

221. Bates D, Mächler M, Bolker B, Walker S (2015) Fitting Linear Mixed-Effects Models Using **lme4**. J Stat Softw 67:. https://doi.org/10.18637/jss.v067.i01

222. Kuznetsova A, Brockhoff PB, Christensen RHB (2017) **lmerTest** Package: Tests in Linear Mixed Effects Models. J Stat Softw 82:. https://doi.org/10.18637/jss.v082.i13

223. Chan YH (2003) Biostatistics 104: correlational analysis. Singapore Med J 44:614–619

224. Crookshank M, Ploeg H-L, Ellis R, MacIntyre NJ (2014) Repeatable calibration of Hounsfield units to mineral density and effect of scanning medium. Adv Biomech Appl 1:15–22. https://doi.org/10.12989/ABA.2013.1.1.015

225. Beck C, Morrice-West AV, Muir P, Hitchens PL, Whitton RC (2025) Quantification of the difference in hounsfield units of an electron density phantom between a conventional and standing computed tomography machine. Vet Res Commun 49:228. https://doi.org/10.1007/s11259-025-10789-7

226. Prevrhal S, Engelke K, Kalender WA (1999) Accuracy limits for the determination of cortical width and density: the influence of object size and CT imaging parameters. Phys Med Biol 44:751–764. https://doi.org/10.1088/0031-9155/44/3/017

227. Lee S-W, Lee C-L, Cho H-M, Park H-S, Kim D-H, Choi Y-N, Kim H-J (2011) Effects of Reconstruction Parameters on Image Noise and Spatial Resolution in Cone-beam Computed Tomography. J Korean Phys Soc 59:2825–2832. https://doi.org/10.3938/jkps.59.2825

228. Burghardt AJ, Link TM, Majumdar S (2011) High-resolution computed tomography for clinical imaging of bone microarchitecture. Clin Orthop 469:2179–2193. https://doi.org/10.1007/s11999-010-1766-x

229. Riggs CM, Whitehouse GH, Boyde A (1999) Structural variation of the distal condyles of the third metacarpal and third metatarsal bones in the horse. Equine Vet J 31:130–139. https://doi.org/10.1111/j.2042-3306.1999.tb03806.x

230. Boyde A, Haroon Y, Jones SJ, Riggs CM (1999) Three dimensional structure of the distal condyles of the third metacarpal bone of the horse. Equine Vet J 31:122–129. https://doi.org/10.1111/j.2042-3306.1999.tb03805.x

231. Riggs CM, Boyde A (1999) Effect of exercise on bone density in distal regions of the equine third metacarpal bone in 2-year-old Thoroughbreds. Equine Vet J 31:555–560. https://doi.org/10.1111/j.2042-3306.1999.tb05283.x

232. Shaffer SK, Garcia TC, Stover SM, Fyhrie DP (2022) Exercise history predicts focal differences in bone volume fraction, mineral density and microdamage in the proximal sesamoid bones of Thoroughbred racehorses. J Orthop Res 40:2831–2842. https://doi.org/10.1002/jor.25312

233. Shaffer SK, Stover SM, Fyhrie DP (2023) Training drives turnover rates in racehorse proximal sesamoid bones. Sci Rep 13:205. https://doi.org/10.1038/s41598-022-26027-y

234. Boros K, Dyson S, Kovács Á, Lang Z, Nagy A (2024) Computed Tomographic Evaluation of the Sagittal Ridge of the Third Metacarpal Bone in Young Thoroughbred Racehorses: A Longitudinal Study. Animals 14:812. https://doi.org/10.3390/ani14050812

235. Anthenill LA, Gardner IA, Pool RR, Garcia TC, Stover SM (2010) Comparison of macrostructural and microstructural bone features in Thoroughbred racehorses with and without midbody fracture of the proximal sesamoid bone. Am J Vet Res 71:755–765. https://doi.org/10.2460/ajvr.71.7.755

236. Shaffer SK, Shelly K, Garcia TC, Samol MA, Hill AE, Fyhrie DP, Stover SM (2022) In vitro motions of the medial and lateral proximal sesamoid bones under mid-stance load conditions are consistent with racehorse fracture configurations. J Biomech 130:110888. https://doi.org/10.1016/j.jbiomech.2021.110888

237. Harrison SM, Chris Whitton R, Kawcak CE, Stover SM, Pandy MG (2014) Evaluation of a subject-specific finite-element model of the equine metacarpophalangeal joint under physiological load. J Biomech 47:65–73. https://doi.org/10.1016/j.jbiomech.2013.10.001

238. Parkin TDH, Clegg PD, French NP, Proudman CJ, Riggs CM, Singer ER, Webbon PM, Morgan KL (2006) Catastrophic fracture of the lateral condyle of the third metacarpus/metatarsus in UK racehorses – fracture descriptions and pre-existing pathology. Vet J 171:157–165. https://doi.org/10.1016/j.tvjl.2004.10.009

239. Jacklin BD, Wright IM (2012) Frequency distributions of 174 fractures of the distal condyles of the third metacarpal and metatarsal bones in 167 Thoroughbred racehorses (1999-2009). Equine Vet J 44:707–713. https://doi.org/10.1111/j.2042-3306.2012.00558.x

240. Pratt-Phillips S, Munjizun A (2023) Impacts of Adiposity on Exercise Performance in Horses. Animals 13:666. https://doi.org/10.3390/ani13040666

241. Ross, MW (1998) Observations in horses with lameness abolished by palmar digital analgesia. In: Proceedings of the Annual Convention of the American Association of Equine Practitioners. American Association of Equine Practitioners, Baltimore, Maryland, USA, pp 230–232

242. Cornelissen BP, Buma P, Rijkenhuizen AB, Barneveld A (1998) Innervation of the equine mature and immature proximal sesamoid bone by calcitonin gene-related peptide and substance P-containing nerves. Am J Vet Res 59:1378–1385

243. Schumacher J, Livesey L, De Graves FJ, Schumacher J, Schramme MC, Hathcock J, Taintor J, Gomez J (2004) Effect of anaesthesia of the palmar digital nerves on proximal interphalangeal joint pain in the horse. Equine Vet J 36:409–414. https://doi.org/10.2746/0425164044868404

244. Mageed M (2022) Standing computed tomography of the equine limb using a multi-slice helical scanner: Technique and feasibility study. Equine Vet Educ 34:77–83. https://doi.org/10.1111/eve.13388

245. Semevolos SA (2017) Osteochondritis Dissecans Development. Vet Clin North Am Equine Pract 33:367–378. https://doi.org/10.1016/j.cveq.2017.03.009

246. Dik KJ, Enzerink E, Van Weeren PR (1999) Radiographic development of osteochondral abnormalities, in the hock and stifle of Dutch Warmblood foals, from age 1 to 11 months. Equine Vet J 31:9–15. https://doi.org/10.1111/j.2042-3306.1999.tb05308.x

247. Van Cauter R, Serteyn D, Lejeune J-P, Rousset A, Caudron I (2023) Evaluation of the appearance of osteochondrosis lesions by two radiographic examinations in sport horses aged from 12 to 36 months. PLOS ONE 18:e0286213. https://doi.org/10.1371/journal.pone.0286213

248. Fraser JA (1971) Some Conditions of the Proximal Sesamoid Bones in the Horse. Equine Vet J 3:20–24. https://doi.org/10.1111/j.2042-3306.1971.tb04434.x

249. Okudaira M, Cresswell EN, Wollman CW, McDonough SP, Engiles JB, Reesink HL (2024) Mineralization of equine proximal sesamoid bones precedes articular cartilage and fibrocartilaginous enthesis maturation in early postgestational development. Am J Vet Res 85:ajvr.24.04.0101. https://doi.org/10.2460/ajvr.24.04.0101

250. Rao T (2024) Understanding survivorship bias: implications for research and decision-making. J Emerg Technol Innov Res 11:604–612

251. Heederik D (2006) Micro-epidemiology of the healthy worker effect? Occup Environ Med 63:83–83. https://doi.org/10.1136/oem.2005.024307

12. Scientific publications

12.1 Publications in peer-reviewed journals related to the thesis

Boros K, Nagy A. Diseases of the fetlock joint in Thoroughbred racehorses. Part 1: The role of biomechanics and bone adaptation in the development of injuries. Literature review. Hungarian Veterinary Journal 2022;144:387-396.

Boros K, Nagy A. Diseases of the fetlock joint in Thoroughbred racehorses. Part 2: Articular and osseous abnormalities. Hungarian Veterinary Journal 2023;145:67-80.

Boros K; Dyson S, Kovács Á, Lang Z, Nagy A. Computed Tomographic Evaluation of the Sagittal Ridge of the Third Metacarpal Bone in Young Thoroughbred Racehorses: A Longitudinal Study. Animals. 2024;14(5):812. https://doi.org/10.3390/ani14050812

Boros K, Dyson S, Pollard D, Nagy A. A longitudinal study of radiodensity and radiographic appearance of the proximal sesamoid bones in Thoroughbred racehorses. Equine Vet J. 2026;58(4):946-958. https://doi.org/10.1111/evj.70075

12.2 Scientific posters, presentations

12.2.1 National

Boros K, Dyson S, Nagy A. Computed tomographic and radiographic findings in the metacarpophalangeal joints of non-lame Thoroughbred yearlings. Hungarian Association of Equine Practitioners Congress 2022, Vecsés , clinical research report

Boros K, Dyson S, Nagy A. Computed tomographic and radiographic findings in the metacarpophalangeal joints of non-lame Thoroughbred yearlings. Hungarian Academy of Sciences, Veterinary Science Committee; Doctoral School of Veterinary Science, Academic Reports 2023, Budapest, clinical research report

Boros K, Dyson S, Nagy A. Computed tomographic evaluation of the sagittal ridge of the third metacarpal bone in Thoroughbred racehorses in their first year of training: a longitudinal study. Hungarian Association of Equine Practitioners Congress 2023, Kecskemét, clinical research report

Boros K, Dyson S, Nagy A. Comparative diagnostic imaging of the metacarpophalangeal joints in Thoroughbred racehorses: a longitudinal study. Hungarian Academy of Sciences, Veterinary

Science Committee; Doctoral School of Veterinary Science, Academic Reports 2024, Budapest, clinical research report

Boros K, Dyson S, Nagy A. Computed tomographic evaluation of the sagittal ridge of the third metacarpal bone in Thoroughbred racehorses in their first year of training: a longitudinal study. Hungarian Symposium of Agricultural Doctoral Students 2024, Budapest, clinical research report

Boros K, Dyson S, Pollard D, Nagy A. Radiographic and computed tomographic evaluation of the proximal sesamoid bones in Thoroughbred racehorses: a longitudinal study. Hungarian Association of Equine Practitioners Congress 2024, Gárdony, clinical research report

Boros K, Dyson S, Pollard D, Nagy A. Radiographic and computed tomographic evaluation of the proximal sesamoid bones in Thoroughbred racehorses: a longitudinal study. Hungarian Academy of Sciences, Veterinary Science Committee; Doctoral School of Veterinary Science, Academic Reports 2025, Budapest, clinical research report

Boros K, Dyson S, Pollard D, Nagy A. Comparative magnetic resonance imaging and computed tomographic evaluation of the metacarpal condyles in Thoroughbred racehorses. University Research Scholarship Programme Conference 2025, Budapest, clinical research report

Boros K, Dyson S, Pollard D, Nagy A. Comparative magnetic resonance imaging and computed tomographic evaluation of the metacarpal condyles in Thoroughbred racehorses. Hungarian Academy of Sciences, Veterinary Science Committee; Doctoral School of Veterinary Science, Academic Reports 2026, Budapest, clinical research report

Boros K. MRI and CT findings in the fetlock joints of Thoroughbred racehorses. Hungarian Academy of Sciences, 200 Years of the Hungarian Academy of Sciences 2026, Budapest

12.2.2 International

Boros K, Dyson S, Nagy A. Computed tomographic and radiographic findings in the metacarpophalangeal joint of Thoroughbred yearlings. British Equine Veterinary Association Congress 2022, Liverpool, clinical abstract, https://doi.org/10.1111/evj.12_13855

Boros K, Dyson S, Nagy A. Computed tomographic evaluation of the sagittal ridge of the third metacarpal bone in Thoroughbred racehorses in their first year of training: a longitudinal study.

European College of Veterinary Sports Medicine and Rehabilitation Congress 2023, Paris, clinical abstract

Boros K, Dyson S, Pollard D, Nagy A. Radiographic and computed tomographic evaluation of the proximal sesamoid bones in Thoroughbred racehorses: a longitudinal study. European Veterinary Diagnostic Imaging Congress 2024, Athens, clinical abstract, https://doi.org/10.1111/vru.13470

Boros K, Pollard D, Nagy A. Longitudinal computed tomographic and magnetic resonance imaging evaluation of bone density changes in the metacarpal condyles of Thoroughbred racehorses. International Conference: Applying Science to the Care of the Thoroughbred Racehorse 2025, Hong Kong, poster presentation

Boros K, Dyson S, Pollard D, Nagy A. Comparative computed tomographic and magnetic resonance imaging evaluation of metacarpal condylar densification in Thoroughbred racehorses. British Equine Veterinary Association Congress 2026, Birmingham, clinical abstract

13. Supplementary material

	Diagnostic anaesthesia	Diagnosis	Total Diff Head (Vector Sum)	Diff Max Head Mean	Diff Max Head SD	Diff Min Head Mean	Diff Min Head SD
Horse 1 LF	Palmar digital	Unrelated to fetlock	16.3	-0.1	19.6	-16.3	27.3
Horse 2 LF	Palmar digital	Unrelated to fetlock	9.5	-2.8	10.1	-9.1	12.1
Horse 3 LF	Abaxial sesamoid	Unrelated to fetlock	26.1	-7.8	10.0	-24.9	12.3
Horse 4 LF	Low four-point	Insufficient lameness for repeat diagnostic anaesthesia the following day	36.9	-8.3	13.4	-35.9	18.2
Horse 5 RF	Low four-point	Unusual condylar resorption with mineralisation of the overlying cartilage	14.1	-5.3	9.3	13.1	10.2
Horse 6 LF	Low four-point	No overt fetlock MRI/CT changes	10.3	-4.1	6.1	-9.4	8.7
Horse 7 LF	Low four-point	No overt fetlock MRI/CT changes	25.0	-12.5	7.9	-21.6	12
Horse 8 LF	Palmar digital	Unrelated to fetlock	12.9	-1.4	5.1	-12.8	6
Horse 9 LF	Palmar digital	Unrelated to fetlock	14.2	-12.3	9.8	-7.1	9
Horse 9 RF	Palmar digital	Unrelated to fetlock	8.8	-8.6	6.8	1.9	8.3

Supplementary item 1. Objective baseline lameness assessment data (obtained in a straight line on a hard surface) of horses, which developed forelimb lameness and underwent diagnostic anaesthesia during the study period. LF – left forelimb; RF – right forelimb; Diff Max Head – The difference (millimetres) in maximum head heights between left and right halves of the stride; Diff Min Head – The difference in minimum head heights between left and right halves of the stride; Total Diff Head – The mean Diff Max and Diff Min Head combined as a

vector. Diagnostic anaesthesia refers to the perineural anaesthetic technique that resulted in substantial improvement in lameness. Perineural anaesthesia of the medial and lateral palmar digital nerves at the level of the ungular cartilages = palmar digital block; at the level of the base of the PSBs = abaxial sesamoid block; perineural anaesthesia of the medial and lateral palmar nerves and the medial and lateral palmar metacarpal nerves just proximal to the fetlock = low four-point block. Diagnosis refers to the final clinical interpretation based on diagnostic anaesthesia and CT/MRI findings.

Variable	Estimate	Standard Error	T-value	P-value
Examination time (continuous)	26.49	1.95	13.56	2.00E-16
Examination time category				
0	Reference			
1	60.09	4.49	13.38	2.00E-16
2	65.93	5.04	13.08	2.00E-16
3	139.44	6.28	22.21	2.00E-16
4	50.65	7.64	6.63	1.01E-10
Number of total starts (continuous)	6.34	0.82	7.74	7.03E-14
PSB grade (continuous)	8.22	4.18	1.97	**0.0497**
PSB grade category				
0	Reference			
1	-11.04	10.1	-1.09	0.275
2	10.32	14.49	0.71	0.477
3	37.15	14.42	2.58	**0.0103**
Abaxial new bone				
No	Reference			
Yes	-6.24	13.26	-0.47	0.638
Abaxial margin concavity				
No	Reference			
Yes	-26.88	17.53	-1.53	0.126
Irregular surface				

No	Reference			
Yes	-9.41	9.78	-0.96	0.337
Age in days (continuous)	0.13	0.01	13.4	2.00E-16
Age in months (continuous)	4.05	0.3	13.32	2.00E-16
Age category (months)				
17 to 20	Reference			
21 to 26	45.25	5.83	7.76	6.07E-14
27 to 33	79.83	6.07	13.15	2.00E-16
34 to 47	105.76	6.37	16.59	2.00E-16
Weight in kg (continuous)	1.05	0.12	8.5	3.51E-16
Height in cm (continuous)	10.51	0.9	11.63	2.00E-16
Weight_height ratio (continuous)	128.82	23.67	5.44	1.01E-07
Sex				
Filly	Reference			
Gelding	-1.96	22.49	-0.09	0.931
Colt	-26.84	18.99	-1.41	0.166
Medial or lateral PSB				
Lateral	Reference			
Medial	11.55	4.98	2.32	**0.021**
Limb laterality				
Left fore	Reference			
Right fore	5.97	5	1.2	0.233

E – exponent

Supplementary item 2. Results of univariable mixed-effects linear regression models, including horse as a random effect, with HU as the outcome, for 40 Thoroughbred flat racehorses which were first examined as yearlings (time 0, n=40) and then four more times, at approximately six months' intervals (time 1 n=31, time 2 n=23, time 3 n=13, time 4 n=8). The PSBs were graded using predefined criteria from 0-3 and the presence or absence of abaxial new bone, abaxial margin concavity and an irregular surface of the palmar distal half of each PSB. Significant p-values are highlighted in bold.

Outcome - New bone formation						
Variable	**Estimate**	**Standard Error**	**Z-value**	**OR**	**95% CI**	**P-value**
Examination time (continuous)	-0.14	0.23	-0.62	0.87	0.56, 0.01	0.538
Examination time category						
0	Reference					
1	-0.43	0.63	-0.68	0.65	0.19, 2.23	0.495
2	-0.31	0.7	-0.44	0.73	0.19, 2.87	0.658
3	-0.27	0.92	-0.29	0.76	0.12, 4.68	0.771
4	-0.72	1.23	-0.59	0.49	0.04, 5.39	0.557
Number of total starts (continuous)	-0.01	0.08	-0.15	0.99	0.85, 1.15	0.882
PSB grade (continuous)	0.78	0.31	2.48	2.18	1.18, 4.04	**0.013**
PSB grade category						
0	Reference					
1	0.39	1.23	0.31	1.47	0.13, 16.44	0.755
2	0.01	1.28	0.01	1.01	0.08, 12.34	0.994
3	2.89	1.01	2.87	17.96	2.49, 129.41	**0.004**
Abaxial margin concavity						
No	Reference					
Yes	-17.15	6880.25	-0.002	3.58E-08	0.00, Inf	0.998
Irregular surface						
No	Reference					
Yes	-19.07	4037.18	-0.01	5.20E-09	0.00, Inf	0.996
Age in months (continuous)	-0.02	0.04	-0.66	0.98	0.91, 1.05	0.511
Age category (months)						
17 to 20	Reference					
21 to 26	0.12	0.66	0.19	1.13	0.31, 4.10	0.85

27 to 33	-0.39	0.75	-0.52	0.68	0.15, 2.97	0.606
34 to 47	-0.36	0.78	-0.46	0.7	0.15, 3.24	0.648
Weight in kg (continuous)	0.0004	0.009	0.05	1.0004	9.82e-01, 1.02	0.964
Height in cm (continuous)	-0.08	0.08	-0.02	0.92	0.79, 1.08	0.309
Weight:height ratio (continuous)	0.77	1.67	0.46	2.17	0.81, 57.61	0.644
Sex						
Filly	Reference					
Gelding	-16.57	591.21	-0.03	6.38E-08	0.00, Inf	0.978
Colt	-0.99	0.85	-1.16	0.37	0.07, 1.96	0.244
Medial or lateral PSB						
Lateral	Reference					
Medial	-1.11	0.53	-2.09	0.33	0.12, 0.93	**0.036**
Limb laterality						
Left fore	Reference					
Right fore	-0.35	0.49	-0.72	0.71	0.27, 1.83	0.472
Outcome - Abaxial margin concavity						
Variable	**Estimate**	**Standard Error**	**Z-value**	**OR**	**95% CI**	**P-value**
Examination time (continuous)	-1.22	0.52	-2.37	0.3	0.11, 0.81	0.018
Examination time category						
0	Reference					
1	-1.45	0.86	-1.68	0.23	0.04, 1.27	0.092
2	-1.97	1.14	-1.72	0.14	0.01, 1.31	0.085
3	-18.86	1057.58	-0.018	6.47E-09	0.00, Inf	0.986
4	-18.38	1057.58	-0.017	1.04E-08	0.00, Inf	0.986
Number of total starts (continuous)	-1.09	0.84	-1.3	0.34	0.07, 1.74	0.194
PSB grade (continuous)	0.22	0.38	0.58	1.24	0.6, 2.59	0.562

PSB grade category						
0	Reference					
1	2.43	1.02	2.4	11.4	1.56, 83.27	0.017
2	1.28	1.43	0.89	3.6	0.22, 59.88	0.372
3	-17.7	9455.77	-0.002	2.06E-08	0.00, Inf	0.999
Abaxial new bone						
No	Reference					
Yes	-15.37	724.08	-0.02	2.12E-07	0.00, Inf	0.983
Irregular surface						
No	Reference					
Yes	0.16	1.17	0.14	1.18	0.12, 11.67	0.889
Age in months (continuous)	-0.22	0.09	-2.5	0.81	0.68, 0.95	0.012
Age category (months)						
17 to 20	Reference					
21 to 26	-1.69	0.86	-1.96	0.18	0.03, 1.00	0.05
27 to 33	-2.29	1.13	-2.03	0.1	0.01, 0.93	0.043
34 to 47	-19.28	1448.16	-0.01	4.23E-09	0.00, Inf	0.989
Weight in kg (continuous)	-0.02	0.01	-1.95	0.98	0.96, 1.00	0.051
Height in cm (continuous)	-0.33	0.12	-2.65	0.72	0.56, 0.92	0.008
Weight:height ratio (continuous)	-2.34	1.77	-1.32	0.1	0.003, 3.12	0.188
Sex						
Filly	Reference					
Gelding	-14.32	724.08	-0.02	6.07E-07	0.00, Inf	0.984
Colt	1.8	1.2	1.5	6.02	0.58, 62.61	0.133
Medial or lateral PSB						
Lateral	Reference					
Medial	1.66	0.82	2.04	5.27	1.06, 3.26	0.042
Limb laterality						

Left fore	Reference					
Right fore	-1.66	0.82	-2.04	0.19	0.04, 0.94	0.042
Outcome - Irregular surface on radiographs						
Variable	**Estimate**	**Standard Error**	**Z-value**	**OR**	**95% CI**	**P-value**
Examination time (continuous)	-0.42	0.19	-2.23	0.66	0.45, 0.95	0.026
Examination time category						
0	Reference					
1	-0.19	0.44	-0.43	0.83	0.35, 1.96	0.67
2	-0.93	0.55	-1.7	0.4	0.14, 1.15	0.09
3	-1.24	0.86	-1.45	0.29	0.05, 1.56	0.148
4	-1.59	1.17	-1.36	0.2	0.02, 2.01	0.174
Number of total starts (continuous)	-0.14	0.08	-1.73	0.87	0.74, 1.02	0.084
PSB grade (continuous)	-0.07	0.33	-0.2	0.94	0.5, 1.77	0.841
PSB grade category						
0	Reference					
1	0.51	0.66	0.77	1.66	0.45, 6.07	0.443
2	1.04	0.95	1.1	2.84	0.44, 18.26	0.271
3	-17.66	4035.54	-0.004	2.14E-08	0.00, Inf	0.997
Abaxial new bone						
No	Reference					
Yes	-19.03	724.08	-0.03	5.44E-09	0.00, Inf	0.979
Abaxial margin concavity						
No	Reference					
Yes	0.16	1.23	0.13	1.18	0.11, 13.03	0.893
Age in months (continuous)	-0.07	0.03	-2.26	0.93	0.88, 0.99	0.024
Agecategory (months)						
17 to 20	Reference					

21 to 26	-0.55	0.53	-1.05	0.57	0.20, 1.62	0.29
27 to 33	-0.81	0.55	-1.48	0.44	0.15, 1.31	0.14
34 to 47	-1.18	0.62	-1.91	0.31	0.09, 1.03	0.056
Weight in kg (continuous)	-0.01	0.01	-1.14	0.99	0.97, 1.01	0.254
Height in cm (continuous)	-0.07	0.07	-1.04	0.93	0.81, 1.07	0.296
Weight:height ratio (continuous)	-1.77	01-Sep	-0.93	0.17	0.004, 7.11	0.353
Sex						
Filly	Reference					
Gelding	0.9	1.42	0.64	2.47	0.15, 40.14	0.525
Colt	1.15	1.01	1.15	3.16	0.44, 22.69	0.252
Medial or lateral PSB						
Lateral	Reference					
Medial	1.58	0.42	3.77	4.86	2.13, 11.05	0.000165
Limb laterality						
Left fore	Reference					
Right fore	0.13	0.36	0.36	1.14	0.56, 2.31	0.719

E – exponent; Inf – infinity.

Supplementary item 3. Results of univariable mixed-effects logistic regression models, including horse as a random effect, with presence of abaxial margin changes as individual outcomes, for 40 Thoroughbred flat racehorses which were first examined as yearlings (Time 0, n=40) and then four more times, at approximately six months' intervals (time 1 n=31, time 2 n=23, time 3 n=13, time 4 n=8). The PSBs were graded using predefined criteria from 0-3 and the presence or absence of abaxial new bone, abaxial margin concavity and an irregular surface of the palmar distal half of each PSB. Significant p-values are highlighted in bold.

Univariable mixed effects linear regression model for MRI measurements				
	Estimate	**Standard error**	**T-value**	**P-value**
Age (months)	0.20	0.04	12.72	<0.001

Limb				
Right fore	0.0003	0.26	0.001	0.999
Left fore	Reference			
Condyle				
Medial	-0.19	0.26	-0.74	0.459
Lateral	Reference			
Examination time point (0-4)	1.27	0.10	12.59	<0.001
Sex				
Colt	-1.11	0.72	-1.55	0.130
Filly	Reference			
Gelding	1.12	0.93	1.20	0.233
Total number of starts	0.40	0.04	9.86	<0.001
Body weight (kg)	0.04	0.01	6.27	<0.001
Height (cm)	0.47	0.05	10.09	<0.001
Body weight:height ratio	3.55	1.17	3.04	0.003
Maximum measurement location				
Abaxial	Reference			
Axial	1.14	0.49	2.32	0.021
Middle	0.64	0.45	1.41	0.158
Mixed	-0.47	1.01	-0.46	0.644

Supplementary item 4. Results of univariable mixed-effects linear regression models, including horse as a random effect, with extent of maximal densification on MR images in the metacarpal condyles as an individual outcome, for 39 Thoroughbred flat racehorses which were first examined as yearlings (Time 0, n=39) and then four more times, at approximately six months' intervals (Time 1 n=31, Time 2 n=23, Time 3 n=13, Time 4 n=8).

Univariable mixed effects linear regression model for CT measurements				
	Estimate	**Standard error**	**T-value**	**P-value**
Age (months)	0.22	0.01	15.28	<0.001

Limb				
Right fore	0.14	0.26	0.54	0.593
Left fore	Reference			
Condyle				
Medial	-0.16	0.26	-0.64	0.525
Lateral	Reference			
Examination time point (0-4)	1.43	0.09	15.26	<0.001
Sex				
Male	-0.50	0.64	-0.77	0.446
Female	Reference			
Gelding	2.77	0.87	3.19	0.002
Total number of starts	0.43	0.04	11.25	<0.001
Body weight (kg)	0.04	0.01	6.82	<0.001
Height (cm)	0.52	0.04	11.71	<0.001
Body weight:height ratio	3.24	1.11	2.92	0.004
Maximum measurement location				
Abaxial	Reference			
Axial	-1.00	0.91	-1.09	0.276
Middle	1.50	0.86	1.74	0.083
Mixed	-3.24	1.74	-1.86	0.063

Supplementary item 5. Results of univariable mixed-effects linear regression models, including horse as a random effect, with extent of maximal CT densification in the condyle as an individual outcome, for 39 Thoroughbred flat Thoroughbred racehorses which were first examined as yearlings (Time 0, n=39) and then four more times, at approximately six months' intervals (Time 1 n=31, Time 2 n=23, Time 3 n=13, Time 4 n=8).

14. Acknowledgements

First and foremost, I would like to express my deepest gratitude to my supervisor, Dr. Annamária Nagy, and my consultant, Dr. Sue Dyson, for their guidance, continuous support, and invaluable expertise throughout my PhD studies. I would also like to sincerely thank all staff members of the Department and Clinic of Equine Medicine for their support and assistance, with special appreciation to those who actively contributed to this project. Special thanks are extended to Gabriella Horváth-Lukics for her assistance with diagnostic imaging procedures and data acquisition. I am deeply grateful to the owners, trainers, and referring veterinarians of the Thoroughbred racehorses included in this research for their cooperation, trust, and commitment to the study. I would also like to acknowledge the racehorses themselves, whose participation made this research possible. Finally, I would like to acknowledge the invaluable statistical support provided by Dr. Danica Pollard, Dr. Ágnes Kovács, and Dr. Zsolt Lang.

Project no. FK 138825 was supported by the Ministry of Innovation and Technology of Hungary from the National Research, Development and Innovation Fund, financed under the FK_21 „OTKA" Fiatal kutatói kiválósági program funding scheme. Project no. TKP2020-NKA-01 has been implemented with the support provided from the National Research, Development and Innovation Fund of Hungary, financed under the Tématerületi Kiválósági Program 2020 (2020-4.1.1-TKP2020) funding scheme. The study was supported by the ÚNKP-22-5 New National Excellence Program of the Ministry for Culture and Innovation from the source of the National Research, Development and Innovation Fund. Project no. 2024-2.1.1-EKÖP-2024-00018 has been implemented with the support provided by the Ministry of Culture and Innovation of Hungary from the National Research, Development and Innovation Fund, financed under the 2024-2.1.1-EKÖP funding scheme.